Title
Novel patterns of activity in the hippocampus

Permalink
https://escholarship.org/uc/item/5zw2m60c

Author
Kay, Kenneth Norman

Publication Date
2016

Peer reviewed|Thesis/dissertation

Novel patterns of activity in the hippocampus

by

Kenneth Kay

DISSERTATION

Submitted in partial satisfaction of the requirements for the degree of

DOCTOR OF PHILOSOPHY

in

Bioengineering

in the

GRADUATE DIVISION

of the

UNIVERSITY OF CALIFORNIA, SAN FRANCISCO

AND

UNIVERSITY OF CALIFORNIA, BERKELEY

To those at work and play

"The purpose of computing is insight, not numbers."

R.W. Hamming

Acknowledgements

To my thesis advisor Loren Frank I owe more than I can say. I highlight three things here. First, when I was rotating, it was Loren who was decisive enough to say that if I wanted to follow through on my vague wish to study the brain in action, then I should join his lab. This was the first of many decision points in which Loren's guidance was exactly right. Second, as a lab member, I was able to develop as a scientist only because of Loren's extraordinary patience, which gave me the time I needed to acquire and analyze data, and mental space enough to develop ideas. Third, Loren's integrity, optimism, and brilliance together have set an unforgettable standard by which to do science.

I thank past and present lab colleagues – Caleb Kemere, Shantanu Jadhav, Maggie Larkin, Steve Kim, Walter German, Daniel Liu, Gideon Rothschild, Jai Yu, Emily Anderson, Mari Sosa, Jason Chung, Demetris Roumis, Anna Gillespie, Mattias Karlsson, Tom Davidson, and Hannah Joo – for so many things: for teaching me, for untold numbers of discussions and impromptu help, for putting up with my meandering lab meetings, for carefully considered feedback, for encouragement, and for all the fun we had.

I give special thanks to my outstanding lab collaborators Mari and Jason. Together we recorded data from multiple subjects, and in subjects with linear probes Jason was completely in charge of implantation. Also, in work described in Chapter 2, Mari did several pilot analyses that led us to look more deeply. I also give special thanks to Mattias and Maggie, whose data collected years ago proved crucial in bringing numerous findings to light.

I thank Xinyi Deng and Uri Eden for their superb work on the clusterless decoding algorithm, which has greatly helped me to understand the hippocampal data.

I thank Sheri Harris, Christy Lykken, Irene Grossrubatscher, and Gomathi Ramakrishnan for their excellent histology and for making the lab a great place to work.

I thank the members of my Thesis Committee – Christoph Schreiner, Philip Sabes, Michael Stryker, and Bob Knight – for their candor and incisive feedback. It has been a great privilege for me to learn from them.

I thank my friends and colleagues, past and present, inside and outside the lab, who, despite my best efforts to resist, have taught me everything I needed to know.

Finally I thank my siblings Kendra, Kelvin, Kendrick, and parents Kenneth and Nora Kay for raising me and for placing great value in science.

Novel patterns of activity in the hippocampus

by

Kenneth Norman Kay

Submitted June 7, 2016
in Partial Satisfaction of the Requirements for
the Degree of Doctor of Philosophy in Bioengineering
in the Graduate Division of the
University of California, San Francisco
and
University of California, Berkeley

Abstract

The observation that the hippocampus is required for memory and spatial navigation has led to extensive study of the hippocampal neural circuit. Past research has focused on established patterns of hippocampal neural activity, such as the classic place cell code and the theta network pattern. However, we still have only a preliminary understanding of how the hippocampus performs cognitive functions. This may be the case because there still remain unknown yet fundamental patterns of hippocampal neural activity.

To investigate this possibility, we recorded neural activity in the hippocampus of rats engaged in a spatial memory task. In this thesis I describe four previously unidentified patterns of hippocampal neural activity: (1) spatially specific neural firing that is more active when animals are at rest, (2) a ~200 ms network pattern that is associated with spatial firing at rest, (3) spatially specific, transient neural firing at the time of behavioral transitions between movement and rest, and (4) a high frequency (65-140 Hz) network pattern that entrains neural firing throughout the hippocampus. I postulate that these patterns of activity have essential roles in complex hippocampal functions.

Thesis supervisor: Loren Frank, Ph. D.
Title: Professor

Abstract on space

In the mammalian brain, the hippocampus constructs a neural map of space understood to be required for memory and spatial navigation. Yet despite decades of research into the hippocampal spatial map, it has remained unclear whether and how the hippocampus represents location when animals are at rest – a behavioral state not only essential in the life of an animal but also integral to complex behaviors dependent on the hippocampus.

In this thesis I present experimental findings that show (1) the hippocampus constructs a representation of location when animals are at rest, (2) the hippocampus engages a specific set of neurons to do so, and (3) the hippocampus briefly activates two unorthodox patterns of neural activity when transitioning to the locational representation associated with rest. These findings indicate that fundamentally distinct spatial representations in the hippocampus are active at different times, and furthermore that alternation between the different spatial representations depends on variables internal to the brain.

Table of Contents

List of Figures

Chapter 1

Chapter 2

List of Illustrations

Introduction

Our knowledge of the world depends on apparently disparate things: on one hand, the biological apparatus of the brain, yet also on the abstract concepts of time and space. Contemporary brain research has begun to address this fundamental matter. Beginning with the discovery of hippocampal "place" cells in 1971 by O'Keefe and Dostrovsky, a collection of experimental work has established that the neural circuit of the brain structure known as the hippocampus constructs an abstract representation of space[1-3]. The defining unit of this representation is the place cell, a hippocampal neuron that fires when animals move through a particular location. Place cell activity thereby constitutes a neural code for current location as animals move through space[4].

While the elucidation of the hippocampal place code has shed light on the neural implementation of spatial cognition, our understanding of how the hippocampal neural circuit represents space is still deeply incomplete. The most striking indication that this is the case is recent work showing that when animals are at rest, hippocampal neurons engage in a radically different neural code for space[†]. This alternative code, conventionally referred to as hippocampal "replay," has two properties distinguishing it from the classic place code. The first is that replay occurs in intermittent bouts of neural firing lasting ~100 ms, in contrast to the place code, which is continuously active during movement. The second is that replay represents past and possible future spatial experience, a radical departure from the local representation of position characteristic of the place code. It is worth mentioning that these and other distinctive properties of replay imply a crucial role in the well-documented memory functions of the hippocampus, a possibility currently under investigation[5-7].

But replay also raises a basic question. If replay is the characteristic neural code of the hippocampus when animals are at rest, does this mean that the hippocampus has no particular representation of current location at rest? Surprisingly, a hippocampal code for current location at rest has not been set forth as an explicitly analyzed experimental fact (though see early anecdotal reports[8-10]) or as a theoretical necessity. In fact, popular behavioral paradigms in the field of neural spatial coding characteristically elicit continuous movement, leaving open the question of what is represented during times when movement is absent and replay is not observed. Furthermore, it is conceivable that brain structures outside of the hippocampus represent current position when animals are at rest, or even that there is no such representation in the brain. In these scenarios, the local representation of space manifest in hippocampal place firing simply dissipates when movement ends.

In fairness, the traditional focus on spatial coding during movement stems from a set of influential experimental findings: (1) classic place cells in hippocampal subregions CA1 and CA3 fire more at high speeds[11-13], (2) classic place cell firing is often active in conjunction with the

---

[†]See Buzsaki (2015) for a comprehensive review.

theta network pattern, a physiological marker plainly expressed in the hippocampal local field potential (LFP) during movement[14-17], (3) classic place cell firing shows an extraordinary temporal relationship with the phase of theta (theta phase precession[18-20]), underscoring the potential significance of the previous finding, and (4) classic place cells fire less and lose their spatial specificity under conditions of restraint[21-25]. These various findings have in the past led to the view that periods of movement accompanied by theta are when the hippocampus is "on-line," while periods of rest correspond to when the hippocampus relaxes from informative processing[2,16,26]. Also, the recent elucidation of hippocampal replay indicates that since the hippocampus during rest engages a different neural code, hippocampal neural activity at rest therefore adds noise to the traditional place signal[27]. These various facts have led to the current scenario in the field in which rest periods are often in practice excluded in analyses of local spatial representations.

Chapter 1 directly addresses the above matter. In the study described therein, we recorded neural activity in the hippocampus of rats not only navigating through space, but also at rest. We found that a distinct subpopulation of neurons in a poorly studied hippocampal subregion known as CA2 was preferentially active when subjects were at rest, and moreover that these neurons continuously fired at specific locations. Thus firing in these neurons constituted a code for location that was distinctly activated at rest. These findings and others in this study indicate that the hippocampus engages fundamentally different neural codes for space from moment to moment during natural behavior: (1) during movement – the classical place code, (2) during intermittent bouts at rest – the replay code, and (3) in a continuous manner at rest – a novel spatial code that recruits a particular subpopulation of hippocampal neurons.

Chapter 2 investigates how fast and how these neural codes transition from one to another. In the study described therein, we analyzed neural activity at times when animals came to a stop or began moving from a period of rest. We observed that, at the time of these behavioral transitions, neurons participating in the rest-associated spatial code could change firing rates as rapidly as the classic place code, shifting between silence and high firing rates within hundreds of milliseconds. Unexpectedly, we also identified two non-classical patterns of hippocampal neural activity that rapidly became active at these same times: (1) a transient and spatially specific increase in firing (lasting less than a second) in a subset of hippocampal neurons, and (2) a widespread high frequency rhythmic network pattern detectable in CA3 and DG. These several findings specify the timescale of activation of distinct neural codes in the hippocampus and identify neural mechanisms that may mediate transitions between them.

1   O'Keefe, J. & Dostrovsky, J. The hippocampus as a spatial map. Preliminary evidence from unit activity in the freely-moving rat. Brain Res 34, 171-175 (1971).

2   O'Keefe, J. & Nadel, L. The hippocampus as a cognitive map. (Oxford University Press, 1978).

3   Andersen, P. in The Hippocampus Book (eds P. Andersen *et al.*) 37-114 (Oxford Univ. Press, 2007).

4   Wilson, M. A. & McNaughton, B. L. Dynamics of the hippocampal ensemble code for space. Science 261, 1055-1058 (1993).

5   Carr, M. F., Jadhav, S. P. & Frank, L. M. Hippocampal replay in the awake state: a potential substrate for memory consolidation and retrieval. Nat Neurosci 14, 147-153 (2011).

6   Pfeiffer, B. E. & Foster, D. J. Hippocampal place-cell sequences depict future paths to remembered goals. Nature 497, 74-79 (2013).

7   Buzsaki, G. Hippocampal sharp wave-ripple: A cognitive biomarker for episodic memory and planning. Hippocampus 25, 1073-1188 (2015).

8   Ranck, J. B., Jr. Studies on single neurons in dorsal hippocampal formation and septum in unrestrained rats. I. Behavioral correlates and firing repertoires. Exp Neurol 41, 461-531 (1973).

9   O'Keefe, J. Place units in the hippocampus of the freely moving rat. Exp Neurol 51, 78-109 (1976).

10   Best, P. J. & Ranck, J. B., Jr. Reliability of the relationship between hippocampal unit activity and sensory-behavioral events in the rat. Exp Neurol 75, 652-664 (1982).

11   McNaughton, B. L., Barnes, C. A. & O'Keefe, J. The contributions of position, direction, and velocity to single unit activity in the hippocampus of freely-moving rats. Exp Brain Res 52, 41-49 (1983).

12   Huxter, J., Burgess, N. & O'Keefe, J. Independent rate and temporal coding in hippocampal pyramidal cells. Nature 425, 828-832 (2003).

13   Zheng, C., Bieri, K. W., Trettel, S. G. & Colgin, L. L. The relationship between gamma frequency and running speed differs for slow and fast gamma rhythms in freely behaving rats. Hippocampus (2015).

14   Vanderwolf, C. H. Hippocampal electrical activity and voluntary movement in the rat. Electroencephalogr Clin Neurophysiol 26, 407-418 (1969).

15   Vanderwolf, C. H. Limbic-diencephalic mechanisms of voluntary movement. Psychological review 78, 83-113 (1971).

16   Buzsaki, G. Theta oscillations in the hippocampus. Neuron 33, 325-340 (2002).

17   Buzsaki, G. Theta rhythm of navigation: link between path integration and landmark navigation, episodic and semantic memory. Hippocampus 15, 827-840 (2005).

18   O'Keefe, J. & Recce, M. L. Phase relationship between hippocampal place units and the EEG theta rhythm. Hippocampus 3, 317-330 (1993).

19   Skaggs, W. E., McNaughton, B. L., Wilson, M. A. & Barnes, C. A. Theta phase precession in hippocampal neuronal populations and the compression of temporal sequences. Hippocampus 6, 149-172 (1996).

20   Schmidt, R. *et al.* Single-trial phase precession in the hippocampus. Journal of Neuroscience 29, 13232-13241 (2009).

21   Foster, T. C., Castro, C. A. & McNaughton, B. L. Spatial selectivity of rat hippocampal neurons: dependence on preparedness for movement. Science 244, 1580-1582 (1989).

22   Song, E. Y., Kim, Y. B., Kim, Y. H. & Jung, M. W. Role of active movement in place-specific firing of hippocampal neurons. Hippocampus 15, 8-17 (2005).

23   Terrazas, A. *et al.* Self-motion and the hippocampal spatial metric. J Neurosci 25, 8085-8096 (2005).

24   Ravassard, P. *et al.* Multisensory control of hippocampal spatiotemporal selectivity. Science 340, 1342-1346 (2013).

25   Aghajan, Z. M. *et al.* Impaired spatial selectivity and intact phase precession in two-dimensional virtual reality. Nat Neurosci 18, 121-128 (2015).

26   Buzsaki, G. Two-stage model of memory trace formation: a role for "noisy" brain states. Neuroscience 31, 551-570 (1989).

27   Zhang, K., Ginzburg, I., McNaughton, B. L. & Sejnowski, T. J. Interpreting neuronal population activity by reconstruction: unified framework with application to hippocampal place cells. J.Neurophysiol. 79, 1017-1044 (1998).

Biological interpretation and the hippocampus

The brain is a bodily organ upon which our survival depends. Despite this fact, we still have only an elementary understanding of how the brain performs some of its most vital functions. What is the way forward?

Brain science is a large field, and there is now more than ever a diverse set of ways of approaching the brain[1,2]. Nonetheless, if understanding the brain is at least in part a problem of biology, then it may be valuable to take a traditional biological approach – namely, to analyze the problem as composed of two distinct yet reciprocal parts: structure and function. As the thinking goes, improvement in our knowledge of one part will yield improvement in our knowledge of the other. You can call this an article of faith, or, if you prefer, a consequence of how evolution works. The conventional interpretation is that if we have some particular function (however simple or complex) we want to understand, we may benefit from a careful consideration of its structural correlates. A bolder interpretation is that we should choose to study not only structures that we suspect will yield functional insight, but also functions that we suspect will yield structural insight.

If only it were that easy. Structural organization in biology spans orders of magnitude of size, and, depending on what particular function we provisionally have in mind, biological structural units may be classified under a variety of schemes. The difficulty moreover works both ways. For example, our conception of some particular biological function may be flawed due to a mismatched or misleading structural correlate. And, adding to the difficulty, an adequate account of a biological function requires knowledge, if not simulation, of the native conditions of the function in question. The native conditions essential to the problem being studied may in turn not be easy to come by in a laboratory setting, or may be inadvertently eliminated in experimental design.

Yet the old way of thinking might not be hopeless. In fact it might not even be unlike how many scientists casually and subconsciously reason about the brain. I propose here that this approach may be quite useful if we proceed explicitly, reductively, and iteratively. We can begin by making clear what our very best guess is for each half of the biological problem that concerns us, doing the same for every smaller constituent problem. After doing so, we will have articulated a collection of gaps in our knowledge. Some of these gaps will be well-known while others obscure, but, more to the point, each would be identified as belonging either to structure or to function. As such, a particular gap in knowledge in a biological problem can be viewed as implying some unit of knowledge we do in fact have. In particular, the unit of biological knowledge that elicits the most dissatisfaction – insofar as it lacks a clear or demonstrable structural or functional counterpart – could then become what we choose to address in our next project, whether observational, experimental, or theoretical. The cycle then repeats, presumably until no units either of structure or of function remain unpaired with a convincing correlate.

The experimental work described in this thesis is an attempt to complete such a cycle. We studied the hippocampus, a brain structure known to be grossly required for episodic memory

and spatial navigation, two vital functions upon which we rely. We had the advantage of building upon past scientific work that reduced the large problem of the hippocampus to a smaller constituent structure-function problem. This smaller problem is the hippocampal place cell, a single neuron whose functional output – an abstract representation of space in the form of neural firing – can provide an animal with potentially life-saving information about where it is located in the world. The hippocampal place cell is an important biological problem because it not only relates to prior structural knowledge (i.e. of neurons), but also is defined by a function that is required for spatial navigation, required for episodic memory, and by itself discernibly useful to a living animal. Thus, when we were considering what to study, at least the function of spatial representation was already established within the overarching problem of the hippocampus.

The difficulty that arises is that the traditional spatial representation expressed by place cells, a neuron-level function, is not convincingly matched with any known structural correlate. Despite the fact that place cells themselves have been identified to be principal neurons in the hippocampus[3], these neurons are not especially structurally distinct from other neurons found throughout the brain, at least not in a way that clarifies the function of spatial representation. Nor has the classic place representation been matched to a structural correlate beyond the individual neuron. Studies of place cells do show that a range of sensory and proprioceptive inputs somehow converge to generate the place cell spatial representation[4-8], but this fact does not effectively single out a specific circuit-level architecture. Moreover, anatomically detailed studies of the hippocampal neural circuit during traditional place cell activity[9], as well as studies inactivating or ablating components of the hippocampus[10-12], also have not led to identification of hippocampal structural units that are important for the traditional place cell representation. Indeed, spatial representations as informative as that of place cells have come to be observed in brain regions outside of the hippocampus[5,13]. This latter fact indicates that the place cell spatial representation, strictly speaking and at least as currently understood, is not convincingly matched to structural features of the hippocampus.

The story would stall at this point if not for recent findings indicating that the traditional functional account of the place cell is fundamentally incomplete. Beginning with studies conducted in the 1990s, the discovery and elucidation of the phenomenon of hippocampal replay has shown that there is in fact a radically different neural representation of space in the hippocampus[14]. In replay, coherent representations of past spatial experiences relevant to ongoing behavior are re-activated – indeed this re-activation occurs in the very same hippocampal place cells that at other times express the traditional local spatial representation. Thus place cells are just as well "replay cells." In this way, replay suggests an alternative functional account of the hippocampus, that is, one involving memory[15].

Critically, unlike the traditional place code, replay has a highly distinct structural correlate that goes beyond the single neuron. As it turns out, replay occurs in conjunction with a prominent hippocampal activity pattern that largely originates in a macroscopic substructure within the

hippocampus. The pattern is known as the sharp wave-ripple and the substructure in question is the CA3 subregion of the hippocampus[14]. Neurons in CA3 form an exceptionally large, highly recurrently connected network[14,16-18], suggesting a neural architecture suited for the memory-like function characterizing replay[14,19-21].

The link between CA3 and re-activation indicates that subregions in the hippocampus are crucial structural units in the study of hippocampal function. Some context is important here: as might be expected for any large part of the brain, the hippocampus has an abundance of established structural components, dimensions, and markers, along with a variety of proposed organizational schemes[22-27].

Despite this, the concept of hippocampal subregion has had an unusual history[17,23,28-30]. On the basis of neuroanatomical findings, Ramón y Cajal himself subdivided different macroscopic portions of hippocampus into subregions he termed *regio superior* and *regio inferior*[28]. Cajal's scheme has since been replaced by a system, formally established in 1934 by Lorente de Nó, in which the hippocampus proper (the hippocampal formation excluding the dentate gyrus and subiculum) is divided into the CA1, CA2, and CA3 subregions[29]. Like Cajal, Lorente de Nó justified the CA divisions on purely anatomical grounds. Yet he clearly went further in his explicit identification of what he termed CA2, a relatively small subregion of the hippocampus he defined by structural features. CA2 was not in Cajal's system, in which *regio superior* and *inferior* correspond respectively to CA1 and CA3, and indeed CA2 has had a controversial history until recent state-of-the-art characterizations[31-34]. A comprehensive review of what we have learned about CA2 since Lorente de Nó can be found elsewhere[34]. The point I hope to make here is that CA2 – a brain region that has been understudied for decades – has for a time been of justifiable interest purely on the basis of its identification as an instantiation of a crucial type of structural unit. It is worth pointing out that this identification was made possible through research that explicitly sought, in this particular case, structural insight. This research ranged from the purely anatomical work of Cajal and Lorente de Nó to physiological studies that aimed to identify the structural correlates important for discrete neurophysiological functions[35-41], however reductive and less well appreciated these functions were at the time.

These notes outline some of our thinking after first taking notice of CA2 histologically in pilot experiments. We therefore set out to determine whether the structurally defined CA2 subregion exhibited neural functions that had previously been established in the hippocampus – that is, whether there was place or replay activity in CA2 neurons. To do so, we targeted the CA2 subregion in a series of recording studies. We moreover used an experimental paradigm[42-45] that was developed to simulate ethologically native conditions under which we expected the hippocampus, and therefore CA2, to be functionally active.

1   Abbott, L. F. Theoretical neuroscience rising. Neuron 60, 489-495 (2008).

2   Marder, E. Understanding brains: details, intuition, and big data. PLoS Biol 13, e1002147 (2015).

3   Spruston, N. Pyramidal neurons: dendritic structure and synaptic integration. Nat Rev Neurosci 9, 206-221 (2008).

4   McNaughton, B. L. *et al.* Deciphering the hippocampal polyglot: the hippocampus as a path integration system. J Exp Biol 199, 173-185 (1996).

5   Moser, E. I., Kropff, E. & Moser, M. B. Place Cells, Grid Cells, and the Brain's Spatial Representation System. Annu. Rev. Neurosci. 19 (2008).

6   Eichenbaum, H. in Hippocampal place fields: relevance to learning and memory (ed S. Mizumori) 409 p. (Oxford University Press, 2008).

7   Ravassard, P. *et al.* Multisensory control of hippocampal spatiotemporal selectivity. Science 340, 1342-1346 (2013).

8   Chen, G., King, J. A., Burgess, N. & O'Keefe, J. How vision and movement combine in the hippocampal place code. Proc Natl Acad Sci U S A 110, 378-383 (2013).

9   Mizuseki, K., Sirota, A., Pastalkova, E. & Buzsaki, G. Theta oscillations provide temporal windows for local circuit computation in the entorhinal-hippocampal loop. Neuron 64, 267-280 (2009).

10   McNaughton, B. L., Barnes, C. A., Meltzer, J. & Sutherland, R. J. Hippocampal granule cells are necessary for normal spatial learning but not for spatially-selective pyramidal cell discharge. Exp Brain Res 76, 485-496 (1989).

11   Brun, V. H. *et al.* Place cells and place recognition maintained by direct entorhinal-hippocampal circuitry. Science 296, 2243-2246 (2002).

12   Nakashiba, T., Buhl, D. L., McHugh, T. J. & Tonegawa, S. Hippocampal CA3 output is crucial for ripple-associated reactivation and consolidation of memory. Neuron 62, 781-787 (2009).

13   Hartley, T., Lever, C., Burgess, N. & O'Keefe, J. Space in the brain: how the hippocampal formation supports spatial cognition. Philos Trans R Soc Lond B Biol Sci 369, 20120510 (2014).

14   Buzsaki, G. Hippocampal sharp wave-ripple: A cognitive biomarker for episodic memory and planning. Hippocampus 25, 1073-1188 (2015).

15   Carr, M. F., Jadhav, S. P. & Frank, L. M. Hippocampal replay in the awake state: a potential substrate for memory consolidation and retrieval. Nat Neurosci 14, 147-153 (2011).

16   Le Duigou, C., Simonnet, J., Telenczuk, M. T., Fricker, D. & Miles, R. Recurrent synapses and circuits in the CA3 region of the hippocampus: an associative network. Front Cell Neurosci 7, 262 (2014).

17   Ishizuka, N., Weber, J. & Amaral, D. G. Organization of intrahippocampal projections originating from CA3 pyramidal cells in the rat. J Comp Neurol 295, 580-623 (1990).

18   Wittner, L., Henze, D. A., Zaborszky, L. & Buzsaki, G. Three-dimensional reconstruction of the axon arbor of a CA3 pyramidal cell recorded and filled in vivo. Brain Struct Funct 212, 75-83 (2007).

19   Marr, D. Simple memory: a theory for archicortex. Philos Trans R Soc Lond B Biol Sci 262, 23-81 (1971).

20   Lisman, J. E., Talamini, L. M. & Raffone, A. Recall of memory sequences by interaction of the dentate and CA3: a revised model of the phase precession. Neural Netw 18, 1191-1201 (2005).

21   Rolls, E. T. A quantitative theory of the functions of the hippocampal CA3 network in memory. Front Cell Neurosci 7, 98 (2013).

22   Amaral, D. G. & Witter, M. P. The three-dimensional organization of the hippocampal formation: a review of anatomical data. Neuroscience 31, 571-591 (1989).

23   Andersen, P. in The Hippocampus Book (eds P. Andersen *et al.*) 37-114 (Oxford Univ. Press, 2007).

24   Klausberger, T. & Somogyi, P. Neuronal diversity and temporal dynamics: the unity of hippocampal circuit operations. Science 321, 53-57 (2008).

25   Fanselow, M. S. & Dong, H. W. Are the dorsal and ventral hippocampus functionally distinct structures? Neuron 65, 7-19 (2010).

26   Mizuseki, K., Diba, K., Pastalkova, E. & Buzsaki, G. Hippocampal CA1 pyramidal cells form functionally distinct sublayers. Nat Neurosci 14, 1174-1181 (2011).

27   Cembrowski, M. S. *et al.* Spatial Gene-Expression Gradients Underlie Prominent Heterogeneity of CA1 Pyramidal Neurons. Neuron 89, 351-368 (2016).

28   Ramón y Cajal, S. Estructura del asta de Ammon y fascia dentata. Ann Soc Esp Hist Nat 22 (1893).

29   Lorente de Nó, R. Studies on the structure of the cerebral cortex. II. Continuation of the study of the ammonic system. J Psychol Neurol 46, 113-177 (1934).

30   O'Keefe, J. & Nadel, L. The hippocampus as a cognitive map. (Oxford University Press, 1978).

31   Woodhams, P. L., Celio, M. R., Ulfig, N. & Witter, M. P. Morphological and functional correlates of borders in the entorhinal cortex and hippocampus. Hippocampus 3, 303-311 (1993).

32   Lein, E. S., Callaway, E. M., Albright, T. D. & Gage, F. H. Redefining the boundaries of the hippocampal CA2 subfield in the mouse using gene expression and 3-dimensional reconstruction. J Comp Neurol 485, 1-10 (2005).

33   Kohara, K. *et al.* Cell type-specific genetic and optogenetic tools reveal hippocampal CA2 circuits. Nat Neurosci 17, 269-279 (2014).

34   Dudek, S. M., Alexander, G. M. & Farris, S. Rediscovering area CA2: unique properties and functions. Nat Rev Neurosci 17, 89-102 (2016).

35   Buzsaki, G., Leung, L. W. & Vanderwolf, C. H. Cellular bases of hippocampal EEG in the behaving rat. Brain Res 287, 139-171 (1983).

36   Buzsáki, G. Hippocampal sharp waves: their origin and significance. Brain research 398, 242-252 (1986).

37   Ylinen, A. *et al.* Sharp wave-associated high-frequency oscillation (200 Hz) in the intact hippocampus: network and intracellular mechanisms. J Neurosci 15, 30-46 (1995).

38   Penttonen, M., Kamondi, A., Sik, A., Acsady, L. & Buzsaki, G. Feed-forward and feed-back activation of the dentate gyrus in vivo during dentate spikes and sharp wave bursts. Hippocampus 7, 437-450 (1997).

39   Csicsvari, J., Hirase, H., Czurko, A., Mamiya, A. & Buzsaki, G. Fast Network Oscillations in the Hippocampal CA1 Region of the Behaving Rat. J Neurosci 19, RC20 (1999).

40   Csicsvari, J., Hirase, H., Mamiya, A. & Buzsaki, G. Ensemble patterns of hippocampal CA3-CA1 neurons during sharp wave-associated population events. Neuron 28, 585-594 (2000).

41   Buzsaki, G. Theta oscillations in the hippocampus. Neuron 33, 325-340 (2002).

42   Frank, L. M., Brown, E. N. & Wilson, M. Trajectory encoding in the hippocampus and entorhinal cortex. Neuron 27, 169-178 (2000).

43   Kim, S. M. & Frank, L. M. Hippocampal lesions impair rapid learning of a continuous spatial alternation task. PLoS ONE 4, e5494 (2009).

44   Karlsson, M. P. & Frank, L. M. Awake replay of remote experiences in the hippocampus. Nat Neurosci 12, 913-918 (2009).

45   Jadhav, S. P., Kemere, C., German, P. W. & Frank, L. M. Awake hippocampal sharp-wave ripples support spatial memory. Science 336, 1454-1458 (2012).

Chapter 1:

A hippocampal network for spatial coding during immobility and sleep[‡]

A hippocampal network for spatial coding during immobility and sleep

Abstract

      How does an animal know where it is when it stops moving? Hippocampal place cells fire at discrete locations as subjects traverse space, thereby providing an explicit neural code for current location during locomotion. In contrast, during awake immobility, the hippocampus is thought to be dominated by neural firing representing past and possible future experience. The question of whether and how the hippocampus constructs a representation of current location in the absence of locomotion has stood unresolved. Here we report that a distinct population of hippocampal neurons, located in the CA2 subregion, signals current location during immobility, and furthermore does so in association with a previously unidentified hippocampus-wide network pattern. In addition, signaling of location persists into brief periods of desynchronization prevalent in slow-wave sleep. The hippocampus thus generates a distinct representation of current location during immobility, pointing to mnemonic processing specific to experience occurring in the absence of locomotion.

Figure 1 | Distinct hippocampal neuron population at CA2.

Figure 2 | N units fire more at low speeds and during immobility.

Figure 3 | N units signal location during immobility.

Figure 4 | A novel hippocampal network pattern marks spatial coding during immobility.

Figure 5 | Hippocampal spatial coding in desynchronized sleep.

Extended Data Figure 1 | Behavioral task and hippocampal recording sites.

Extended Data Figure 2 | Observation of firing during immobility.

Extended Data Figure 3 | Firing properties of CA1, CA2, and CA3 units.

Extended Data Figure 4 | Spatial firing of CA1, CA2, and CA3 units.

Extended Data Figure 5 | N unit spatial coding.

Extended Data Figure 6 | Locomotor STAs and theta analysis.

Extended Data Figure 7 | N wave: a novel hippocampal network pattern at 1-4 Hz.

Extended Data Figure 8 | CA1 and CA3 principal neurons fire in association with the N wave.

Extended Data Figure 9 | N wave-coupled CA1 and CA3 principal neurons.

Extended Data Figure 10 | Hippocampal spatial coding in the rest environment.

Introduction

The hippocampus is essential for memory and spatial navigation, but we still do not know how these cognitive functions are made possible by the hippocampal neural circuit. Examination of hippocampal neural activity during naturalistic behaviors yields a landmark clue: during locomotion, hippocampal principal neurons, known as "place" cells, fire when subjects traverse discrete locations in space[1,2]. Place cell firing thus provides an internal representation of space understood to be required for both spatial navigation and episodic memory[1,3,4]. Yet despite extensive study of place cells, it remains an open question whether place firing reliably persists in the absence of movement, and, if so, whether distinct hippocampal neurons and network mechanisms are engaged. This matter is of fundamental importance since immobility punctuates spatial exploration[5,6] and features in a range of behaviors dependent on the hippocampus[1,7,8], including contextual fear conditioning[9] and trace conditioning[10].

Previous work focusing on hippocampal neural activity during immobility has identified firing related to past and even upcoming experience[11-15]. Most striking is the observation that place cells during immobility often re-activate in brief bouts at locations outside of their spatial receptive fields. These brief re-activations occur in conjunction with hippocampal sharp wave-ripples (SWRs)[16,17], massively synchronous network events lasting ~100 ms and reflecting high firing rates and strong excitatory drive in hippocampal subregions CA1[1,16-19], CA3[17-20], and DG[20]. Recent work indicates that place cell firing during SWRs frequently represents spatial sequences remote from the animal's current position[14,17,21-23], further raising the question of whether and how the hippocampus sustains a representation of current position during immobility.

A distinct neuron population at CA2

We recorded neural activity in hippocampal subregions CA1, CA2, CA3, and DG (**Fig. 1a**) in rats engaged in a hippocampus-dependent spatial memory task[21,25], with interleaved rest sessions in an enclosed box. In the task, subjects were trained to alternate between each of three locations (reward wells) in a W-shaped maze (**Extended Data Fig. 1a**). In examining single neuron (unit) activity, we observed principal units (**Fig. 1b**) that fired at continuously high rates during immobility (**Extended Data Fig. 2a**). This basic observation led us to investigate hippocampal activity in this behavioral state.

We first found that, although SWRs were prominent during immobility, SWR periods comprised only a small proportion of time spent immobile (<10%, **Extended Data Fig. 2b**), suggesting that SWRs could not account for the observed continuous firing. Next, in examining unit firing at the time of SWRs, we were struck by putative principal units recorded in CA2 that consistently decreased firing during both task and rest SWRs, in contrast to CA1 and CA3 principal units, which increased firing (**Fig. 1c, d**). Indeed virtually all CA1 and CA3 principal units fired more during SWRs (permutation tests at p < 0.05, CA1: 478 out of 489 units, CA3: 271 out of 276 units), while a substantial proportion of putative principal units recorded at CA2 sites were

13

either inhibited or showed no change in firing rate during SWRs, despite otherwise firing hundreds to thousands of spikes during single task epochs (84 out of 226 CA2 site units, with 56 of 84 significantly inhibited during SWRs; **Fig. 1e**, **Extended Data Fig. 3**). We termed these atypical units at CA2 sites "N" units (non-positively modulated by SWRs) to distinguish them from conventionally responding "P" units (positively modulated).

N units fire more during immobility

We next examined the relationship of N unit firing to ongoing behavior. We found that N units fired mainly at low movement speeds and during immobility (**Fig. 2a**). To characterize this relationship, we first evaluated the correlation between unit firing rate and speed (**Fig. 2b**). The CA1 and CA3 unit populations both showed overall positive correlation, consistent with previous reports[26-28] (Pearson r, firing rate vs. log speed; mean ± s.d.; CA1: 0.11 ± 0.10, CA1 vs. 0, $p < 10^{-58}$, signed-rank; CA3: 0.06 ± 0.11, CA3 vs. 0, $p < 10^{-14}$, signed-rank). Remarkably, the CA2 N and CA2 P unit populations showed dramatically different distributions: P units were positively correlated while N units were almost exclusively negatively correlated (mean ± s.d.; CA2 P: 0.10 ± 0.13, CA2 P vs. 0, $p < 10^{-11}$, signed-rank; CA2 N: -0.10 ± 0.09, CA2 N vs. 0, $p < 10^{-10}$, signed-rank; CA2 N vs. CA2 P, $p < 10^{-19}$, rank-sum). N units also fired at higher rates than all other unit populations during immobility (**Fig. 2c**). These findings indicated a fundamental distinction between N units and classic hippocampal place cells.

N units signal location during immobility

We next assessed whether N units showed spatial firing. We found that N units showed less spatial coverage than the other unit populations (**Fig. 3a, b, Extended Data Fig. 4**). In contrast, CA2 P units typically showed large spatial fields, consistent with recent reports[29-31].

In conjunction with low spatial coverage, N unit firing maps showed concentrated firing at locations where subjects were immobile (**Fig. 3a, Extended Data Fig. 4c**). To quantify possible spatial specificity in firing during immobility, we focused on firing at the maze reward wells since immobility at these locations was common across all subjects. Our analysis revealed that individual N units characteristically fired at specific single reward wells while remaining silent at the others (**Fig. 3c, d**, **Extended Data Fig. 5a**). Importantly, the location of N unit firing did not require direct association with reward since spatially specific firing was also observed at other maze locations (**Extended Data Fig. 5b-d**; seen previously in **Fig. 2a**, **Fig. 3a**, **Extended Data Fig. 4c**). These findings indicate that N unit firing constitutes a precise neural code for location during immobility.

A signature of spatial coding during immobility

We were struck by the fact that the firing pattern of N units was not only unorthodox (**Fig. 1**) but also had unambiguous behavioral (**Fig. 2**) and representational (**Fig. 3**) correlates. We

14

hypothesized that this distinctive firing was the result of an unidentified input pattern in the hippocampus. To evaluate this possibility, we calculated CA2 site (N and P) unit spike-triggered averages (STAs) of hippocampal local field potential (LFP)[18], analyzing locomotor and immobility periods separately (**Fig. 4a**).

In contrast to STAs from locomotor periods (characterized by the expected ~8 Hz theta frequency modulation[18,32], **Extended Data Fig. 6**), STAs from non-SWR immobility periods (**Fig. 4b, c**, **Extended Data Fig. 7a**) showed that N units fired at the time of a positive transient LFP pattern lasting ~200 ms. The pattern was smallest on the parent electrode in CA2, larger in CA3, and largest at DG, suggesting broad engagement of the hippocampal circuit. Furthermore, unlike N units, P units showed a mean STA characterized by a negative transient similar to the canonical sharp wave transient of SWRs[33] (**Fig. 4b, c**).

Power spectral analysis (**Fig. 4d**) further specified the contrasting LFP patterns. The power spectral density (PSD) of CA2 N and P unit immobility STAs and of SWR sharp waves showed fundamental frequencies <5 Hz, a bandwidth distinct to that of theta[18,32] (5-11 Hz). In agreement, STAs of LFP filtered at 1-4 Hz showed the same pattern of transients as in the wide-band STAs (**Extended Data Fig. 7a**), indicating that filtering at 1-4 Hz effectively isolates the large-amplitude transients associated with CA2 N units, CA2 P units, and SWRs. Importantly, the N unit STA pattern exceeded 0 mV (**Extended Data Fig. 7b, c**), in fundamental contrast to SWR sharp waves[33], which manifested as negative transients. Thus N units fired in association with an LFP pattern distinct from canonical hippocampal LFP patterns[1,17,18] (theta and SWRs). We termed this pattern "N wave" (N unit-identified wave), a ~200 ms LFP transient with positive polarity at hippocampal recording sites (specifically CA2, CA3, and DG principal cell layers) at which SWR sharp waves are negative.

We then asked whether neurons outside of CA2 were also N wave-coupled. We identified N wave-coupled units in CA1, CA3, and DG (**Fig. 4e-i, Extended Data Figs. 7d-g, 8, 9**), indicating that the N wave reflects a hippocampus-wide network pattern. Critically, a distinct subset of principal units was N wave-coupled (CA1: 50 units, CA3: 34 units, **Fig. 4g-i, Extended Data Figs. 8, 9**). As with CA2 N units, these units fired more during immobility than during movement (**Extended Data Fig. 8b**) and showed unequivocal location-specific firing during immobility (**Fig. 4g, i** and **Extended Data Figs. 8d, e, 9**), thereby linking the N wave network pattern to spatial coding during immobility across the hippocampus.

Hippocampal spatial coding in sleep

Does spatial coding during immobility also occur under quiescent behavioral conditions? Intriguingly, past work has shown that, during slow-wave sleep, ~5% of CA1 place cells continuously fire during episodes in which hippocampal neural activity becomes highly desynchronized, reflected by low-amplitude LFP[34]. In this sleep state, termed small-irregular activity (SIA)[1,34,35], CA1 place cells were found to signal the location where the subject fell asleep

(nesting position)[34]. Recent findings show that CA2 neurons send strong excitatory input to CA1[36-38], raising the possibility that coding of nesting position is staged upstream in CA2.

To test this possibility, we evaluated hippocampal neural activity during rest sessions. First, during sleep, we observed periods of high-amplitude LFP, corresponding to a hippocampal sleep state dominated by SWRs (termed LIA[1,18,34,35]), frequently interrupted by periods of low-amplitude LFP in which the subject did not rouse, which we identified as periods of SIA (**Fig. 5a**). Next, in examining unit firing during sleep, we observed striking instances in which N units fired preferentially during SIA periods, falling silent during LIA (**Fig. 5b**). Analogously to awake immobility in the task (**Fig. 2c**), the N unit population fired at higher rates than all other unit populations during SIA (green, **Fig. 5c**) and also during awake immobility in the rest environment (dark grey, **Fig. 5c**). However, unlike the task condition, there was no significant overall correlation between firing rate and speed for N units during awake periods in the rest environment (**Extended Data Fig. 10a**), indicating that properties of the task maze or the cognitive demands of the task have essential roles in regulating N unit firing.

We then asked whether N units represented locations in the rest environment. We found that N units showed spatially specific firing during awake periods (**Fig. 5d**, **Extended Data Fig. 10b**) that persisted in awake immobility periods (**Extended Data Fig. 10c-i**) and furthermore into SIA: specifically, the CA1 and N unit populations met dual criteria for nesting position coding during SIA, while the CA3 population unexpectedly failed both criteria (criteria in Supplemental Methods; **Fig. 5e, f**, **Extended Data Fig. 10j-l**). In addition, during awake immobility in the rest environment, the N unit population showed a dominant coupling to the N wave network pattern, suggesting similar or equivalent circuit mechanisms underlying spatial firing during immobility in quiescent conditions as spatial firing during immobility in the task (**Extended Data Fig. 10m**).

Discussion

These findings identify a distinct hippocampal network at the anatomical (**Fig. 1**), behavioral (**Fig. 2**), representational (**Fig. 3**), and neural circuit (**Figs. 1, 4**) levels, and also indicate its activation in sleep (**Fig. 5**). In the awake animal, neural firing in this network is marked by a distinct hippocampal network pattern (N wave), occurs during immobility in subsets of neurons in CA1, CA2, CA3, and DG, and is location-specific, constituting an explicit neural code for current position. Thus the classic locomotor hippocampal place code switches, during immobility, to an alternative hippocampal neural code that nonetheless maintains spatial specificity.

Past observations of a lack of place cell firing in restrained animals have led to the suggestion that place firing is driven by input correspondent with an animal's preparedness to make limb movements that would displace the animal from its current position, a condition termed "motor set"[39,40]. Moreover, in rodents, hippocampal theta has been proposed to be a marker of motor set[1,35,41], and thus by inference a marker of hippocampal place firing. Here we observe

spatial firing dependent on neither theta nor motor set, indicating that distinct mechanisms can generate spatial firing and in fact do so complementarily.

A neural code for location during awake immobility enables the brain to provide a spatial context to events occurring during immobility such as consumption of food, sensory stimuli, and deliberation, allowing for the formation of location-specific memories when the animal is still. Moreover, we suggest that the various hippocampus-dependent behaviors characterized by immobility[1,5-10] engage this network, and that activity in this network may correspond to activity seen in human[42], monkey[43], and bat[44] hippocampus, where the theta network pattern occurs less frequently. Importantly, analysis of firing during immobility has not been prominent in traditional approaches to hippocampal spatial coding, in which behavioral paradigms eliciting continuous locomotion or post hoc exclusion of immobility periods is the norm.

Remarkably, a distinct population of hippocampal neurons located at CA2 (N units) signaled location during not only awake immobility but also sleep. An internal representation of current location active during sleep could adaptively influence representations reactivated in sleep in support of memory consolidation[45-47], and, concurrently, could serve to maintain a sleeping animal's bearings despite diminished receptivity to sensory stimuli.

Finally, the localization of N units at CA2 suggests that N units correspond to CA2 neurons, while CA2 P units correspond to intermingling CA1 and CA3 neurons at the CA2 anatomical locus. In parallel with the unique firing pattern of N units, CA2 neurons exhibit a variety of properties unique among hippocampal neurons, including a unique synaptic configuration[36-38,48,49]. Moreover, a recent study reports suppressed firing in three identified CA2 neurons during SWRs[50], indicating that N units and CA2 neurons are overlapping populations or in fact identical. Recent work also links CA2 neurons to the generation of time-dependent spatial representations[29], spatial pattern completion[30,31], and social memory[38]. These cognitive functions and possibly others may rely on the alternative forms of hippocampal neural activity identified here.

1   O'Keefe, J. & Nadel, L. The hippocampus as a cognitive map. (Oxford University Press, 1978).

2   Wilson, M. A. & McNaughton, B. L. Dynamics of the hippocampal ensemble code for space. Science 261, 1055-1058 (1993).

3   Buzsaki, G. & Moser, E. I. Memory, navigation and theta rhythm in the hippocampal-entorhinal system. Nat Neurosci 16, 130-138 (2013).

4   Eichenbaum, H. & Cohen, N. J. Can we reconcile the declarative memory and spatial navigation views on hippocampal function? Neuron 83, 764-770 (2014).

5   Eilam, D. & Golani, I. Home base behavior of rats (Rattus norvegicus) exploring a novel environment. Behav Brain Res 34, 199-211 (1989).

6   Wallace, D. G., Hamilton, D. A. & Whishaw, I. Q. Movement characteristics support a role for dead reckoning in organizing exploratory behavior. Anim Cogn 9, 219-228 (2006).

7   Bannerman, D. M. *et al.* Regional dissociations within the hippocampus--memory and anxiety. Neurosci Biobehav Rev 28, 273-283 (2004).

8   Pentkowski, N. S., Blanchard, D. C., Lever, C., Litvin, Y. & Blanchard, R. J. Effects of lesions to the dorsal and ventral hippocampus on defensive behaviors in rats. Eur J Neurosci 23, 2185-2196 (2006).

9   Maren, S., Phan, K. L. & Liberzon, I. The contextual brain: implications for fear conditioning, extinction and psychopathology. Nat Rev Neurosci 14, 417-428 (2013).

10   Christian, K. M. & Thompson, R. F. Neural substrates of eyeblink conditioning: acquisition and retention. Learn Mem 10, 427-455 (2003).

11   Takahashi, M., Lauwereyns, J., Sakurai, Y. & Tsukada, M. A code for spatial alternation during fixation in rat hippocampal CA1 neurons. J Neurophysiol 102, 556-567 (2009).

12   MacDonald, C. J., Carrow, S., Place, R. & Eichenbaum, H. Distinct hippocampal time cell sequences represent odor memories in immobilized rats. J Neurosci 33, 14607-14616 (2013).

13   Hattori, S., Chen, L., Weiss, C. & Disterhoft, J. F. Robust hippocampal responsivity during retrieval of consolidated associative memory. Hippocampus 25, 655-669 (2015).

14   Carr, M. F., Jadhav, S. P. & Frank, L. M. Hippocampal replay in the awake state: a potential substrate for memory consolidation and retrieval. Nat Neurosci 14, 147-153 (2011).

15   Pfeiffer, B. E. & Foster, D. J. Hippocampal place-cell sequences depict future paths to remembered goals. Nature 497, 74-79 (2013).

16   Buzsaki, G., Horvath, Z., Urioste, R., Hetke, J. & Wise, K. High-frequency network oscillation in the hippocampus. Science 256, 1025-1027 (1992).

17   Buzsaki, G. Hippocampal sharp wave-ripple: A cognitive biomarker for episodic memory and planning. Hippocampus (2015).

18   Buzsaki, G., Leung, L. W. & Vanderwolf, C. H. Cellular bases of hippocampal EEG in the behaving rat. Brain Res 287, 139-171 (1983).

19   Csicsvari, J., Hirase, H., Mamiya, A. & Buzsaki, G. Ensemble patterns of hippocampal CA3-CA1 neurons during sharp wave-associated population events. Neuron 28, 585-594 (2000).

20   Penttonen, M., Kamondi, A., Sik, A., Acsady, L. & Buzsaki, G. Feed-forward and feed-back activation of the dentate gyrus in vivo during dentate spikes and sharp wave bursts. Hippocampus. 7, 437-450 (1997).

21   Karlsson, M. P. & Frank, L. M. Awake replay of remote experiences in the hippocampus. Nat Neurosci 12, 913-918 (2009).

22   Davidson, T. J., Kloosterman, F. & Wilson, M. A. Hippocampal replay of extended experience. Neuron 63, 497-507 (2009).

23   Gupta, A. S., van der Meer, M. A., Touretzky, D. S. & Redish, A. D. Hippocampal replay is not a simple function of experience. Neuron 65, 695-705 (2010).

24   Lorente de Nó, R. Studies on the structure of the cerebral cortex. II. Continuation of the study of the ammonic system. J. Psychol. Neurol. 46, 113-177 (1934).

25   Kim, S. M. & Frank, L. M. Hippocampal lesions impair rapid learning of a continuous spatial alternation task. PLoS ONE 4, e5494 (2009).

26   McNaughton, B. L., Barnes, C. A. & O'Keefe, J. The contributions of position, direction, and velocity to single unit activity in the hippocampus of freely-moving rats. Exp Brain Res 52, 41-49 (1983).

27   Huxter, J., Burgess, N. & O'Keefe, J. Independent rate and temporal coding in hippocampal pyramidal cells. Nature 425, 828-832 (2003).

28   Zheng, C., Bieri, K. W., Trettel, S. G. & Colgin, L. L. The relationship between gamma frequency and running speed differs for slow and fast gamma rhythms in freely behaving rats. Hippocampus (2015).

29   Mankin, E. A., Diehl, G. W., Sparks, F. T., Leutgeb, S. & Leutgeb, J. K. Hippocampal CA2 activity patterns change over time to a larger extent than between spatial contexts. Neuron 85, 190-201 (2015).

30   Lu, L., Igarashi, K. M., Witter, M. P., Moser, E. I. & Moser, M. B. Topography of Place Maps along the CA3-to-CA2 Axis of the Hippocampus. Neuron 87, 1078-1092 (2015).

31   Lee, H., Wang, C., Deshmukh, S. S. & Knierim, J. J. Neural Population Evidence of Functional Heterogeneity along the CA3 Transverse Axis: Pattern Completion versus Pattern Separation. Neuron 87, 1093-1105 (2015).

32   Mizuseki, K., Sirota, A., Pastalkova, E. & Buzsaki, G. Theta oscillations provide temporal windows for local circuit computation in the entorhinal-hippocampal loop. Neuron 64, 267-280 (2009).

33   Buzsaki, G. Hippocampal sharp waves: their origin and significance. Brain Res 398, 242-252 (1986).

34   Jarosiewicz, B., McNaughton, B. L. & Skaggs, W. E. Hippocampal population activity during the small-amplitude irregular activity state in the rat. J Neurosci 22, 1373-1384 (2002).

35   Vanderwolf, C. H. Hippocampal electrical activity and voluntary movement in the rat. Electroencephalogr Clin Neurophysiol 26, 407-418 (1969).

36   Chevaleyre, V. & Siegelbaum, S. A. Strong CA2 pyramidal neuron synapses define a powerful disynaptic cortico-hippocampal loop. Neuron 66, 560-572 (2010).

37   Kohara, K. *et al.* Cell type-specific genetic and optogenetic tools reveal hippocampal CA2 circuits. Nat Neurosci 17, 269-279 (2014).

38   Hitti, F. L. & Siegelbaum, S. A. The hippocampal CA2 region is essential for social memory. Nature 508, 88-92 (2014).

39   Foster, T. C., Castro, C. A. & McNaughton, B. L. Spatial selectivity of rat hippocampal neurons: dependence on preparedness for movement. Science 244, 1580-1582 (1989).

40   McNaughton, B. L., Battaglia, F. P., Jensen, O., Moser, E. I. & Moser, M. B. Path integration and the neural basis of the 'cognitive map'. Nat Rev Neurosci 7, 663-678 (2006).

41   Buzsaki, G. Theta rhythm of navigation: link between path integration and landmark navigation, episodic and semantic memory. Hippocampus 15, 827-840 (2005).

42   Watrous, A. J. *et al.* A comparative study of human and rat hippocampal low-frequency oscillations during spatial navigation. Hippocampus 23, 656-661 (2013).

43   Jutras, M. J., Fries, P. & Buffalo, E. A. Gamma-band synchronization in the macaque hippocampus and memory formation. J Neurosci 29, 12521-12531 (2009).

44   Ulanovsky, N. & Moss, C. F. Hippocampal cellular and network activity in freely moving echolocating bats. Nat Neurosci 10, 224-233 (2007).

45   Lee, A. K. & Wilson, M. A. Memory of sequential experience in the hippocampus during slow wave sleep. Neuron 36, 1183-1194 (2002).

46   Girardeau, G., Benchenane, K., Wiener, S. I., Buzsaki, G. & Zugaro, M. B. Selective suppression of hippocampal ripples impairs spatial memory. Nat Neurosci 12, 1222-1223 (2009).

47   Ego-Stengel, V. & Wilson, M. A. Disruption of ripple-associated hippocampal activity during rest impairs spatial learning in the rat. Hippocampus 20, 1-10 (2010).

48   Caruana, D. A., Alexander, G. M. & Dudek, S. M. New insights into the regulation of synaptic plasticity from an unexpected place: hippocampal area CA2. Learn Mem 19, 391-400 (2012).

49   Rowland, D. C. *et al.* Transgenically targeted rabies virus demonstrates a major monosynaptic projection from hippocampal area CA2 to medial entorhinal layer II neurons. J Neurosci 33, 14889-14898 (2013).

50   Valero, M. *et al.* Determinants of different deep and superficial CA1 pyramidal cell dynamics during sharp-wave ripples. Nat Neurosci 18, 1281-1290 (2015).

Acknowledgements

Methods

Subjects, neural recordings, and behavioral task. Eight male Long-Evans rats that were 4 to 9 months old (500–600 g) were food deprived to 85% of their baseline weight and pre-trained to run on a 1-m linear track for liquid reward (sweetened evaporated milk). After subjects alternated reliably, they were implanted with microdrives containing 14 (two subjects), 21 (three subjects), or 30 (three subjects) independently movable four-wire electrodes (tetrodes[2,51]) targeting dorsal hippocampus (all rats) and medial entorhinal cortex (one rat), in accordance with University of California San Francisco Institutional Animal Care and Use Committee and US National Institutes of Health guidelines. The minimum number of subjects was established beforehand as four or more, as this is considered to be the minimum necessary to yield data with sufficient statistical power to evaluate the type of effects investigated in this study.

In two subjects, right and left dorsal hippocampus were targeted at AP: -3.7 mm, ML: ±3.7 mm. In one subject, dorsal hippocampus was targeted at AP: -3.6 mm, ML: +2.2 mm, in

addition to medial entorhinal cortex at AP: -9.1, ML: 5.6, at a 10 degree angle in the sagittal plane. Data from these several subjects have been reported in earlier studies[5,31-33]. In five subjects, right dorsal hippocampus was targeted at AP: -3.3 to -4.0 mm, ML: +3.5 to +3.9 mm, moreover, in two of these subjects, the septal pole of right hippocampus was targeted with an additional six tetrodes targeted to AP: -2.3 mm, ML: +1.1 mm. Targeting locations were used to position stainless steel cannulae containing 6, 14, 15, or 21 independently driveable tetrodes. The cannulae were circular except in four cases targeting dorsal hippocampus in which they were elongated into ovals (major axis ~2.5 mm, minor axis ~1.5 mm; two subjects with major axis 45° relative to midline, along the transverse axis of dorsal hippocampus; two subjects with major axis 135° relative to midline, along the longitudinal axis of dorsal hippocampus). Data exclusively from tetrodes targeting right dorsal hippocampus were analyzed in this study.

In five subjects, viral vectors with optogenetic transgenes were targeted to either right dorsal CA2 (three subjects, AAV2/5-CaMKII-hChR2(H134R)-EYFP, UNC Vector Core, 135 nl at AP: -3.6 mm, ML: +4.2 mm, DV: -4.5 mm), dorsal DG (one subject, AAV2/5-I12B[34]-ChR2-GFP, 225 nl at AP: -3.75 mm, ML: +2.2 mm, DV: 3.9 mm and AP: -3.75 mm, ML: +1.8 mm, DV: -4.5 mm), or right supramammilary nucleus (one subject, AAV2/5-hSyn-ChETA-EYFP, Penn Vector Core, 135 nl at AP: -4.3 mm, ML: +1.8 mm, and -8.9 mm along a trajectory angled at 6° in the coronal plane). Viruses were delivered during the implant surgery using a glass micropipette (tip manually cut to ~25 um diameter) attached to an injector (Nanoject, Drummond Scientific). In addition, a driveable optical fiber (62.5/125 µm core/cladding) was integrated in the tetrode microdrive assembly to enable light delivery to hippocampus. This fiber was advanced to its final depth (2.5-3 mm) within 7 days of implantation. Data reported in this study were collected prior to light stimulation. No overt differences in neural activity were observed in subjects that received virus. In particular, CA2 recording sites reporting heterogeneous unit populations (**Extended Data Fig. 3c**) were found in subjects either receiving or free of viral vectors.

Over the course of two weeks following implantation, the tetrodes were advanced to the principal cell layers of CA1 (all subjects), CA2 (5 subjects), CA3 (all subjects), and DG (3 subjects). For DG, tetrodes were advanced to the cell layer using a previously described protocol in which the tetrodes were slowly advanced within DG (~10 µm increments) and unit activity monitored over long periods of rest[52]. DG cell layer was identified by the presence of highly sparsely firing putative principal units. In several subjects, tetrodes were also left in cortex overlying dorsal hippocampus. Neural signals were recorded relative to a reference (REF) tetrode positioned in corpus callosum above right dorsal hippocampus. The REF tetrode reported voltage relative to a ground screw installed in skull overlying cerebellum, and local field potential (LFP) from this tetrode was also recorded. All tetrode final locations were histologically verified (see below).

After 5-7 days of recovery after surgery, subjects were once again food deprived to 85% of their baseline weight, and again pre-trained to run on a linear track for liquid reward. At ~14

days after surgery, six subjects were then introduced to one task W-maze (**Extended Data Fig. 1a**) and recorded for 3 to 6 days before being introduced to a second task W-maze, located in a separate part of the recording room and rotated 90° relative to the first. On recording days in which the second task W-maze was used, recordings were also conducted in the first task W-maze. In two subjects, recordings were conducted in both task W-mazes on every recording day. The W-mazes were 76 x 76 cm with 7-cm-wide track sections. The two task W-mazes were separated by an opaque barrier.

In each W-maze, subjects were rewarded for performing a hippocampus-dependent continuous alternation task[5,13,36] (**Extended Data Fig. 1a**). Liquid reward (sweetened evaporated milk) was dispensed via plastic tubing connected to a hole at the bottom of each of the three reward wells (wells A, B, and C), miniature bowls 3 cm in diameter. In three subjects, reward was dispensed via syringes operated manually by an experimenter who was located in a separate part of the recording room. In five subjects, entry of subjects' head into reward well was sensed by an infrared beam break circuit attached to the well, and reward was automatically delivered by syringe pumps (OEM syringe pumps, Braintree Scientific) either immediately or after an imposed delay lasting from 0.5 to 2 s. In these subjects, digital time stamps corresponding to well entry and reward delivery were recorded and used for illustration in **Fig. 3c**, but were otherwise not used in determining entry times or occupancy of the subjects at the wells for consistency among all subjects. Task epochs lasting 15 minutes were preceded and followed by rest epochs lasting ~20 minutes in a high-walled black box (floor edges 25-35 cm and height 50 cm), during which rats often groomed, quietly waited, and slept. Two subjects also ran in an open field environment for scattered food (grated cheese) after W-maze recordings, with additional interleaved rest epochs. Tetrode positions were adjusted after each day's recordings.

Data were collected using the NSpike data acquisition system (L.M.F. and J. MacArthur, Harvard Instrumentation Design Laboratory). During recording, an infrared diode array with a large and a small cluster of diodes was affixed to headstage preamps to enable tracking of head position and head direction. Following recording, position and direction were reconstructed using a semi-automated analysis of digital video (30 Hz) of the experiment. Spike data were recorded relative to the REF tetrode, sampled at 30 kHz, digitally filtered between 600 Hz and 6 kHz (2-pole Bessel for high- and low-pass), and threshold crossing events were saved to disk. Local field potentials (LFPs) were sampled at 1.5 kHz and digitally filtered between 0.5 Hz and 400 Hz. LFPs analyzed were relative to the REF tetrode except where otherwise indicated.

Individual units (putative single neurons) were identified by clustering spikes using peak amplitude, principal components, and spike width as variables (MatClust, M.P.K.). Only well-isolated neurons with stable spike waveform amplitudes were clustered. A single set of cluster bounds defined in amplitude and width space could often isolate units across an entire recording session. In cases where there was a shift in amplitudes across time, units were clustered only when that shift was coherent across multiple clusters and when plots of amplitude versus time

showed a smooth shift. No units were clustered in which part of the cluster was cut off at spike threshold.

Histology and recording site assignment. After recordings, subjects were anesthetized with isoflurane**,** electrolytically lesioned at each tetrode (30 µA of positive current for 3 s applied to two channels of each tetrode), and allowed to recover overnight. In one subject, no electrolytic lesions were made, and tetrode tracks rather than lesions were used to identify recording sites. Subjects were euthanized with pentobarbital and were perfused intracardially with PBS followed by 4% paraformaldehyde in PBS. The brain was post-fixed *in situ* overnight, after which the tetrodes were retracted and the brain removed, cryo-protected (30% sucrose in PBS), and embedded in OCT compound. Coronal (7 subjects) and sagittal (1 subject) sections (50 µm) were taken with a cryostat. Sections were either Nissl-stained with cresyl violet or stained with the fluorescent Nissl reagent NeuroTrace Blue (1:200) (Life Technologies, N-21479). In four subjects, the sections were blocked (5% donkey serum in 0.3% Triton-X in TBS, used for all incubations) for 1 hr, incubated with RGS14[24,37] antibody (1:400) (Antibodies Inc., 75-140) overnight, washed, and subsequently incubated with fluorescent secondary antibody (1:400) (Alexa 568, Life Technologies). CA2 recording sites were designated as those in which the electrolytic lesion or end of tetrode track overlapped with the dispersed cytoarchitectural zone characteristic of CA2[24,29-31,53-56]. This strategy was deliberately inclusive to maximize detection of putative CA2 neurons with novel physiological responses (N units, **Fig. 1**, **Extended Data Fig. 3**). It is important to note that CA2 sites defined in this way include recording locations that have been designated in previous studies as "CA3a."

Data Analysis. All analyses were carried out using custom software written in Matlab (Mathworks).

SWR detection. Detection of SWRs was prerequisite for all data analyzed in this study, and was performed only when at least three CA1 cell layer recordings were available. Offline, a multisite average approach was used to detect SWRs[57]. Specifically, LFPs from all available CA1 cell layer tetrodes were filtered between 150–250 Hz, then squared and summed across tetrodes. This sum was smoothed with a Gaussian kernel ($\sigma = 4$ ms) and the square root of the smoothed sum was analyzed. SWRs were detected when the signal exceeded 2 s.d. of the recording epoch mean for at least 15 ms. SWR periods were then defined as the periods, containing the times of threshold crossing, in which the power trace exceeded the mean. SWR onset was defined as the start of a SWR period. Detection of SWRs was performed only when subjects' head speed was <4 cm/s. For SWR-triggered spike raster plots and PSTH plots, a 0.5 s exclusion period was imposed to isolate SWRs occurring only after non-SWR periods; otherwise, analyses of SWRs included all detected SWRs.

Unit inclusion. Two unit sets were analyzed in this study. In the first (task unit set), units included fired at least 100 spikes outside of SWRs in at least one task epoch. In the second set (rest unit set), units included fired at least 100 spikes outside of SWRs in at least one rest epoch,

moreover specifically in awake periods (see below). The rest unit set was established to evaluate spatial representations and network patterns in the rest environment. For both unit sets, all included units were required to have available data for least 300 (typically >1000) concurrently detected SWRs in either task or rest epochs. Since relatively less is understood about hippocampal neurons in CA2, units recorded at CA2 in the rest unit set were included in the study only if they met the task unit set criterion to ensure that neurons engaged during active behavior were evaluated. All unit population findings in this study refer to the task unit set, with the exception of those presented in **Fig. 5f** and **Extended Data Fig. 10**, which refer to the rest unit set.

Principal vs. interneuronal unit classification. For each unit set, scatter plots of firing rate, spike width, and autocorrelation function mean (calculated from 0 to 40 ms; low values indicating burst firing) showed two distinct clusters[18,32,58-61] (example plot of task unit set in **Fig. 1c**). Putative principal units corresponded with the low firing rate (<4 Hz), large spike width, low autocorrelation mean cluster, while putative interneuronal units corresponded to the cluster characterized by high firing rate, small spike width, and high autocorrelation mean. Twenty-one units with ambiguous features were left unclassified. All units in the study were isolated (clustered) and classified prior to STA analysis.

N vs. P unit classification. Periods when head speed was <4 cm/s were segregated into SWR vs. non-SWR periods, and the change in firing rate during SWRs calculated. The period types were then permuted (N = 1000) to obtain a distribution of firing rate differences given the null hypothesis of no association of firing rate with period type. P units were those units showing a difference in firing rate that was >95% of values from the null distribution, either for SWRs of any single task epoch or for rest epoch SWRs. N units were those that showed a failure of significance for SWRs in every task epoch and also for rest epoch SWRs. This approach minimized false positives in the detection of N units. Negatively modulated (inhibited) units were formally identified as a subset of N units (examples in **Fig. 1c, d** and additional observations in **Extended Data Fig. 3b**) showing a firing rate difference during SWRs that was <95% of the values from the null hypothesis distribution for rest epoch SWRs and also for SWRs of at least one task epoch.

A small number of CA1 principal units (11 out of 504) and CA3 principal units (7 out of 289) were classified as N units (N vs. P proportions for the task unit set shown in **Fig. 1e**); these units were excluded from all analyses. After exclusion of N units for CA1 and CA3, total putative principal unit counts in the task unit set were CA1: 478, CA3: 271, CA2 P: 142, CA2 N: 84; in the rest unit set, CA1: 163, CA3: 76, CA2 P: 76, CA2 N: 68. "N units" and "P units" solely refer to the distinct unit populations recorded at CA2 sites, and are equivalent to "CA2 N" and "CA2 P."

Behavioral state. Periods of locomotion were defined as times when head speed was >4 cm/s. Periods of non-SWR immobility were times when head speed was <4 cm/s separated from locomotor periods by 2 s buffer intervals (preceding and following) and excluding SWR periods.

Thus brief interruptions in locomotion did not qualify as formally detected periods of immobility.

Firing rate estimation. For each unit, instantaneous firing rate (IFR) was estimated by convolving the unit's spike train (1-ms bins) with a Gaussian kernel ($\sigma = 250$ ms). Mean firing rates in the task (**Fig. 2c**, **Extended Data Fig. 8b**) were calculated from the task epoch in which the unit had the highest mean firing rate combined with additional task epochs of the same environment (specific W-maze) when available. Mean firing rates in the rest environment (**Fig. 5c**) were calculated from all available rest epochs, and were only calculated for units for which LIA and SIA sleep data were available. Firing rates during SWRs were calculated for SWR periods in either task epochs (**Fig. 2c**, **Extended Data Fig. 8b**) or rest epochs (**Fig. 5c**).

Firing vs. speed correlation. For each unit, the Pearson correlation coefficient (r) was calculated between IFR and the logarithm of head speed[28,62,63] for non-SWR periods. The correlation was calculated from the task epoch in which the unit had the highest mean firing rate combined with additional task epochs of the same W-maze when available. Only units with significant correlations ($p < 0.05$) were analyzed (CA1: 475/477 units, CA2 P: 141/142 units, CA2 N: 83/84 units, CA3: 270/271 units). It is worth noting that the findings relating CA2 N unit firing to speed in the task condition (**Fig. 2**) are not a direct consequence of the N unit classification criteria, which refer strictly to a lack of increased firing during SWRs.

Spatial firing. To quantify spatial coverage, 2D position data (corresponding to subjects' head location) for all subjects was first converted to linear position. Linear position was measured as the distance from the center reward well along the linear arms of the W-shaped task maze. In addition, all linear positions were classified as belonging to one of four possible trajectories of the behavioral task, namely, outbound and inbound trajectories between the center well and each of the two outer wells (diagrammed in **Extended Data Fig. 1a**). The end of each continuous trajectory assignment period corresponded to the separation of the subject's linear position from that of the target well of the given trajectory (>2 cm from well).

No trajectory assignment was performed for periods of data corresponding to three cases: (1) excursions in which in the subject departed and returned to the same well, (2) excursions in which the subject occupied a maze segment that was not part of the three linear segments defining the animal's current trajectory, and (3) times during which the subject's linearized head direction (either forward or backward along the current maze segment) did not match the defined direction of the animal's current trajectory. These unassigned periods represented a minority proportion of the data (33% across all task sessions) and were not included either in spatial plots referencing trajectory (occupancy-normalized firing maps in **Extended Data Fig. 4b**) or in subsequent spatial coverage analysis, which relied on unambiguous trajectory assignment in accordance with known direction- and trajectory-dependence of hippocampal spatial firing[26,64-66]. Less stringent restriction of positional data produced qualitatively equivalent results.

For each unit, an occupancy-normalized firing map was calculated for each of the four

task trajectories. First, total spike counts and occupancy durations were calculated for 2-cm spatial bins on each trajectory. Both the occupancy and spike counts per bin were smoothed with a Gaussian (σ = 4 cm), then spike counts were divided by occupancy to produce the unit's smoothed occupancy-normalized firing map. The peak spatial firing rate was the maximum value in the occupancy-normalized map. A bin counted toward spatial coverage (**Fig. 3b**) if its occupancy-normalized rate was >2 Hz. Spatial coverage was quantified in each unit's highest mean firing rate task epoch. Seven units (CA1: 2 units, CA2 N: 5 units) were not included in spatial coverage quantification because of a failure of subjects to visit one of the maze arms in the units' highest firing rate task epochs. Quantification using additional velocity cutoffs and spatial firing thresholds is shown in **Extended Data Fig. 4a**.

Two-dimensional occupancy-normalized firing maps were constructed with 1-cm (W-maze) or 0.5-cm (rest environment) square bins. For example plots, these maps were smoothed with a symmetric 2D Gaussian (σ = 3 cm for maze; σ = 1.5 cm for rest environment); for nesting position analyses in the rest environment, no smoothing was performed. Data during SWR periods were excluded from all spatial firing plots and analyses.

Well firing. Well periods were defined as times when the subject's linear position matched that of the reward well (<2 cm separation). Well visits were defined as well periods that lasted at least 2 s and were preceded earlier in the recording epoch by a well period at a different well. In instances in which subjects re-visited the well they departed from before visiting another well, a well visit was only registered after an exclusion period of 5 s. Well entry times (designated t = 0 in well raster plots) were defined as the beginning of well visits.

To calculate the well specificity index (WSI) of a unit, the well firing rate at each of the three wells of the task was first determined. Well firing rate was specifically calculated from the intersection of well periods with non-SWR immobility periods (well intersectional time). Next, each of the three well firing rates was divided by the numerical sum of the three well firing rates (normalization) to create a three-category (well A vs. B vs. C) probability distribution of firing activity. This probability distribution was subsequently treated as a circular distribution with a vector whose length corresponded to the probability mass for well A placed at 0°, a vector for well B at 120°, and a vector for well C at 240°. The magnitude of the vector sum (resultant), defined as the WSI, was used as a measure of well-specific firing. The WSI directly reflects specificity of firing: a WSI = 0 corresponds to equal firing at all three wells (completely non-specific), WSI = 0.5 corresponds to firing at two wells, and WSI = 1 corresponds to firing at one well.

The WSI was calculated in a unit's highest mean firing task epoch, and was only calculated when (i) at least 100 spikes were observed during well intersectional time, (ii) at least 5 s of well intersectional time was available for each of the three wells, (iii) the firing rate (during well intersectional time) for at least one well exceeded 0.5 Hz. These minimum activity criteria ensured that the WSI was calculated only for units that were unequivocally active at wells and for which adequate data at each well were available.

Theta analysis. To estimate theta phase, LFP from the REF tetrode (located in corpus callosum overlying right dorsal hippocampus[67]) was filtered at 5-11 Hz. The phase of the Hilbert transform of the filtered REF LFP was then designated as the theta phase[32,67]. For a given unit, theta phase locking analysis was performed for locomotor periods (>4 cm/s) in task epochs, and moreover only when at least 50 spikes where present in these periods.

Spike- and SWR-triggered averaging of LFP (STA and RTA). Spike-triggered averages of LFP (STAs) were calculated for spiking in task epochs, moreover specifically for distinct two period types: locomotion and non-SWR immobility. For a given unit, STAs were calculated only when at least 100 spikes in the period type were observed. In each subject, the recording electrodes for each of four LFP reference regions (REF and CA2, CA3, and DG when available) were kept constant over all recording days. Each LFP recording site either reported principal units for its correspondent region (if CA2, CA3, DG) or was within 60 μm of the depth range at which principal units were detected, as determined from records of tetrode adjustment depths. In cases where the LFP reference region was the same as the region in which the unit was located, the parent electrode of the unit was chosen as the LFP reference.

For each unit for which an STA was calculated, a matched SWR-triggered average of LFP (RTA) was calculated, using the same LFP reference site and averaging across all SWRs detected in the same task recording epochs as the unit. RTAs were calculated by averaging LFP aligned to the time of peak power (designated t = 0) in the multisite ripple band power (power at 150-250 Hz across CA1 sites, see above) for each SWR.

To evaluate the spectral components of the STAs and RTAs, the power spectral density (PSD) of individual unit STAs and RTAs (2-sec LFP traces) was calculated using Welch's method (pwelch, Matlab Signal Processing Toolbox). Spectral analysis is shown for STAs/RTAs of LFP recorded in DG (**Fig. 4d**), as DG LFP showed the largest amplitude low-frequency signals.

N wave firing. To detect unit firing in association with the N wave, unit STAs were analyzed. Specifically, unit STAs were classified into distinct groups using the following procedure. First, non-SWR immobility STAs and RTAs were calculated from LFP filtered at 1-4 Hz. Since the N wave as originally identified (**Fig. 4c**) was largest at DG, then CA3, and then CA2, the STAs were calculated for LFP at DG sites when available, then at CA3 when available, then at CA2. Furthermore, for an LFP recording site to be used to calculate classifiable STAs, the RTA at that site had to be significantly negative at t = 0 (p < 0.001 level, signed-rank). In a small number of cases in which this condition was not satisfied, LFP from the next available region, if available, was used. Thus SWR sharp waves were verified to manifest as negative deflections at recording sites used to calculate STAs.

A unit STA was classified in two specific cases: (1) when the STA at the time of spiking (t = 0) was positive and the nearest local extremum was a maximum (peak), and (2) when the STA at the time of spiking was negative and nearest local extremum was a minimum (trough). A small number of units showing positive troughs or negative peaks were left unclassified (CA1: 10 out of

146 units, CA2 N units: 1 out of 58 units, CA3: 3 out of 137 units, interneurons: 10 out of 63 units, plotted at bottom in **Extended Data Figs. 7b, 7d, 8a**). Units satisfying (1) and (2) are referred to as "positive STA" and "negative STA" unit populations, respectively. Units satisfying (1) were identified as firing in association with the N wave (N wave-coupled).

Sleep state identification. In rest epochs, awake periods were identified as times in which head speed was >4 cm/s in addition to times <4 cm/s within 7 s of a previous movement >4 cm/s. Thus, given the behavioral state criteria (see above), for each distinct period in which a subject stopped moving, no more than 5 seconds were included as awake immobility.

Candidate sleep periods were identified as times <4 cm/s preceded by 60 s with no movement >4 cm/s. REM periods within candidate sleep times were identified following an established procedure[68]. Specifically, the ratio of Hilbert amplitudes (smoothed with a Gaussian kernel, $\sigma = 1$ s) of theta (5-11 Hz) to delta (1-4 Hz) filtered LFP was calculated for all available CA1 tetrodes (referenced to cerebellar ground), and the mean taken over tetrodes. For each rest epoch, a threshold (range: 1.2-1.8) was manually set to capture sustained periods (10 s minimum duration) in which the theta:delta ratio was elevated. LFP and position data from each detected REM period were visually inspected.

For a given day's set of candidate sleep times outside of REM periods, LFP from each available CA1, CA3, and DG recording site was squared then smoothed with a Gaussian kernel ($\sigma = 300$ ms). The square root of the smoothed signal was then z-scored and summed across sites. The sum trace was in turn z-scored to obtain an aggregate hippocampal LFP amplitude. For each rest epoch, the distribution of aggregate LFP amplitudes was plotted (example trace and distribution in **Fig. 5a**). From a rest epoch in which bimodality was observed, the value at the local minimum separating the two modes was chosen as the SIA z-score threshold for the day. SIA periods were defined as non-REM times in which the aggregate LFP amplitude was below the threshold, and LIA otherwise. In a minority of cases, a threshold was chosen to isolate a heavy left tail of the distribution, later verified in the LFP to correspond to SIA periods. SIA thresholds across all recording days (n = 73 days) were -0.67 ± 0.24 (z-score, mean ± s.d.), and median period durations were SIA: 1.20 s; LIA: 2.48 s; REM: 27 s. Visual inspection of LFPs confirmed that SIA periods could often be ~1 s in duration[34], indicating rapid switching between distinct sleep states (**Fig. 5a**, **b**). Also, as previously reported[34], slight movements without overt awaking could at times observed during SIA (**Fig. 5b**). Lastly, though SWRs in sleep typically occurred during LIA, SWRs at times occurred within identified SIA periods[34]. Thus, to isolate SIA periods optimally, SWR periods were not included in calculations referencing SIA periods.

Sleep periods were candidate sleep periods at least 90 s in duration and containing extended (>5 s) continuous LIA periods. Across all recording days, 465 sleep periods (median duration: 218 s) were identified.

Nesting position coding. Unit firing rates during SIA were calculated for individual sleep periods. Sleep periods in which a unit's SIA firing rate was >2 Hz were categorized as SIA ON for the unit,

and SIA OFF otherwise. Next, the 2D spatial firing map (non-smoothed, see above) for the unit from awake periods in the same ~20-minute rest epoch was referenced. During awake periods, the total number of spikes and total time spent at positions >5 cm from the subject's head position at the beginning of the sleep period (nesting position) were categorized as Nest OUT, and likewise Nest IN for positions <5 cm. If there were additional sleep periods of a given type (SIA ON or SIA OFF) available for a unit, then the spike counts and durations spent were summed within the Nest OUT/IN categories for the respective nesting positions of the additional sleep periods. Firing rate for a given category (e.g. SIA ON, Nest OUT) was calculated as the total number of spikes divided by the total time.

A unit coding for nesting position is expected to show two firing patterns (dual criteria): if classified as SIA ON in a given sleep period, the unit is expected to show higher firing rates, during awake periods, at positions nearer to the nesting position (Nest IN, <5 cm) corresponding to the sleep period; conversely, if classified as SIA OFF in a given sleep period, the unit is expected to show higher firing rates, during awake periods, at positions farther from the nesting position (Nest OUT, >5 cm) corresponding to the sleep period.

Unit populations were tested for nesting position coding with two approaches. In the first, absolute firing rates were compared between Nest IN vs. OUT periods for both SIA ON and SIA OFF groups[34] (**Extended Data Fig. 10j**). In the second (**Fig. 5f**), firing rates in the Nest IN vs. Nest OUT conditions were compared for each unit by calculating a measure termed the nesting position specificity index, calculated as $2 * fr_{IN} / (fr_{IN} + fr_{OUT}) - 1$. Using this measure, a firing rate in Nest IN that is twice as high as in Nest OUT yields a value of 1/3; three times as high yields a value of 1/2.

For either the absolute firing rate or the specificity index approach, the dual criteria for nesting position coding in a unit population were (1) higher firing during Nest IN vs. Nest OUT for the SIA ON group and (2) higher firing during Nest OUT vs. Nest IN for the SIA OFF group.
Statistics. All statistical tests were two-sided. No statistical methods were used to predetermine sample size.
Code availability. All custom-written code is available upon request.

51   Gray, C. M., Maldonado, P. E., Wilson, M. & McNaughton, B. Tetrodes markedly improve the reliability and yield of multiple single- unit isolation from multi-unit recordings in cat striate cortex. J Neurosci Methods 63, 43-54 (1995).

52   Neunuebel, J. P. & Knierim, J. J. Spatial firing correlates of physiologically distinct cell types of the rat dentate gyrus. J Neurosci 32, 3848-3858 (2012).

53   Ishizuka, N., Cowan, W. M. & Amaral, D. G. A quantitative analysis of the dendritic organization of pyramidal cells in the rat hippocampus. J Comp Neurol 362, 17-45 (1995).

54   Woodhams, P. L., Celio, M. R., Ulfig, N. & Witter, M. P. Morphological and functional correlates of borders in the entorhinal cortex and hippocampus. Hippocampus 3, 303-311 (1993).

55   Amaral, D. G. & Lavenex, P. in The Hippocampus Book   (eds P. Andersen *et al.*) 37-114 (Oxford Univ. Press, 2007).

56   Cui, Z., Gerfen, C. R. & Young, W. S., 3rd. Hypothalamic and other connections with dorsal CA2 area of the mouse hippocampus. J Comp Neurol 521, 1844-1866 (2013).

57   Csicsvari, J., Hirase, H., Czurko, A., Mamiya, A. & Buzsaki, G. Fast Network Oscillations in the Hippocampal CA1 Region of the Behaving Rat. J Neurosci 19, RC20 (1999).

58   Ranck, J. B., Jr. Studies on single neurons in dorsal hippocampal formation and septum in unrestrained rats. I. Behavioral correlates and firing repertoires. Exp Neurol 41, 461-531 (1973).

59   Fox, S. E. & Ranck, J. B., Jr. Electrophysiological characteristics of hippocampal complex-spike cells and theta cells. Exp Brain Res 41, 399-410 (1981).

60   Skaggs, W. E. & McNaughton, B. L. Replay of neuronal firing sequences in rat hippocampus during sleep following spatial experience. Science 271, 1870-1873 (1996).

61   Csicsvari, J., Hirase, H., Czurko, A., Mamiya, A. & Buzsaki, G. Oscillatory coupling of hippocampal pyramidal cells and interneurons in the behaving rat. J Neurosci 19, 274-287 (1999).

62   Kemere, C., Carr, M. F., Karlsson, M. P. & Frank, L. M. Rapid and Continuous Modulation of Hippocampal Network State during Exploration of New Places. PLoS One 8, e73114 (2013).

63   Chen, Z., Resnik, E., McFarland, J. M., Sakmann, B. & Mehta, M. R. Speed controls the amplitude and timing of the hippocampal gamma rhythm. PLoS One 6, e21408 (2011).

64   Frank, L. M., Brown, E. N. & Wilson, M. Trajectory encoding in the hippocampus and entorhinal cortex. Neuron 27, 169-178 (2000).

65   Wood, E. R., Dudchenko, P. A., Robitsek, R. J. & Eichenbaum, H. Hippocampal neurons encode information about different types of memory episodes occurring in the same location. Neuron 27, 623-633 (2000).

66   Ito, H. T., Zhang, S. J., Witter, M. P., Moser, E. I. & Moser, M. B. A prefrontal-thalamo-hippocampal circuit for goal-directed spatial navigation. Nature 522, 50-55 (2015).

67   Lubenov, E. V. & Siapas, A. G. Hippocampal theta oscillations are travelling waves. Nature 459, 534-539 (2009).

68   Mizuseki, K., Diba, K., Pastalkova, E. & Buzsaki, G. Hippocampal CA1 pyramidal cells form functionally distinct sublayers. Nat Neurosci 14, 1174-1181 (2011).

69   Jadhav, S. P., Kemere, C., German, P. W. & Frank, L. M. Awake hippocampal sharp-wave ripples support spatial memory. Science 336, 1454-1458 (2012).

70   Lee, S. E. *et al.* RGS14 is a natural suppressor of both synaptic plasticity in CA2 neurons and hippocampal-based learning and memory. Proc Natl Acad Sci U S A 107, 16994-16998 (2010).

71   Suzuki, S. S. & Smith, G. K. Spontaneous EEG spikes in the normal hippocampus. I. Behavioral correlates, laminar profiles and bilateral synchrony. Electroencephalogr Clin Neurophysiol 67, 348-359 (1987).

72   Buzsaki, G. Two-stage model of memory trace formation: a role for "noisy" brain states. Neuroscience 31, 551-570 (1989).

73   Harris, K. D., Hirase, H., Leinekugel, X., Henze, D. A. & Buzsaki, G. Temporal interaction between single spikes and complex spike bursts in hippocampal pyramidal cells. Neuron 32, 141-149 (2001).

74   Mizuseki, K., Royer, S., Diba, K. & Buzsaki, G. Activity dynamics and behavioral correlates of CA3 and CA1 hippocampal pyramidal neurons. Hippocampus 22, 1659-1680 (2012).

75   Harvey, C. D., Collman, F., Dombeck, D. A. & Tank, D. W. Intracellular dynamics of hippocampal place cells during virtual navigation. Nature 461, 941-946 (2009).

76   Epsztein, J., Brecht, M. & Lee, A. K. Intracellular determinants of hippocampal CA1 place and silent cell activity in a novel environment. Neuron 70, 109-120 (2011).

77   Grienberger, C., Chen, X. & Konnerth, A. NMDA receptor-dependent multidendrite Ca(2+) spikes required for hippocampal burst firing in vivo. Neuron 81, 1274-1281 (2014).

78   Bittner, K. C. *et al.* Conjunctive input processing drives feature selectivity in hippocampal CA1 neurons. Nat Neurosci 18, 1133-1142 (2015).

79   Klausberger, T. & Somogyi, P. Neuronal diversity and temporal dynamics: the unity of hippocampal circuit operations. Science 321, 53-57 (2008).

80   Diba, K., Amarasingham, A., Mizuseki, K. & Buzsaki, G. Millisecond timescale synchrony among hippocampal neurons. J Neurosci 34, 14984-14994 (2014).

81   Royer, S. *et al.* Control of timing, rate and bursts of hippocampal place cells by dendritic and somatic inhibition. Nat Neurosci 15, 769-775 (2012).

82   Skaggs, W. E., McNaughton, B. L., Gothard, K. & Markus, E. in Advanced in Neural Information Processing Systems   (eds S. Hanson, J. D. Cowan, & C. L. Giles) 1030-1037 (Morgan Kaufmann Publishers, 1993).
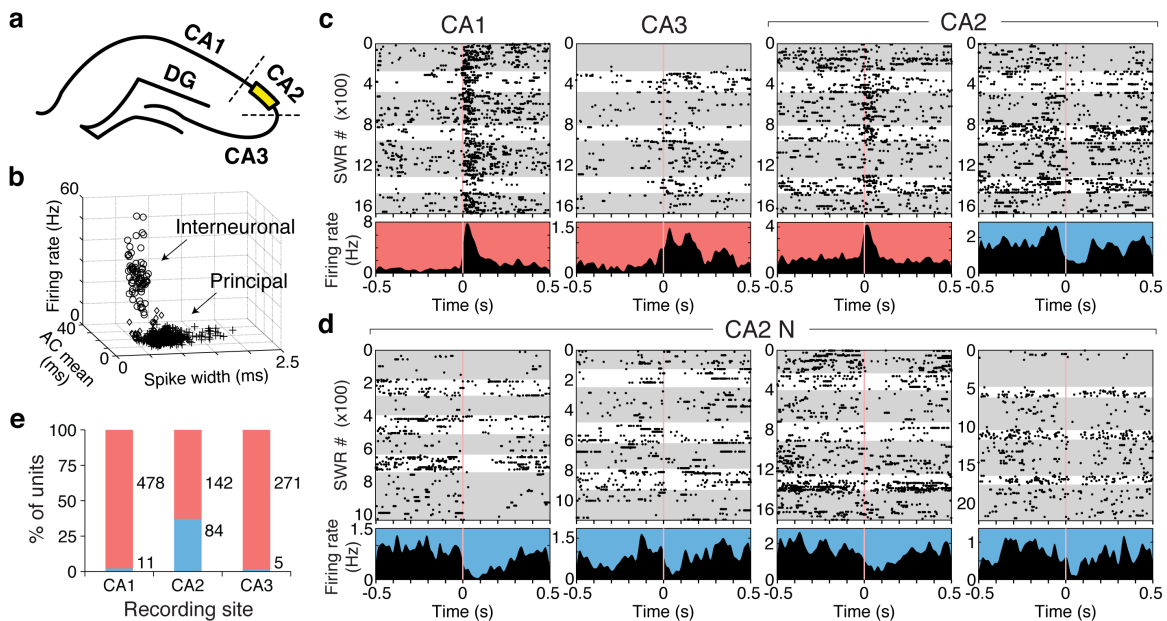
Figure 1

Figure 1 | Distinct hippocampal neuron population at CA2.
a, Diagram of hippocampal recording sites. Recording locations were designated as CA2 sites if found to overlap with the CA2 cytoarchitectural locus[24] (dotted lines). CA2 molecular markers are schematized as a yellow band. Additional description is provided in **Extended Data Fig. 1**.
b, Classification of putative principal vs. interneuronal units. Shown is a scatter plot of all hippocampal neural units in the task data set for the three features used to classify units in this study. AC mean: autocorrelation function mean. Open circles: interneuronal (n = 78); plus symbols: principal (n = 991); open diamonds: unclassified (n = 21).
c, Firing aligned to SWRs (t = 0: time of SWR onset) in four simultaneously recorded hippocampal putative principal units. Upper sections: SWR-triggered spike rasters (black dots). Grey zones demarcate rest epochs; white zones demarcate task epochs. Lower sections: peri-SWR time histogram (PSTH; 1-ms bins) smoothed with a Gaussian kernel (σ = 10 ms). Red background indicates increased firing during SWRs; blue background indicates lack of increase. The CA2 site units were recorded on the same tetrode.
d, Firing aligned to SWRs in four example CA2 N units. Each unit was recorded from a different subject.
e, Percentages of P (red) vs. N (blue) units at CA1, CA2, and CA3 recording sites. Numbers correspond to unit counts.
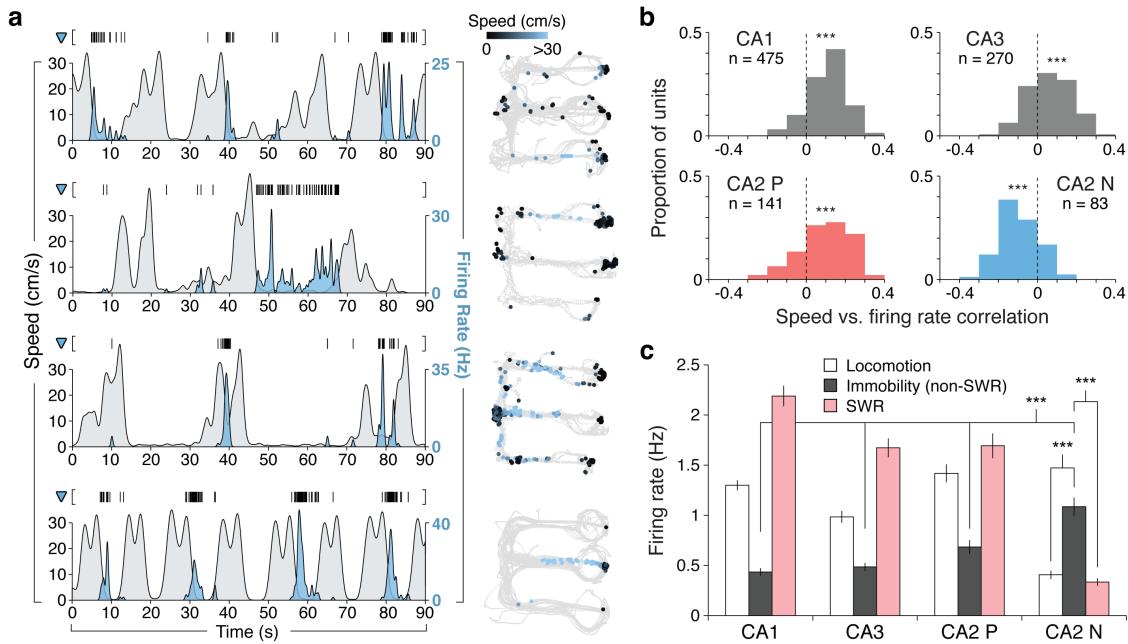
Figure 2

Figure 2 | N units fire more at low speeds and during immobility.
a, Firing of four example CA2 N units during task behavior. Each row corresponds to an N unit, with spike rasters plotted above the traces. Left y-axis and grey fill trace: head speed (cm/s) of the subject. Right y-axis and blue fill trace: instantaneous firing rate (Hz). Right panels: spatial firing maps from corresponding task epochs. Grey: positions visited; colored points (darker color values at lower speeds): positions at which firing occurred, with each point opaque and plotted chronologically.
b, Distribution of correlations (Pearson's r) between firing rate and log speed for each hippocampal unit population. Asterisks: ***, $p \ll 0.001$ (vs. r = 0).
c, Mean firing rates during task epochs (mean ± s.e.m.; # of units: CA1: 478, CA3: 271, CA2 P: 142, CA2 N: 84). Across unit populations, N units showed the highest firing rates during non-SWR immobility (Kruskal-Wallis ANOVA, Tukey's post hoc tests for CA2 N > each other population, $p < 0.001$). Moreover, N unit firing was higher during non-SWR immobility than during locomotion ($p < 10^{-10}$, signed-rank) and also SWRs ($p < 10^{-12}$, signed-rank). Asterisks: ***, $p < 0.001$ or $p \ll 0.001$.
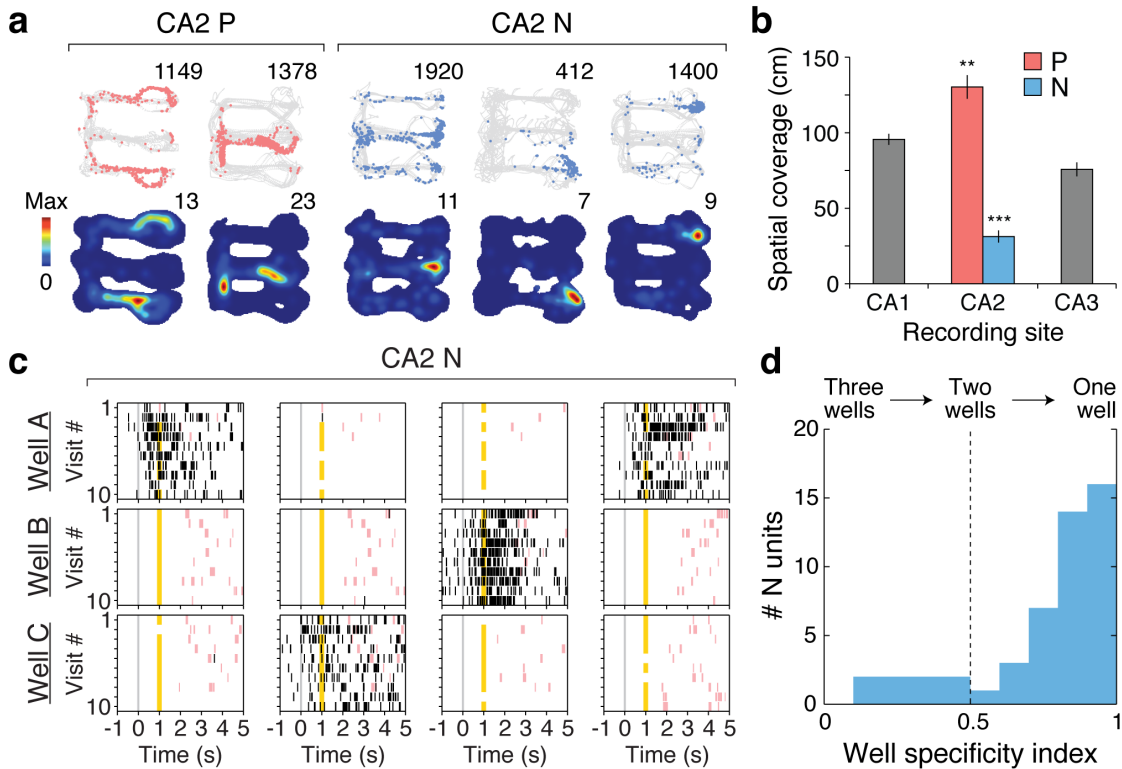
Figure 3

Figure 3 | N units signal current location during immobility.
a, Spatial firing maps of five example CA2 site units. Each column corresponds to a unit. Upper row: positions visited (grey) and positions where the unit fired (colored points: P units in red, N units in blue). Total number of spikes is reported at upper right. Lower row: occupancy-normalized firing maps. Peak spatial firing rate is reported at upper right. Subjects stopped locomoting at the ends of the maze arms to receive reward and also stopped intermittently elsewhere in the maze (**Extended Data Fig. 1a**).
b, Spatial coverage in the hippocampal unit populations (mean ± s.e.m.; # of units: CA1: 476, CA2 P: 142, CA2 N: 79, CA3: 271). The CA2 N and P unit populations showed the lowest and highest spatial coverages, respectively (Kruskal-Wallis ANOVA, Tukey's post hoc tests, CA2 P > each other population, p = 0.0015; CA2 N < each other population, $p < 10^{-6}$). Asterisks: **, $p < 0.01$; ***, $p \ll 0.001$.
c, Reward well firing of four example CA2 N units. Each column corresponds to a unit. For each well, the last ten visits (in a task recording epoch) are shown. Grey line: time of well entry (t = 0); yellow line: time of reward delivery (omitted in error trials). SWR periods are shown as pink zones. The two leftmost units were recorded simultaneously and on the same tetrode.
d, Well specificity distribution in the N unit population. Mean ± s.e.m.: 0.78 ± 0.03 (n = 53 units).
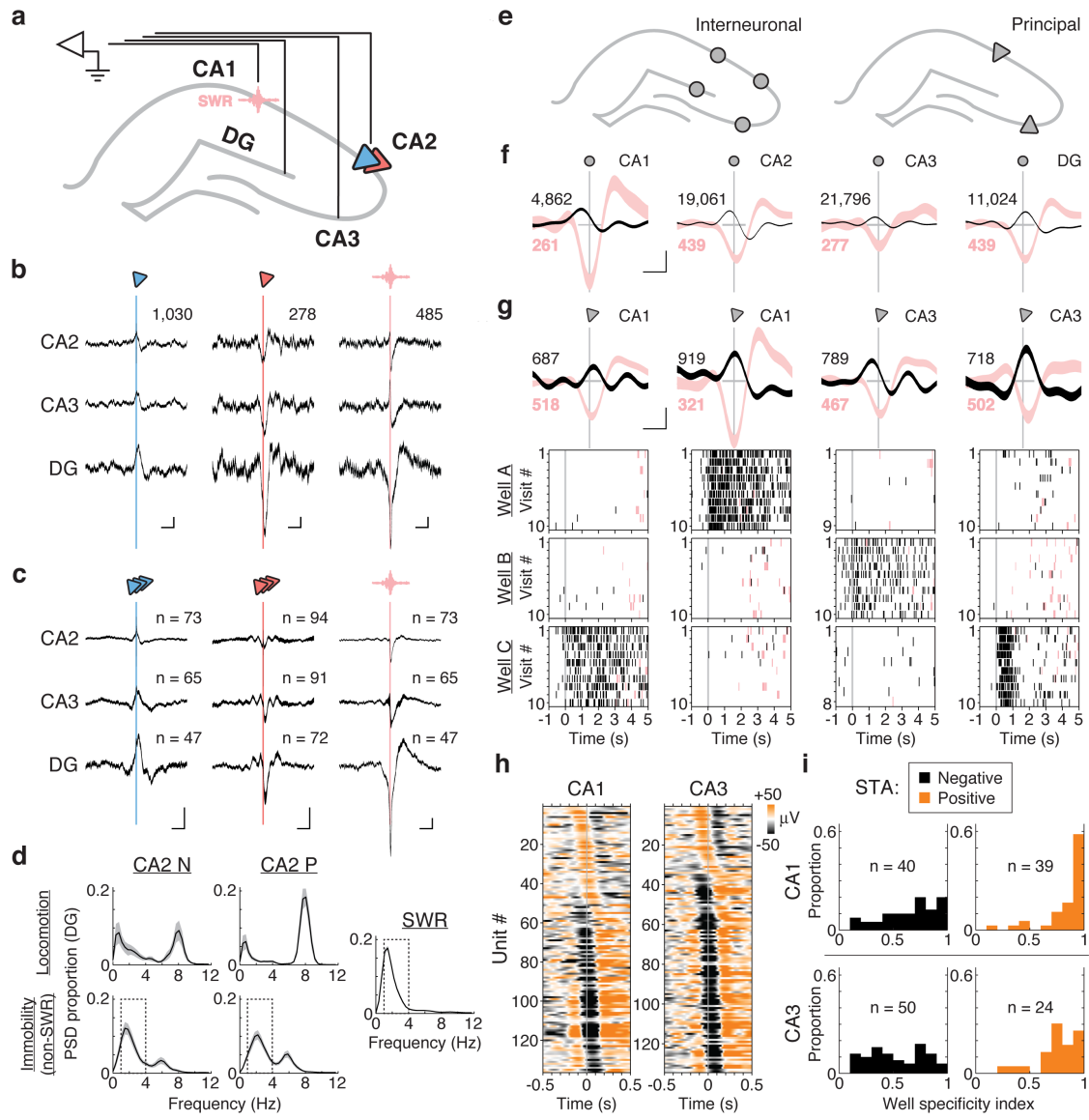
Figure 4

Figure 4 I A novel hippocampal network pattern marks spatial coding during immobility.
a, Schematic of recording configuration. SWRs (pink symbol) were detected with CA1 site electrodes, while wide-band LFP was taken from CA2, CA3, and DG site electrodes. Blue and red symbols refer to CA2 N and CA2 P units, respectively, analyzed in **b-d**.
b, Example CA2 N (blue symbol, first column) and CA2 P (red symbol, second column) unit spike-triggered average (STA) and SWR-triggered average (RTA; pink symbol, third column) of hippocampal CA2, CA3, and DG LFP from non-SWR immobility periods. Vertical lines indicate the time of spiking (STA) or time of SWR (RTA). The two units were recorded simultaneously and on the same tetrode. SWRs averaged in the RTA were detected in the same recording epochs as the units. The total number of events averaged is reported at upper right. Trace width indicates ± s.e.m. over single LFP traces. Trace length: 2 s. Scale bars: x: 250 ms, y: 100 µV.
c, Mean STAs for CA2 N and CA2 P unit populations for non-SWR immobility periods. The mean RTA was calculated from single RTAs matching the recording epochs of N unit STAs, and thus have the same sample size. Trace width indicates ± s.e.m. over unit STAs/RTAs. Trace length: 2 s. Scale bars: x: 250 ms, y: 100 µV.
d, Power spectral density (PSD) of STAs and RTAs of DG LFP. The mean PSD is plotted as a black line, with ± s.e.m. over single averages plotted in grey (locomotor periods: CA2 N, n = 39 units; CA2 P, n = 85; non-SWR immobility periods: CA2 N, n = 47; CA2 P, n = 72; RTAs matched to CA2 N units: n = 47).
e, Schematic of additional hippocampal neurons analyzed with STAs. Interneuronal units (left, grey circles) recorded in the principal cell layers of CA1, CA2, CA3 and DG analyzed in **f** and **Extended Data Fig. 7d-g**. Principal units (right, grey triangles) recorded in CA1 and CA3 analyzed in **g-i** and **Extended Data Figs. 8** and **9**. STAs in **f-i** were taken for 1-4 Hz LFP, analyzing spikes from non-SWR immobility periods.
f, N wave firing in four example interneuronal units. Plotted are unit STAs and RTAs. Trace width indicates ± s.e.m. (STA) or ± 2 s.e.m. (RTA) over single LFP traces. Vertical line: time of spiking (STAs) or SWRs (RTAs). The hippocampal region in which the unit was recorded is reported at upper right. The number of spikes or SWRs averaged is indicated at upper and lower left, respectively. Trace length: 1 s. Horizontal line (200 ms in length): 0 µV. DG LFP was used in each example except for the CA3 unit, which used CA3 LFP. Scale bars: x: 200 ms, y: 50 µV for STA (black), 100 µV for RTA (pink).
g, N wave firing and well specificity in four example CA1/CA3 principal units. Top: unit STAs and RTAs, following the plotting conventions in **f**. DG LFP was used in each example. Bottom: well firing rasters correspondent with each unit. Grey line: time of well entry (t = 0). SWR periods plotted as pink zones.
h, CA1 and CA3 unit STAs. Color indicates voltage. For each unit, LFP (1-4 Hz) from DG, CA3, or CA2 (in decreasing order of preference) was used. Unit STAs were grouped by polarity at the time of spiking (t = 0) and sorted by the time of the local extremum (peak for positive; trough for negative) nearest the time of spiking. Units with positive voltage peaks at the time of spiking were classified as N wave-coupled.
i, Well specificity distributions for CA1 and CA3 principal unit populations classified by STA. For both CA1 and CA3 populations, units with positive STAs (N wave-coupled) showed higher well specificity than units with negative STAs (mean ± s.e.m.; CA1 pos.: 0.85 ± 0.03; CA1 neg.: 0.65 ± 0.04, CA1 pos. vs. CA1 neg., $p < 10^{-5}$, rank-sum; CA3 pos.: 0.77 ± 0.04; CA3 neg.: 0.53 ± 0.04, CA3 pos. vs. CA3 neg., p < 0.001, rank-sum).
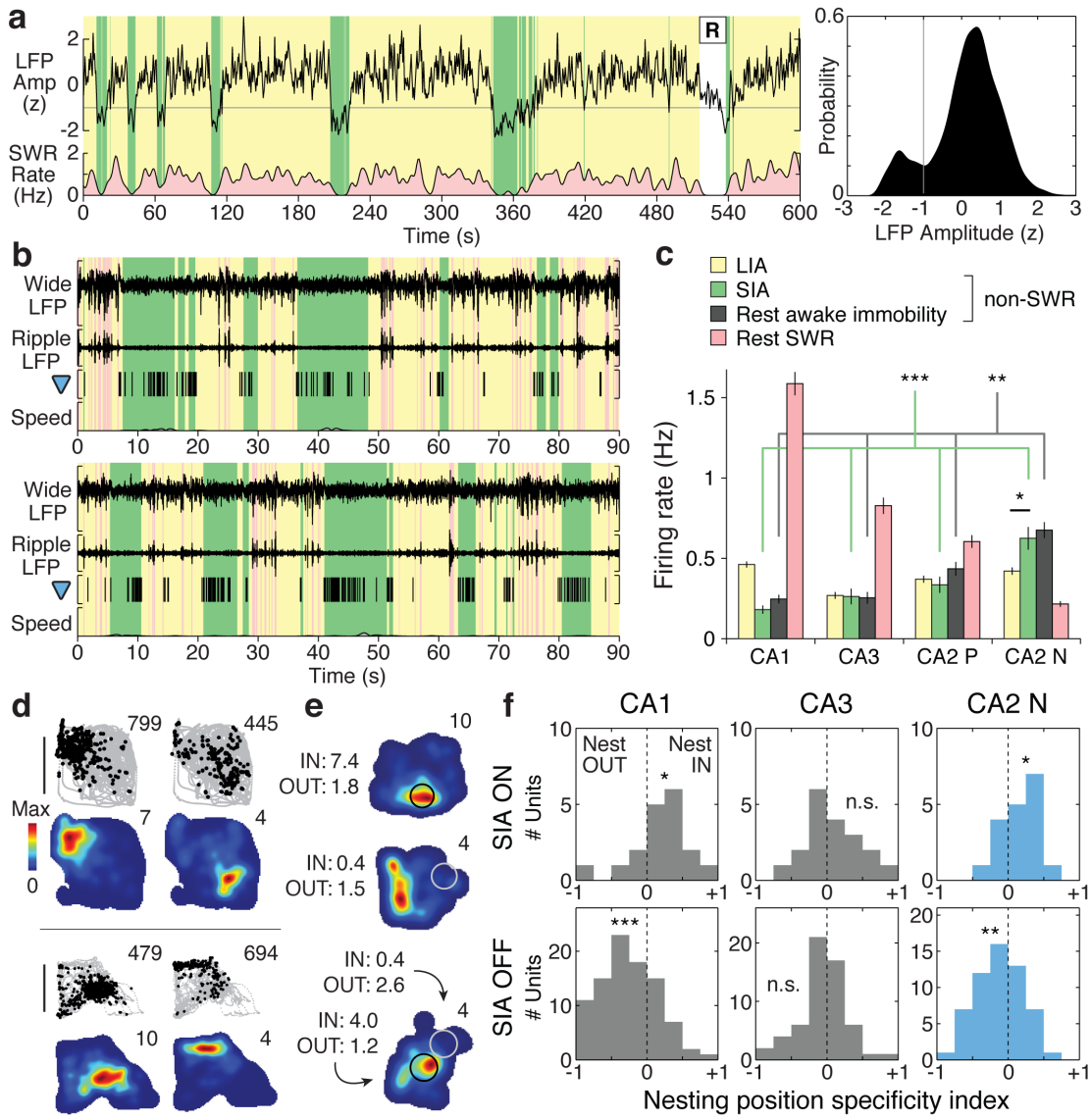
Figure 5

Figure 5 | Hippocampal spatial coding in desynchronized sleep.
a, Detection of sleep states using hippocampal LFP. Left, 10-minute trace of aggregate hippocampal LFP amplitude during sleep, with times classified as LIA (yellow), SIA (green), or REM (R) periods. SWR rate was estimated by counting SWRs in 1-s bins and smoothing with a Gaussian (σ = 2 s). Right, kernel density estimate (Gaussian kernel, σ = 0.1) of aggregate hippocampal LFP amplitude during non-REM sleep for the recording epoch from which the plotted trace was taken. Grey line: amplitude threshold used to distinguish SIA (below threshold) and LIA (above threshold) periods.
b, Sleep firing in two example CA2 N units. Top traces: wide-band LFP (Wide, 0.5-400 Hz, scale bar: 2 mV) and ripple-band LFP (Ripple, 150-250 Hz, scale bar: 300 μV) traces from a simultaneous recording in CA1. SWR, LIA, and SIA periods are plotted as pink, yellow, and green zones, respectively. Grey-filled trace (y-axis: 0 to 10 cm/s): head speed. Subsequent analysis in **d-f** indicated that SIA firing was dependent on whether the location at which the animal slept was near the spatial firing field of the CA2 N unit.
c, Mean firing rates during rest epochs (mean ± s.e.m.; # of units: CA1: 400, CA3: 220, CA2 P: 126 units, CA2 N: 76 units). CA2 N units fired more during SIA than LIA (p = 0.011, signed-rank) and at higher rates than other unit populations during SIA periods (green) and during awake immobility periods (grey) (Kruskal-Wallis ANOVA, Tukey's post hoc tests; $p < 0.001$ for SIA; p = 0.0051 for awake immobility). As in **Fig. 2c**, these comparisons indicate population-level engagement in sleep states, encompassing both higher and lower rate firing as a result of spatially specific firing in single units. Asterisks: *, $p < 0.05$; **, $p < 0.01$; ***, $p < 0.001$.
**d,** Example spatial firing maps of two pairs of simultaneously recorded CA2 N units in the rest environment. Data from waking periods plotted. Upper plots: positions visited (grey) and positions where the unit fired (black points). Total number of spikes is reported at upper right. Lower plots: occupancy-normalized firing maps. Peak spatial firing rate is reported at upper right. Scale bar: 20 cm.
e, Three example CA2 N units coding for nesting position. Shown are occupancy-normalized firing maps from awake periods in a rest recording epoch. Indicated on each map is the nesting position (circle, 5 cm radius) of the subject for a sleep period detected in the same recording epoch. For a given sleep period, the unit was classified either as SIA ON (>2 Hz firing rate during SIA; black circle) or SIA OFF (<2 Hz; white circle). Reported at left are the mean awake firing rates within (Nest IN) and outside (Nest OUT) the encircled nesting region. In the third example, two distinct nesting positions corresponding to two distinct sleep periods were observed.
**f**, Nesting position specificity index distribution in CA1, CA3, and CA2 N unit populations. The CA1 and CA2 N populations met dual criteria (see Supplementary Methods) for nesting position coding, while the CA3 unit population did not. Mean ± s.e.m.: CA1, SIA ON (n = 18 units): 0.18 ± 0.09, p = 0.043; CA1, SIA OFF (n = 92): -0.26 ± 0.04, $p < 10^{-6}$; CA3, SIA ON (n = 19): 0.09 ± 0.09, p = 0.47; CA3, SIA OFF (n = 58): -0.04 ± 0.04, p = 0.50, signed-rank; CA2 N, SIA ON (n = 18): 0.18 ± 0.06, p = 0.020; CA2 N, SIA OFF (n = 57): -0.12 ± 0.04, p = 0.0087. All statistical tests were signed-rank. Asterisks: *, $p < 0.05$; **, $p < 0.01$; ***, $p < 0.001$ or $p \ll 0.001$; n.s., not significant at $p < 0.05$.
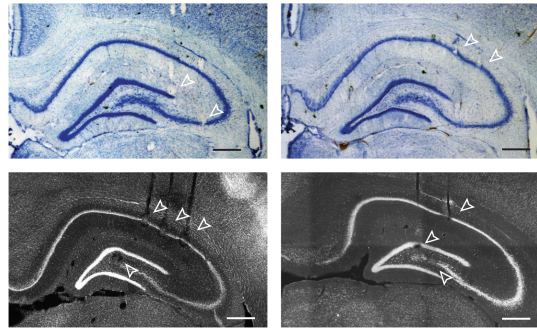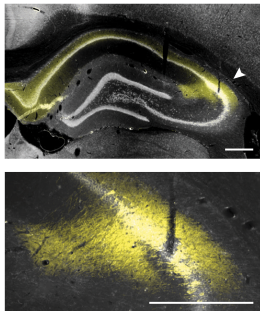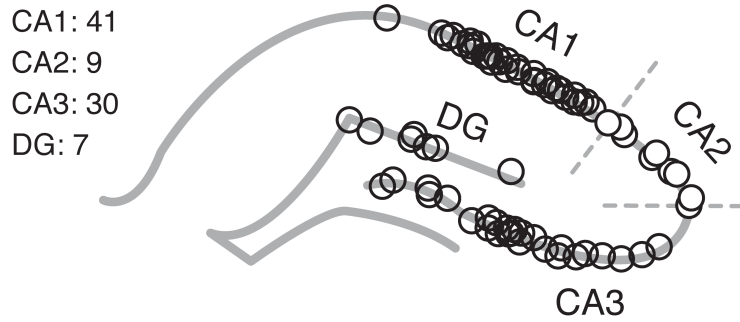
Extended Data Figure 1

a

b

c

d

e

CA1: 41
CA2: 9
CA3: 30
DG: 7
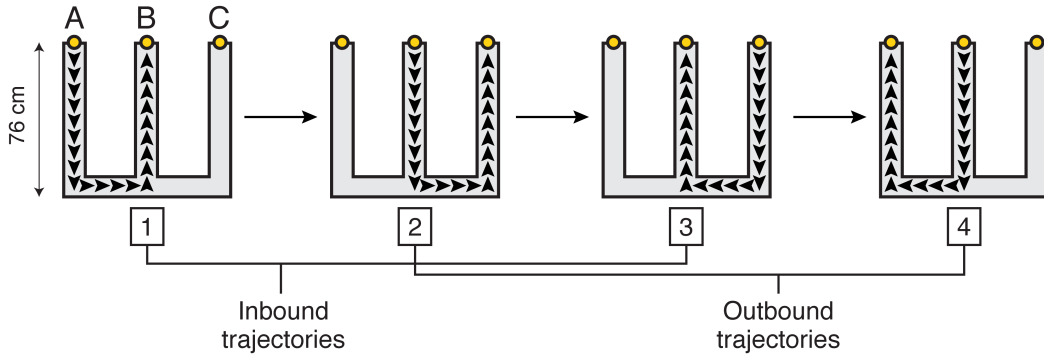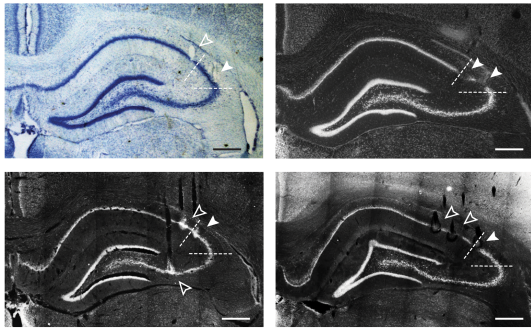
**Extended Data Figure 1 I Behavioral task and hippocampal recording sites.**

a, Continuous spatial alternation task[21,25,64,69]. The task environment is a W-shaped maze with a center arm and two outer arms. Reward (~0.3 mL of sweetened evaporated milk) is dispensed through 3-cm diameter wells (designated "A," "B," and "C" for reference in data plots), located at the end of each arm. Rats are rewarded for performing the trajectory sequence shown, in which the correct destination after visiting the center well is the less recently visited outer well. All subjects stopped locomoting upon reaching the reward wells to check for (by licking) and consume reward. Subjects also stopped intermittently elsewhere on the track (most frequently at maze junctions), particularly in earlier exposures to the task.

b, **c,** Example hippocampal histological sections showing tetrode tracks and electrolytic lesions in CA1, CA2, CA3, and DG. Nissl-stained sections show neuronal cell bodies in dark blue, while sections stained with Neurotrace show neuronal cell bodies in light grey. Panel **b** shows example sections with sites overlapping with the CA2 cytoarchitectural locus[24,29-31,37,53-56] (enclosed by dotted lines; characterized by dispersion of the hippocampal cell layer in the region between CA1 and CA3). Filled arrowheads indicate sites overlapping with CA2, while empty arrowheads indicate non-CA2 recording sites. The CA2 site assignment was deliberately inclusive to maximize detection of units at CA2 with novel physiological responses (N units, **Fig. 1**, **Extended Data Fig. 3**). Scale bars: 500 μm.

d, Coronal hippocampal section stained with a neuronal cell body marker (light grey; NeuroTrace) and CA2 marker (yellow; RGS14[37,48,70]). Bottom, magnified view of a track left by a CA2 site tetrode. Scale bars: 500 μm.

e, Survey of recording sites included in the study data set. Left, diagram of recording site locations in a representative hippocampal section. Shown are recording sites (circles) of seven subjects from which coronal hippocampal sections were taken (CA1: 41 sites, CA2: 9 sites, CA3: 30 sites, DG: 7 sites; two additional CA2 sites near the septal pole of hippocampus not shown). Dotted lines enclose the CA2 anatomical locus, with overlapping recording sites shown as filled circles. The majority of CA1 recordings were in CA1c, while the majority of CA3 recordings were in CA3b.
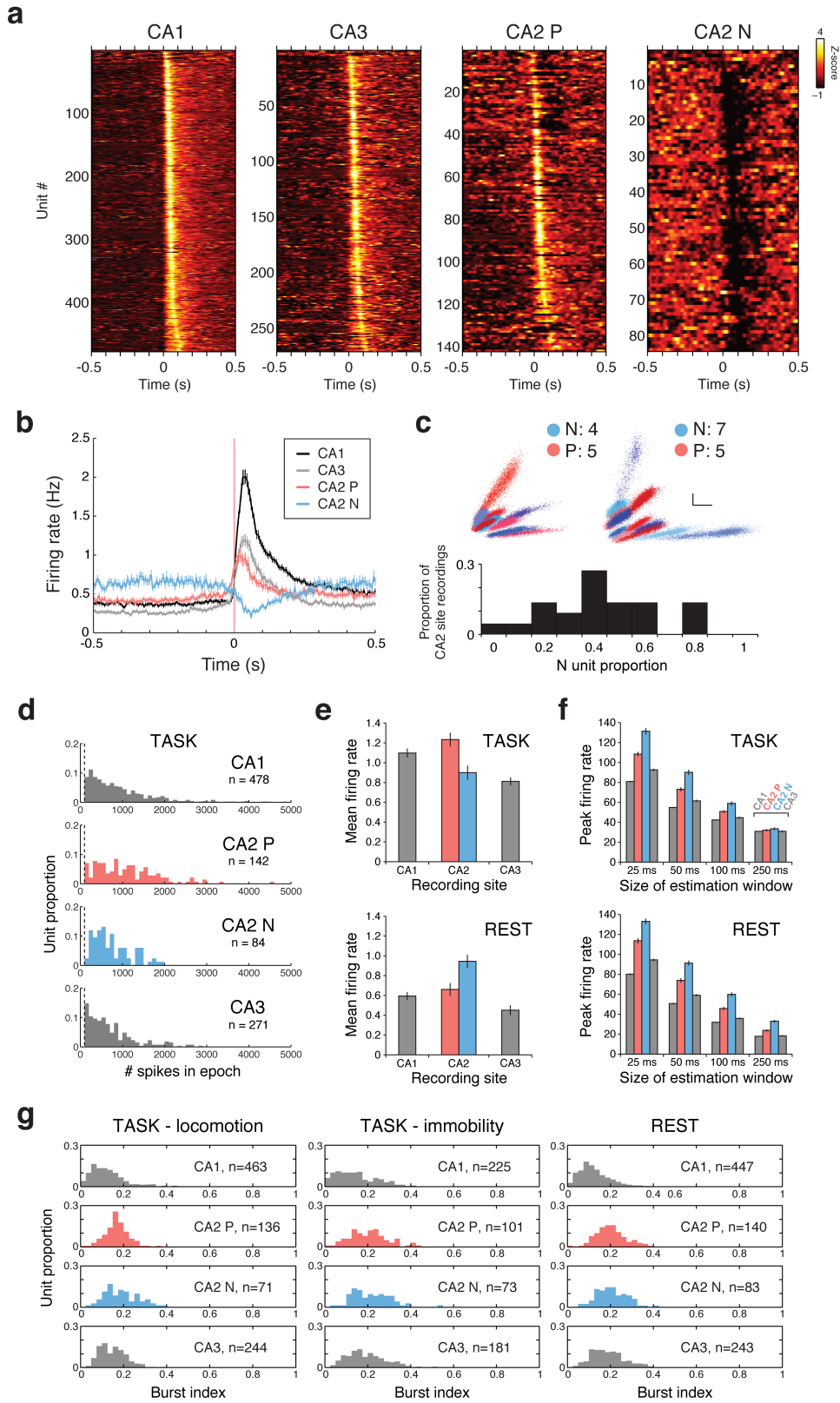
Extended Data Figure 2

a

b
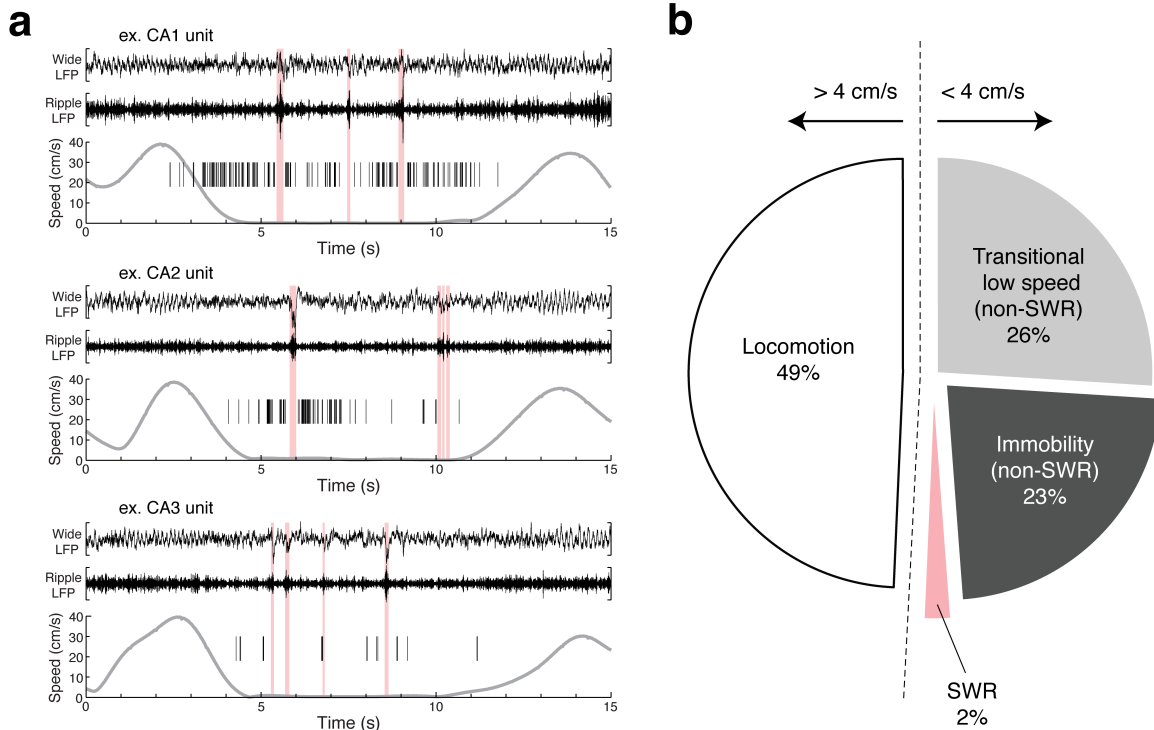
Extended Data Figure 2 | Observation of firing during immobility.
a, Non-SWR immobility firing in three example principal units recorded in CA1, CA2, and CA3. Each firing raster is shown as vertical lines overlaid on a plot of the subject's head speed (grey trace). Top traces: wide-band LFP (0.5-400 Hz, scale bar: 800 μV) and ripple-band LFP (150-250 Hz, scale bar: 100 μV) traces from a simultaneous recording in CA1, to show hippocampal network state. SWR periods are plotted as pink zones. Note that substantial firing occurs in the absence of (i) locomotion, (ii) detectable SWRs, and (iii) detectable theta (regular ~8 Hz rhythm visible in the LFP during moving periods).
b, Proportions of time spent in different period types over all task recording epochs (n = 222 task recording epochs, 8 subjects) in the data set. During the performance of the task, a substantial proportion of time was spent at low speeds and immobility, moreover when SWRs were not detected. Transitional low speed periods were times when the subject's speed was <4 cm/s and within 2 s (earlier or later) of periods of movement >4 cm/s, while immobility periods were times when the speed was <4 cm/s but separated more than 2 s (earlier or later) from periods of movement >4 cm/s. Note that SWR periods comprised only a minority of time spent at low speeds, consistent with past observations[17,71,72].

Extended Data Figure 3

Extended Data Figure 3 | Firing properties of CA1, CA2, and CA3 units.

a, Peri-SWR time histograms (PSTHs; SWR onset at t = 0) of firing for all principal units in the task unit set. SWRs from both task and rest epochs were used to calculate PSTHs (1-ms bins), which were smoothed with a Gaussian kernel (σ = 10 ms). Each unit's mean PSTH was then z-scored (color bar) and plotted in a row. Units are sorted by the time of the maximum z-scored rate from 0 to +100 ms.

b, PSTHs for the four hippocampal unit populations (mean ± s.e.m.; # of units: CA1: 478 units; CA3: 271; CA2 P: 142; CA2 N: 84) analyzed in this study. Using formal criteria (described in Supplementary Methods), units that were inhibited during SWRs constituted a majority subset (56 of 84) of N units, and were observed in every subject with CA2 site recordings (5 subjects, inhibition apparent in examples in **Fig. 1d** and N unit PSTHs in **a**). Here, the reduction of firing in these neurons manifests in the N unit population response as a dip in firing rate at the time of SWRs (N unit population in blue), in contrast to the CA1, CA3, and CA2 P unit populations, all of which showed sharp increases in firing during SWRs[19]. Time bins: 5 ms.

c, Proportion of N units in CA2 site recordings. Upper plots: spike amplitudes measured on two channels of a tetrode for two example CA2 site recordings (left and right). Colors indicate spikes of N (blue-based tones) and P (red-based tones) units. The number of well-isolated principal units of each type is reported at upper right. Scale bars (x and y): 100 µV. Lower plot: proportion of N units across CA2 site recordings with at least four clustered putative principal units. CA2 recording sites typically reported N and P units concurrently, indicating that the spiking of two distinct hippocampal principal cell types was detectable at a single CA2 recording site.

d, Unit spike counts in 15-minute task epochs for each principal unit population. The counts were taken from each unit's highest mean rate task epoch. Spikes that occurred during SWR periods were not included in these counts.

e, Mean firing rate for each principal unit population (mean ± s.e.m). The mean rates were calculated from the highest rate epoch for each unit, either among task (top, TASK) or rest (bottom, REST) epochs. TASK # units (task unit set): CA1: 478 units; CA2 P: 142; CA2 N: 84; CA3: 271. REST # units (subset of task unit set with available rest epoch data): CA1: 454 units; CA2 P: 142; CA2 N: 84; CA3: 252. All spikes and epoch times were included.

f, Peak firing rate for each principal unit population (mean ± s.e.m). The peak rates were estimated from the highest rate epochs for each unit, either among task (top, TASK) or rest (bottom, REST) epochs. The peak rate was the maximum instantaneous firing rate (IFR) exhibited by the unit. Here, the IFR was estimated by convolving each unit's spike train (1-ms bins) with Gaussian kernels of different sizes (x-axis, times refer to s.d. of the kernel). TASK # units (task unit set): CA1: 478 units; CA2 P: 142; CA2 N: 84; CA3: 271. REST # units (subset of task unit set with available rest epoch data and at least 100 spikes in a rest epoch): CA1: 421, CA2 P: 138, CA2 N: 82, CA3: 197 units. All spikes and epoch times were included.

g, Burst firing in each principal unit population. The burst index of a unit was defined as the proportion of inter-spike intervals (ISI) less than 6 ms[73,74]. Burst indices were calculated separately for three conditions: locomotion (left panels) and immobility (center) in task epochs, and also for rest epochs (right). In a given condition, a minimum of 100 spikes was required for a unit to be analyzed. Moreover, for locomotor and immobility periods from task epochs, only ISIs of spikes that were successive within single uninterrupted periods of a given type were included. Lastly, in this analysis, SWR periods were not excluded. Notably, CA2 N units showed high levels of bursting, suggesting that these units correspond to hippocampal principal (pyramidal) neurons[58,59,61,75-78].

Extended Data Figure 4
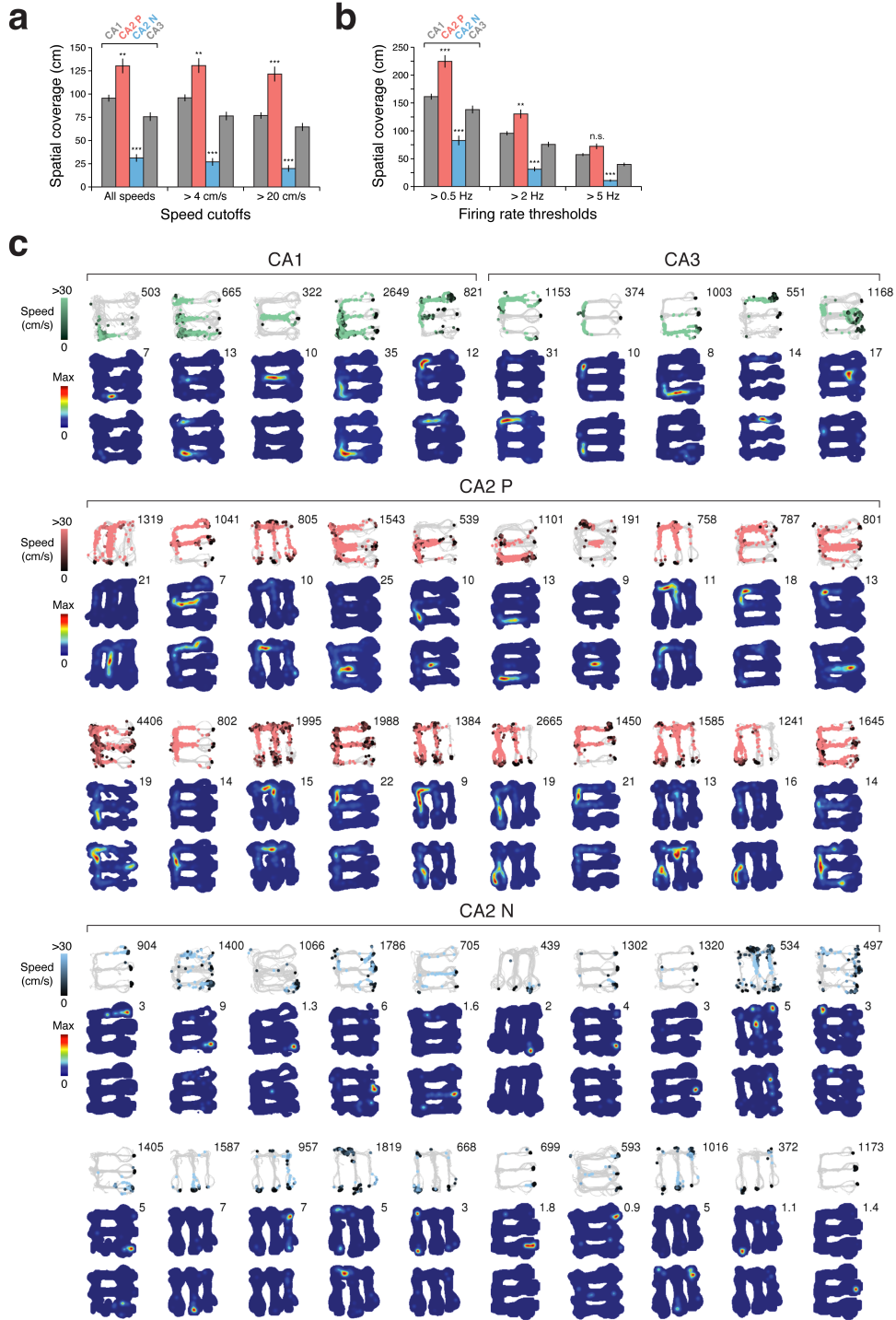
Extended Data Figure 4 | Spatial firing of CA1, CA2, and CA3 units.
For the analyses in **a** and **b**, unit sample sizes are the same as in **Fig. 3b**.
a, Spatial coverage at different speed cutoffs (mean ± s.e.m.), in which only data from periods satisfying the speed condition were analyzed. For each speed cutoff, a firing rate threshold of 2 Hz was used. The all speeds condition is the same as in Fig. 3b. CA2 P > each other unit population, Kruskal-Wallis ANOVA, Tukey's post hoc tests, p = 0.0015 for all speeds, p = 0.0021 for >4 cm/s, and $p < 10^{-5}$ for >20 cm/s. CA2 N < each other unit population, Kruskal-Wallis ANOVA, Tukey's post hoc tests, $p < 10^{-6}$ for all speeds, $p < 10^{-7}$ for >4 cm/s, and $p < 10^{-8}$ for >20 cm/s. Asterisks: **, $p < 0.01$; ***, $p < 0.001$ or $p \ll 0.001$.
b, Spatial coverage at different firing rate thresholds (mean ± s.e.m.). For each threshold level, spikes at all speeds were analyzed. CA2 P > each other unit population, Kruskal-Wallis ANOVA, Tukey's post hoc tests, $p < 10^{-5}$ for >0.5 Hz, p = 0.0015 for >2 Hz, and p = 0.11 for >5 Hz. CA2 N < each other unit population, Kruskal-Wallis ANOVA, Tukey's post hoc tests, $p < 10^{-4}$ for >0.5 Hz, $p < 10^{-6}$ for >2 Hz, and $p < 10^{-7}$ for >5 Hz. Asterisks: **, $p < 0.01$; ***, $p < 0.001$ or $p \ll 0.001$, n.s., not significant at $p < 0.05$.
c, Example spatial firing maps for CA1, CA3, CA2 P, and CA2 N units. Each column corresponds to data from an individual unit from a single 15-minute task epoch. Upper row: raw maps showing positions visited by the subject (grey) and positions where the unit fired (colored opaque points, plotted chronologically and with darker color values at lower speeds). The total number of spikes (outside of SWRs) in the epoch is reported at upper right. Lower two rows: occupancy-normalized firing maps, with the first row showing maps generated from data from outbound trajectories (center to left or right arms) and the second row inbound trajectories (left or right to center arm; **Extended Data Fig. 1a**). The spatial peak firing rate (highest rate for a occupancy-normalized bin) is shown at upper right. Shown are data from each unit's highest mean firing rate task epoch. Data from SWR periods were excluded from all plots. Notably, N units could show substantial firing at locations distinct from the reward wells (N unit examples with spike counts of 534, 497, 957, 1819, 668, 1016, 372).

Extended Data Figure 5

a

b

c Non-reward well positions

d Non-reward well positions &
>2 Hz place bins
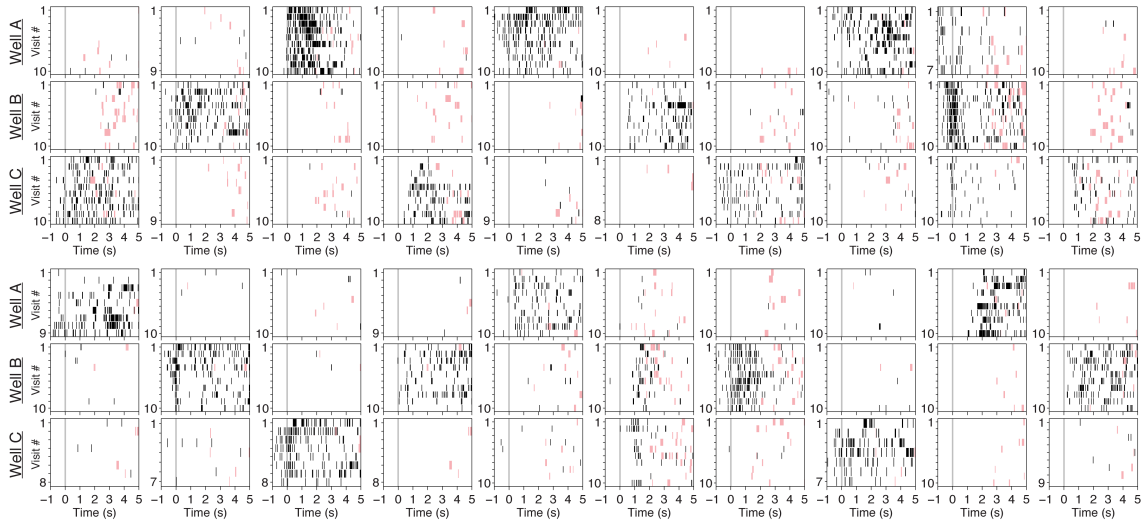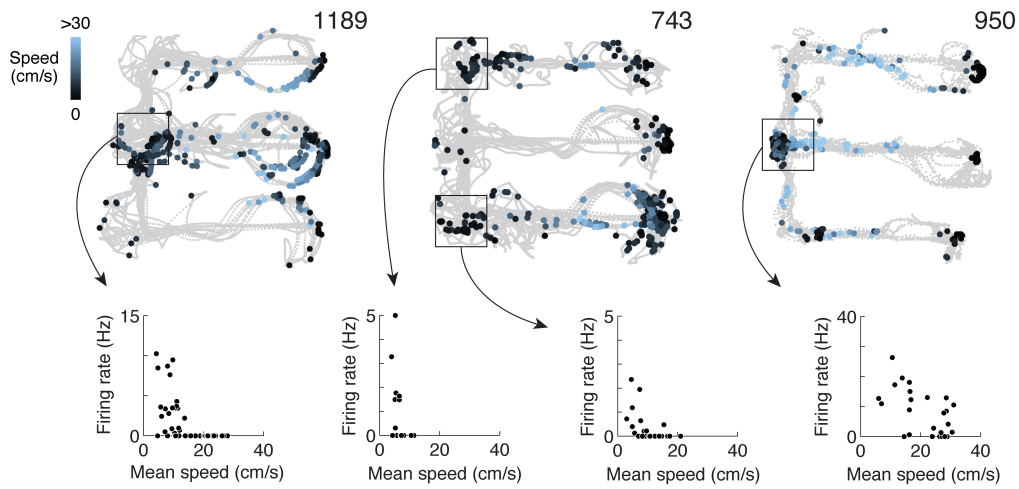
Extended Data Figure 5 | N unit spatial coding.
a, Reward well firing rasters of 20 example N units. For each unit, data from the final ten (if available) entries of the subject's head into each of the three task reward wells (A, B, C) from a single task epoch are shown. The time of well entry (t = 0) is plotted as a grey line. SWR periods are plotted in the background as pink zones. Note that firing for a given N unit was typically specific to one of the three reward wells.
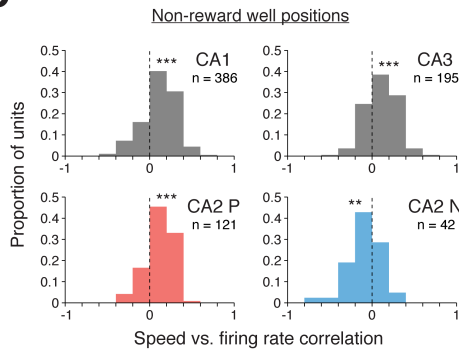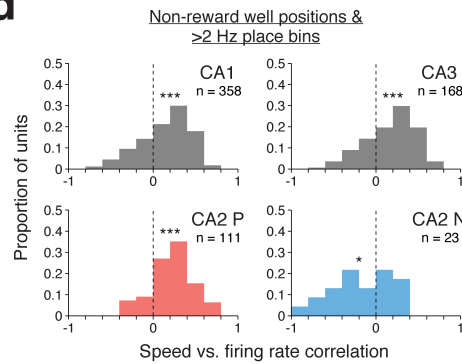**b**, Non-reward well firing in three example N units. The rightmost example is the same as the third example in **Fig. 2a**. Upper row: spatial firing maps. Locations visited by the subject are plotted in grey, while locations at which the unit fired are plotted as colored opaque points (in blue) plotted chronologically and with darker color values at lower speeds. Total spike counts are indicated at upper right. In the task (Supplementary Methods and **Extended Data Fig. 1a**), reward was delivered to the subjects only at the ends of the maze arms, thus locations elsewhere in the maze were not directly associated with reward. Lower row: firing rate vs. speed of distinct visits to specific maze junctions (indicated with a square on spatial firing maps). Junction visits were identified as periods during which the subject's linear position (Supplementary Methods) was within 10 cm of a maze junction. Firing rate was the total number of spikes divided by the visit duration. Mean speed was the average instantaneous head speed during the visit. To limit analysis to discrete traversals through a junction, visits that were both less than 1 s in duration and also had mean speeds <10 cm/s were disregarded. Note that N units tended to fire at lower speed junction visits, and that some junction visits at higher speeds elicited no firing.
c, Firing rate dependence on speed at non-reward task locations. Distribution of correlations (Pearson's r) between firing rate and log speed for each unit population. This analysis is the same as in **Fig. 2b** except restricted to periods when the subject was located >30 cm from reward wells, moreover including only units that fired at least 50 spikes outside of SWRs at these locations. As in the location-inclusive case (**Fig. 2b**), the N unit population uniquely showed an anti-correlation ($r < 0$) of firing rate with speed. Pearson's r, mean ± s.d.; CA1: 0.12 ± 0.20, CA1 vs. 0, $p < 10^{-23}$, signed-rank; CA3: 0.11 ± 0.18, CA3 vs. 0, $p < 10^{-13}$, signed-rank; CA2 P: 0.12 ± 0.16, CA2 P vs. 0, $p < 10^{-10}$, signed-rank; CA2 N: -0.09 ± 0.20, CA2 N vs. 0, $p = 0.0056$, signed-rank; CA2 N vs. CA2 P, $p < 10^{-8}$, rank-sum. Only units with significant correlations ($p < 0.05$) were included (CA1: 386/393 units, CA3: 195/196 units, CA2 P: 121/121 units, CA2 N: 42/42 units). Asterisks: **, $p < 0.01$; ***, $p < 0.001$.
d, Same analysis as **c**, except with an additional restriction to periods when the subject was located in positions where a unit had occupancy-normalized spatial coverage >2 Hz. Pearson's r, mean ± s.d.; CA1: 0.14 ± 0.30, CA1 vs. 0, $p < 10^{-16}$, signed-rank; CA3: 0.17 ± 0.30, CA3 vs. 0, $p < 10^{-10}$, signed-rank; CA2 P: 0.22 ± 0.23, CA2 P vs. 0, $p < 10^{-12}$, signed-rank; CA2 N: -0.17 ± 0.33, CA2 N vs. 0, $p = 0.031$, signed-rank; CA2 N vs. CA2 P, $p < 10^{-6}$, rank-sum. Only units with significant correlations ($p < 0.05$) were included (CA1: 358/364 units, CA3: 168/168 units, CA2 P: 111/111 units, CA2 N: 23/24 units). Asterisks: *, $p < 0.05$; ***, $p < 0.001$.
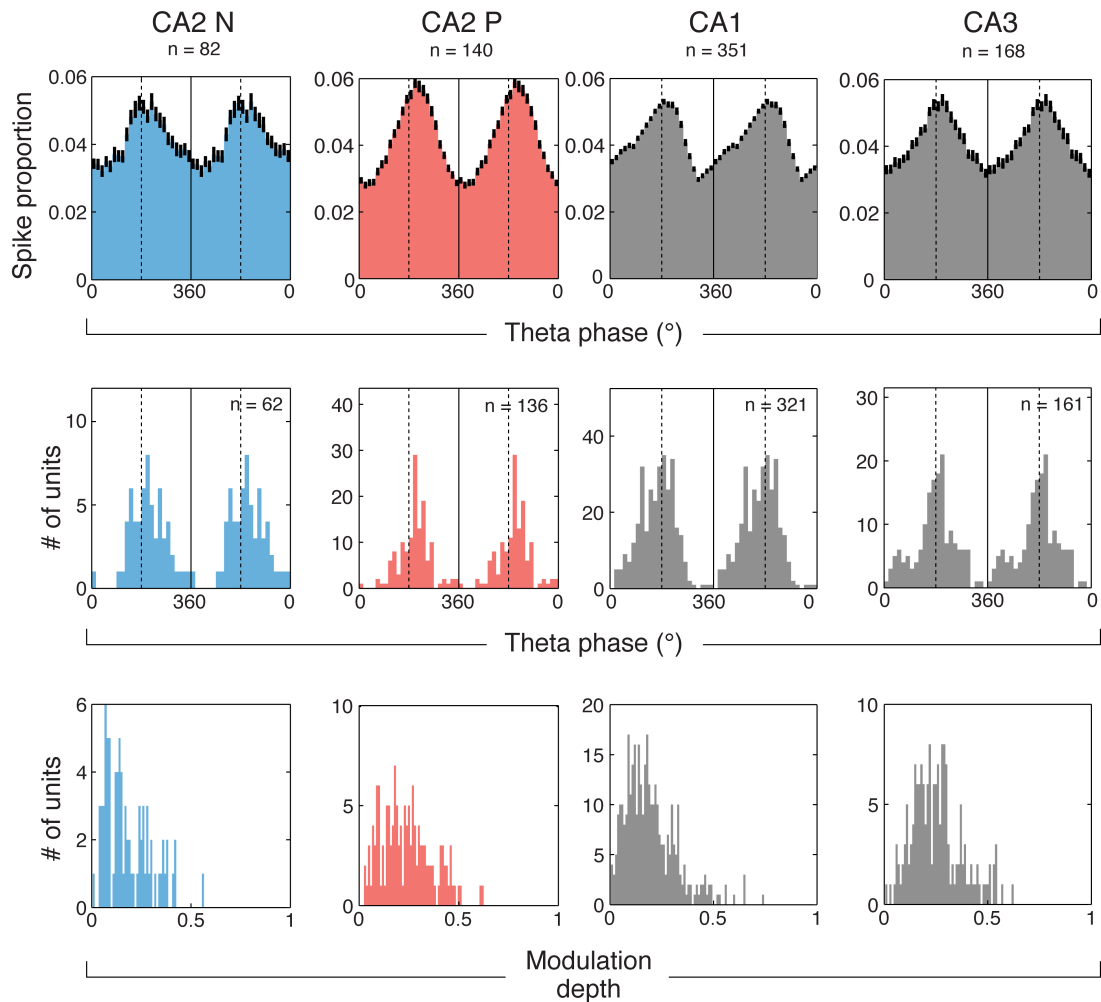
Extended Data Figure 6

a

b
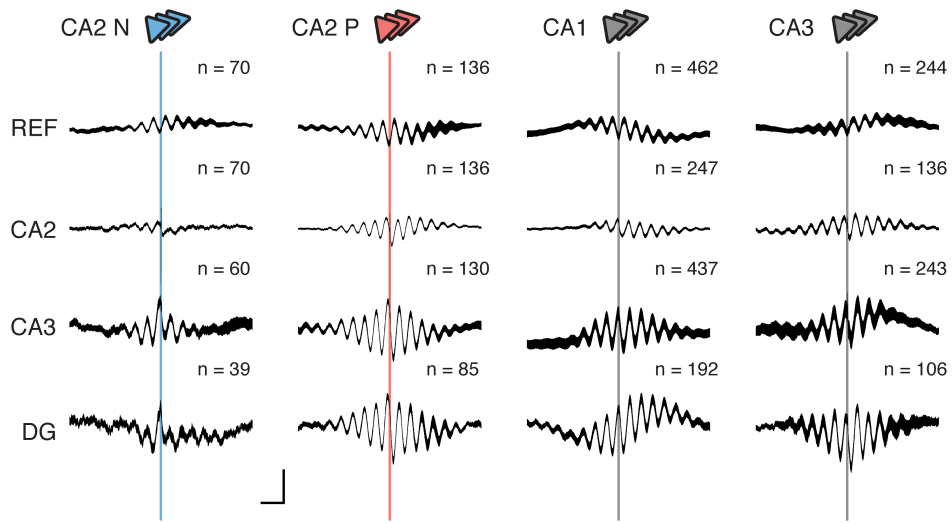
Extended Data Figure 6 | Locomotor STAs and theta analysis.
Unit spiking at speeds >4 cm/s was analyzed.
a, Locomotor STAs. Plotted are mean STAs of hippocampal LFP for each principal unit population. LFP from four distinct recording sites (REF, CA2, CA3, DG) are plotted in rows. Vertical lines correspond to the time of spiking. The width of the trace indicates ± s.e.m. across individual unit STAs. The total trace length is 2 s. REF: reference electrode located in corpus callosum overlying dorsal hippocampus, reporting signals relative to a cerebellar ground screw. Scale bars: x: 250 ms, y: 50 µV.
b, Theta phase locking analysis of each principal unit population. For comparison of theta phase preferences between unit populations in simultaneously recorded data, analysis was restricted to subjects in which all four unit types (CA1, CA3, CA2 N and CA2 P) were recorded. First row: mean circular distribution of spikes for each unit population. Error bars: ± s.e.m. across individual units. Second row: the distribution of mean circular phases for significantly modulated units ($p < 0.05$, Rayleigh tests, total number of significant units reported at upper right). Bottom row: the distribution of modulation depths (resultant length) for all units. In plots with theta phase (bin size: 15°; troughs at 180°, indicated in dotted lines), two cycles are shown to aid visual comparison. Surprisingly, we did not observe a ~90° phase lead of CA3 relative to CA1 as reported in a previous study[32], perhaps due to differences in CA3 recording locations.

Extended Data Figure 7

a

0.5-400 Hz

CA2 N   CA2 P   CA1   CA3   SWR

b

CA2 N STA   RTA

c

d   Interneuronal STA   RTA

e

f

g   Negative STA interneuronal units   Positive STA interneuronal units
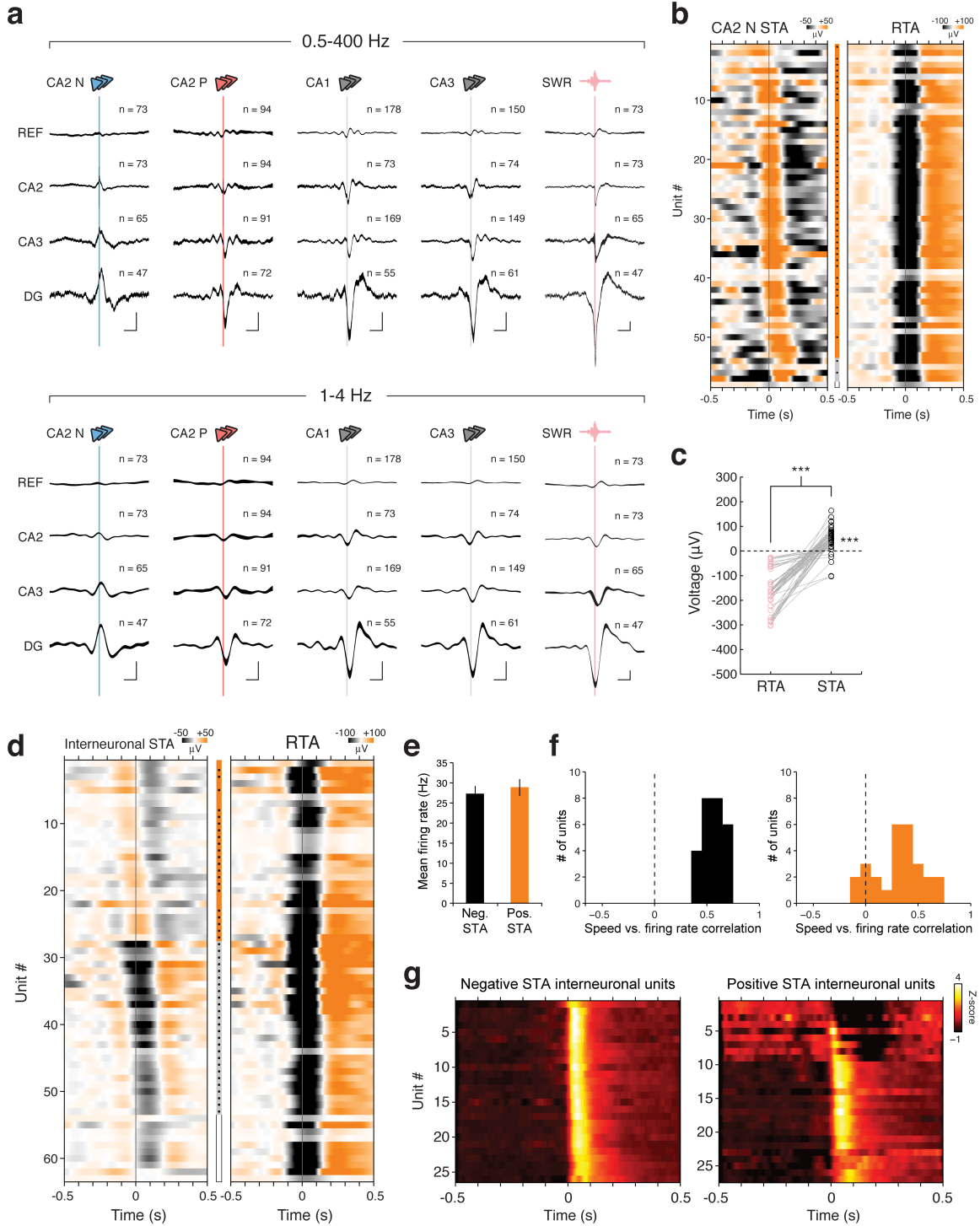
Extended Data Figure 7 | N wave: a novel hippocampal network pattern at 1-4 Hz.
a, Non-SWR immobility STAs of wide-band (0.5-400 Hz, upper section) and low frequency-band (1-4 Hz, lower section) filtered LFP. Plotted are mean STAs of hippocampal LFP for each principal unit population (first four columns). LFP from four distinct recording sites (REF, CA2, CA3, DG) are plotted in rows. The mean RTA (fifth column) was calculated from individual RTAs that were matched (same recording epochs) to each CA2 N unit, and thus have the same sample sizes as N units. Vertical lines correspond to the time of spiking (STAs) or SWRs (RTA). The width of the trace indicates ± s.e.m. over individual unit STAs or RTAs. The total trace length is 2 s. REF: reference electrode located in corpus callosum overlying dorsal hippocampus, reporting signals relative to a cerebellar ground screw. Scale bars: x: 250 ms, y: 50 µV.
b, All CA2 N unit STAs for spiking during non-SWR immobility. Unit STAs are grouped by polarity at the time of spiking (t = 0) and sorted by the time of the extremum (peak for positive; trough for negative) nearest the time of spiking. For each unit, LFP (1-4 Hz) from CA2, CA3, or DG (in increasing order of preference when available) was used. Colors indicate voltage (color bar). STAs are plotted on the left, while RTAs are plotted on the right. The center bar indicates the voltage polarity of the STA (orange: positive, black: negative) at the time of spiking (STAs) or SWRs (RTAs), with a dot indicating significance vs. 0 µV (p < 0.05, rank-sum). The STA of an unclassified unit (see Supplementary Methods) is indicated with an empty box.
c, STA vs. matched RTA voltage amplitudes (1-4 Hz LFP measured at t = 0; STA: time of spike, RTA: time of peak ripple power) for individual CA2 N units (n = 58). CA2 N unit STA amplitudes (black circles) were larger than that of their matched RTAs (pink circles) (mean ± s.e.m., STA: 47 ± 6 µV, RTA: -168 ± 10 µV; $p < 10^{-10}$, signed-rank) and also 0 µV ($p < 10^{-7}$, signed-rank). Asterisks: ***, p << 0.001.
d, All interneuronal unit STAs for spiking during non-SWR immobility periods. Interneuronal units were analyzed for coupling to LFP since hippocampal interneurons show temporally precise firing relationships with all canonical hippocampal network patterns[79]. Seventy-eight putative interneuronal units were recorded in or near the cell layers of CA1, CA2, CA3, and DG; of these units, 63 were recorded when valid CA2, CA3, or DG LFP recordings were simultaneously available and reporting SWR sharp waves as negative transients. Of the 63 units, 27 fired in association with the N wave (criteria in Supplementary Methods; CA1: 10, CA2: 4, CA3: 7, and DG: 6). In the plot, unit STAs are grouped by polarity at the time of spiking (t = 0) and sorted by the time of the extremum (peak for positive; trough for negative) nearest the time of spiking. For each unit, LFP (1-4 Hz) from CA2, CA3, or DG (in increasing order of preference when available) was used. Colors indicate voltage (color bar). STAs are plotted on the left, while RTAs are plotted on the right. The center bar indicates the voltage polarity of the STA (orange: positive, black: negative) at the time of spiking (t = 0), with a dot indicating significance vs. 0 µV (p < 0.05, signed-rank). Unit STAs left unclassified (see Supplementary Methods) are indicated with an empty box.
e, Mean firing rate of interneuronal units (mean ± s.e.m.) with negative (black; n = 36) vs. positive (orange; n = 27) STAs.
f, Firing rate vs. speed correlation (Pearson's r) of interneuronal units with negative (black) vs. positive (orange) STAs. Task epochs were analyzed.
g, Peri-SWR time histograms (PSTHs) of firing for interneuronal units with negative (left) and positive (right) STAs. Negative STA units uniformly exhibited a sharp peak in firing at the time of SWRs while positive STA units showed instances in which unit firing decreased from baseline levels (unit # 1-4, 6, 8) or showed an increase in firing that was less sharp (unit # 23-25)[79-81].

Extended Data Figure 8

a

CA1 / CA3

STA, RTA panels with Unit # on y-axis (10–140 for CA1, 10–130 for CA3), Time (s) from -0.5 to 0.5 on x-axis.

STA: -50 / +50 μV; RTA: -100 / +100 μV

b

Firing rate (Hz), y-axis 0 to 5.

Legend: Locomotion, Immobility (non-SWR), SWR

x-axis: CA1 neg, CA1 pos, CA3 neg, CA3 pos

***

c

Spatial coverage (cm), y-axis 0 to 140.

Legend: Negative STA, Positive STA

x-axis: CA1, CA3

d Significant STA

CA1: n = 29, n = 25
CA3: n = 42, n = 17

Unit proportion (0 to 0.6) vs Well specificity index (0 to 1)

e Theta power cutoff

CA1: n = 25, n = 34
CA3: n = 39, n = 21

Unit proportion (0 to 0.6) vs Well specificity index (0 to 1)

52

Extended Data Figure 8 | CA1 and CA3 principal neurons fire in association with the N wave.

Units showing positive STAs for spiking during non-SWR immobility periods were identified as firing in association with the N wave.

a, All CA1 and CA3 principal unit STAs for spiking during non-SWR immobility periods. Only units with >100 spikes during these periods were analyzed. Unit STAs are grouped by polarity at the time of spiking (t = 0) and sorted by the time of the extremum (peak for positive; trough for negative) nearest the time of spiking. For each unit, LFP (1-4 Hz) from CA2, CA3, or DG (in increasing order of preference when available) was used. Colors indicate voltage (color bar at upper right). STAs are plotted on the left, while RTAs are plotted on the right. The center bar indicates the voltage polarity of the STA (orange: positive, black: negative) at the time of spiking (t = 0), with a dot indicating significance vs. 0 μV (p < 0.05, signed-rank). Unit STAs left unclassified (see Supplementary Methods) are plotted at bottom and indicated with an empty box.
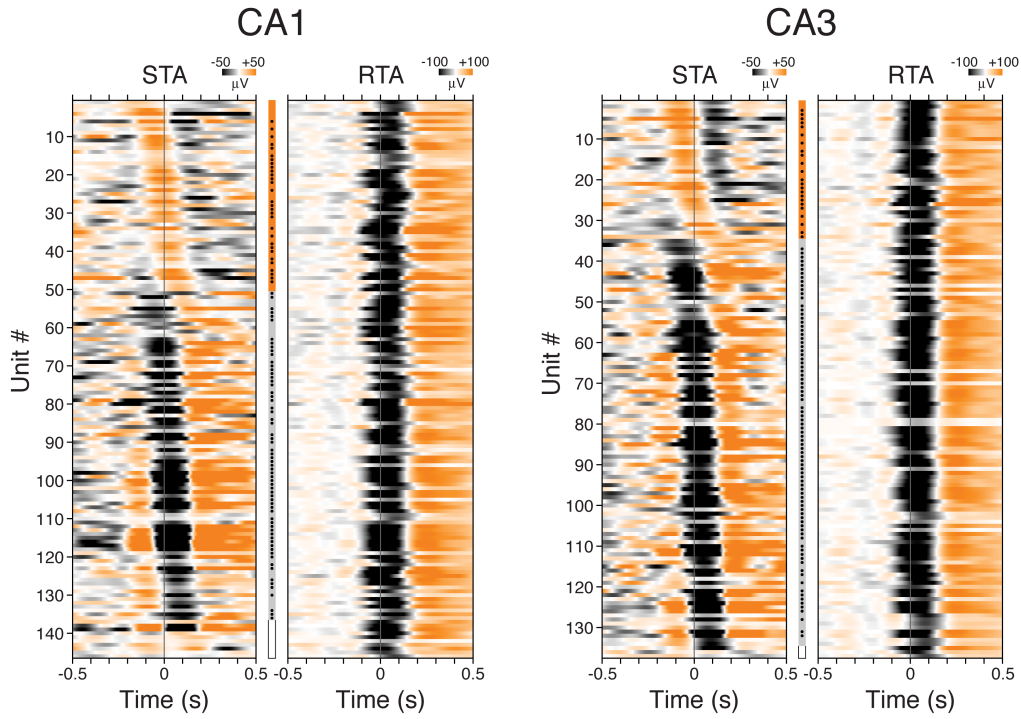
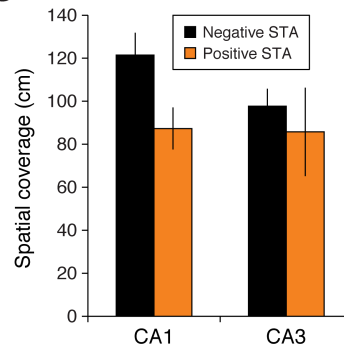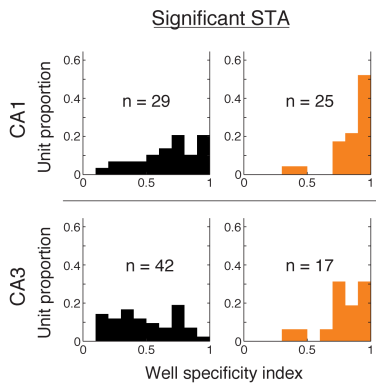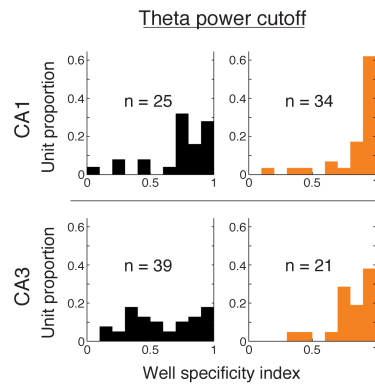**b**, Firing rates for STA-classified unit populations during task epochs (mean ± s.e.m.; # of units: CA1 negative: 86, CA1 positive: 50, CA3 negative: 100, CA3 positive: 34). In both CA1 and CA3, units with positive STAs showed higher firing rates during non-SWR immobility (CA1 positive vs. CA1 negative, $p < 10^{-9}$, rank-sum; CA3 positive vs. CA3 negative, $p < 10^{-5}$, rank-sum), similar to CA2 N units (**Fig. 2c**).

c, Spatial coverage in CA1 and CA3 units with negative vs. positive STAs (mean ± s.e.m.; # of units: CA1 negative: 86, CA1 positive: 50, CA3 negative: 100, CA3 positive: 34). CA1 units with positive STAs showed somewhat lower spatial coverage than units with negative STAs (CA1 negative vs. CA1 positive, p = 0.046, rank-sum), while an analogous difference in CA3 was not statistically significant (CA3 negative vs. CA3 positive, p = 0.12, rank-sum).

d, Well specificity distributions in CA1 and CA3 units that had STA amplitudes (at time of spiking) significantly different from 0 μV (the units marked as significant in **a** and with available well data). For both CA1 and CA3, units with positive STAs showed higher well specificity (mean ± s.e.m., CA1 negative: 0.66 ± 0.04, CA1 positive: 0.86 ± 0.03; CA1 negative vs. CA1 positive, $p < 10^{-4}$, rank-sum; CA3 negative: 0.49 ± 0.04, CA3 positive: 0.79 ± 0.04, CA3 negative vs. CA3 positive, $p < 10^{-4}$, rank-sum).

e, Well specificity distributions in CA1 and CA3 units with theta power cutoff. For each task epoch, the distribution of power in the theta band (5-11 Hz), averaged over CA1 recording sites, was calculated for immobility non-SWR periods. Spikes occurring during times in which the theta band power was in the upper quartile of this distribution were then excluded from well specificity calculations. For both CA1 and CA3, units with positive STAs showed higher well specificity (mean ± s.e.m., CA1 negative: 0.73 ± 0.05, CA1 positive: 0.87 ± 0.04; CA1 positive vs. CA1 negative, p < 0.002, rank-sum; CA3 negative: 0.58 ± 0.04, CA3 positive: 0.80 ± 0.04; CA3 negative vs. CA3 positive, p < 0.004, rank-sum).

Extended Data Figure 9
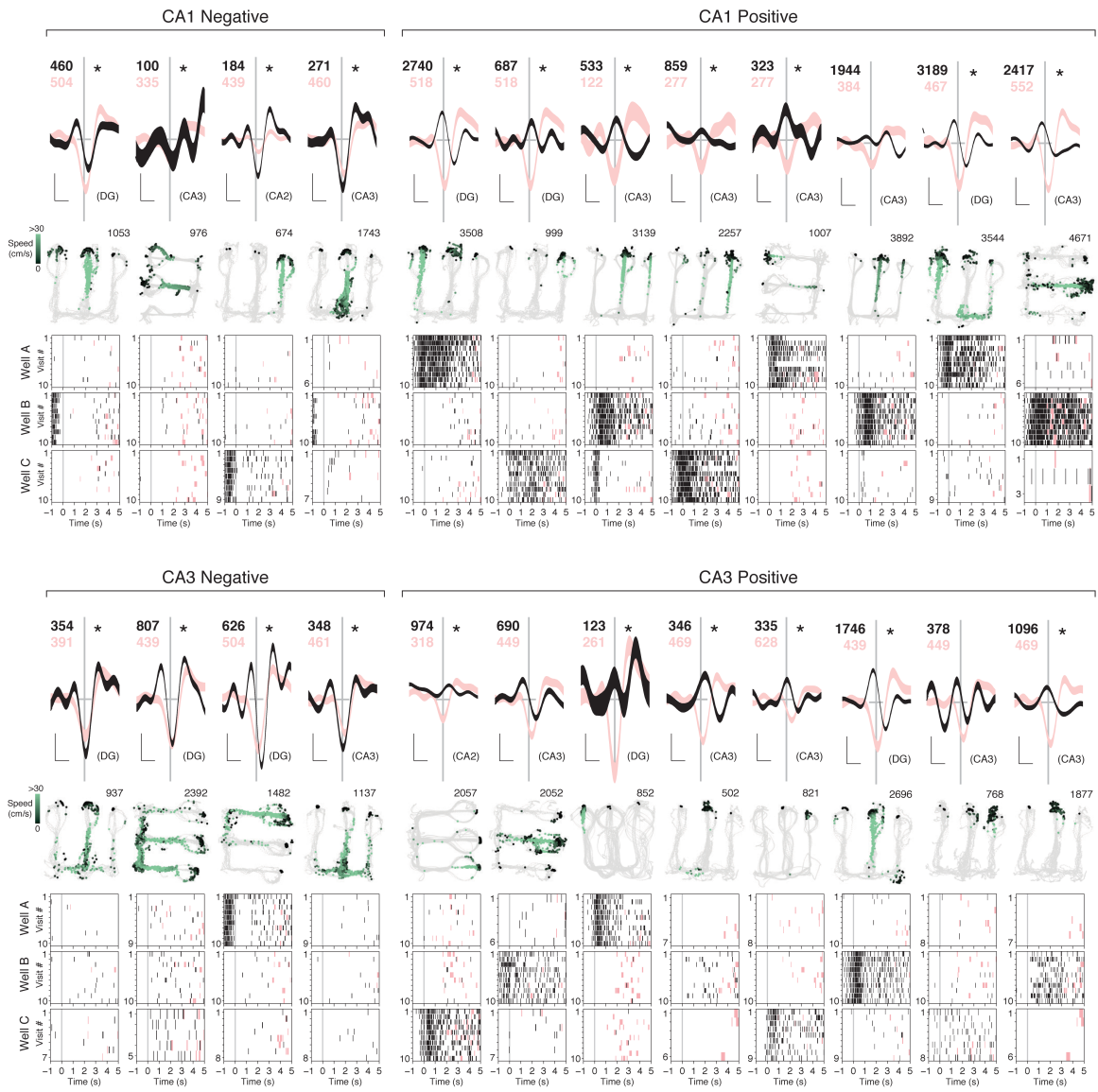
Extended Data Figure 9 | N wave-coupled CA1 and CA3 principal neurons.
Examples of CA1 and CA3 principal units with negative vs. positive STAs during non-SWR immobility. Each column corresponds to data from an individual unit. **Upper sections**: Non-SWR immobility STA (black trace, ± s.e.m. over individual LFP traces) and RTA (pink trace, ± 2 * s.e.m. over individual LFP traces). Vertical lines correspond to the time of spiking (for STAs) or time of SWRs (for RTAs). The total number of spikes (for STAs) and SWRs (for RTAs) averaged is reported at upper left. The region in which the LFP (at 1-4 Hz) was recorded is indicated at lower right. STAs with amplitudes (measured at the time of spiking) significantly different from 0 µV (p < 0.05, rank-sum) are marked by an asterisk at upper right. The total trace length is 1 s. A horizontal bar centered at the time of spiking indicates 0 µV and corresponds to 200 ms. Scale bars: x: 200 ms, y: 50 µV for STA (black trace); 100 µV for RTA (pink trace). **Middle sections**: Spatial firing maps. Positions visited by the subject are plotted in grey while positions at which the unit fired are shown as colored opaque points (in green) plotted chronologically and with darker color values at lower speeds. The total number of spikes in the epoch is reported at upper right. Shown is the 15-minute task epoch in which the unit had the highest mean firing rate. Spikes during SWRs are omitted from all plots. **Lower sections**: Well firing rasters. The time of well entry (t = 0) is plotted as a grey line. SWR periods are plotted in the background as pink zones.

Extended Data Figure 10
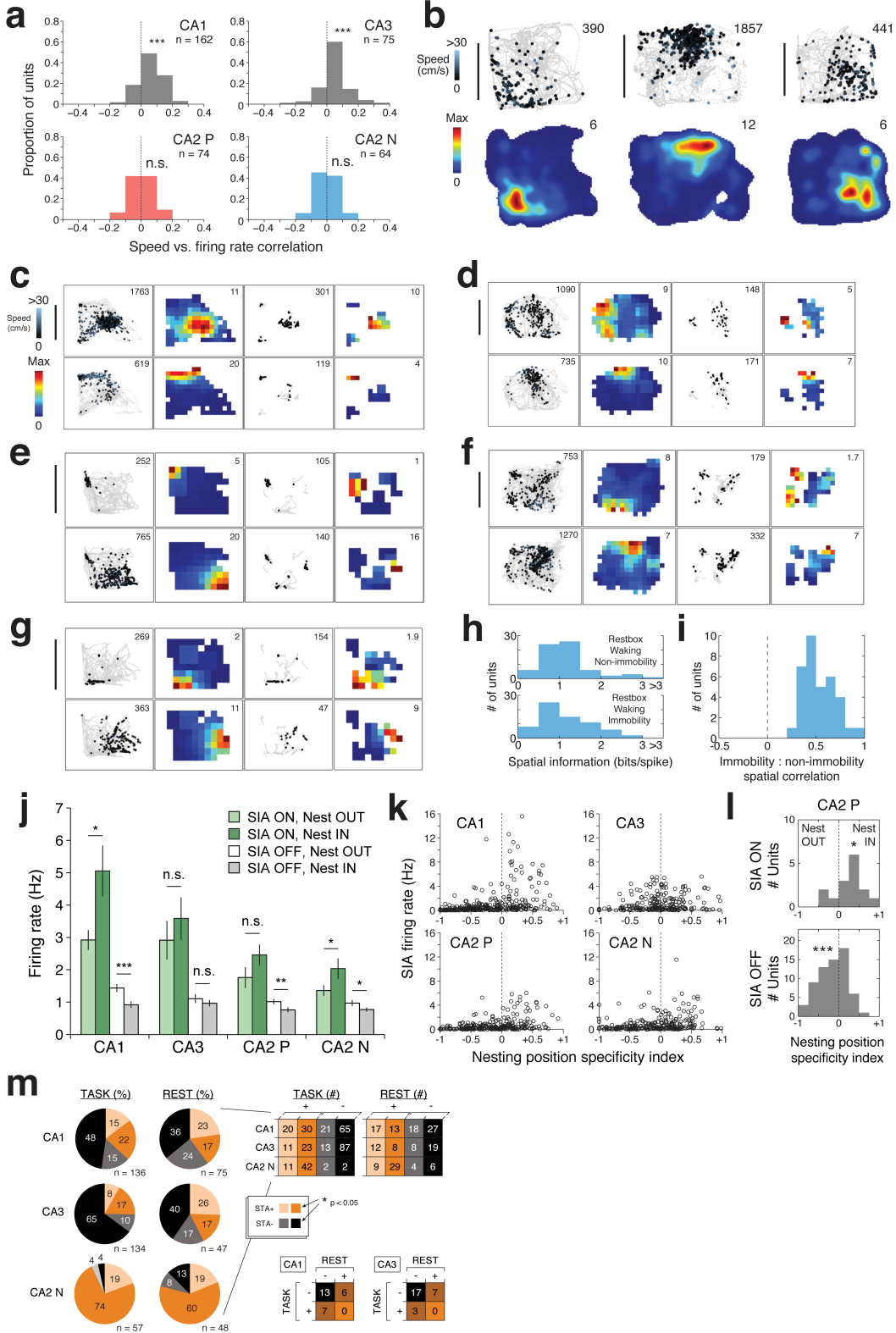
Extended Data Figure 10 | Hippocampal spatial coding in the rest environment.
a, Distribution of correlations (Pearson's r) between firing rate and log speed for each unit population in awake periods in the rest environment. Mean ± s.d.; CA1 (n = 162 units): 0.06 ± 0.07, CA1 vs. 0, $p < 10^{-17}$, signed-rank; CA3 (n = 75): 0.05 ± 0.08, CA3 vs. 0, $p < 10^{-6}$, signed-rank; CA2 P (n = 74): 0.01 ± 0.07, CA2 P vs. 0, p = 0.55, signed-rank; CA2 N (n = 64): 0.00 ± 0.07, CA2 N vs. 0, p = 0.77, signed-rank, CA2 N vs. CA2 P, p = 0.47. Only units with significant correlations (p < 0.05) were included (CA1: 162/163 units, CA3: 75/76, CA2 P: 74/76 units, CA2 N: 64/68 units). The N unit population did not show a significant relationship between firing rate and speed, unlike in the task environment (**Fig. 2b**). The positive correlation between firing rates and speed was also absent in the CA2 P population, suggesting a broader weakening of speed-dependent changes in hippocampal firing in the rest environment. This could be due to the restricted range of speeds in the rest environment enclosure and/or a fundamental influence of task conditions (**Extended Data Fig. 1**) on hippocampal neural activity.
b, Three additional example N unit spatial firing maps in the rest environment. Plotted are data from awake periods. Each column corresponds to data from an individual unit. Upper row: raw maps showing positions visited by the subject (grey) and positions where the unit fired (colored opaque points, plotted chronologically and with darker color values at lower speeds). Total number of spikes (outside of SWRs) in the epoch is reported at upper right. Lower row: occupancy-normalized firing maps. Peak spatial firing rate is reported at upper right. Scale bar: 20 cm.
c-g, Awake immobility spatial firing in five example co-recorded pairs of N units from single rest recording epochs. The example pair in **c** is the same as shown at bottom in **Fig. 5d**. For each example pair, a unit corresponds to a row. The leftmost two columns (raw and occupancy-normalized firing maps) correspond to data from awake periods, while the rightmost two columns (raw and occupancy-normalized firing maps) correspond to data from awake immobility periods. Reported at upper right are total spike counts (raw maps) or peak spatial rates (occupancy-normalized maps). Bin size: 2.5 cm. Scale bar: 20 cm. Here, the occupancy-normalized maps shown were generated from unsmoothed occupancy-normalized maps by taking the mean firing rate of bins of a 3x3 grid centered on the bin, disregarding bins that were not occupied by the subject. Quantification in **h** and **i** was performed on unsmoothed occupancy-normalized maps.
h, Spatial information[82] of N units in awake periods outside of immobility periods (upper plot, 1.12 ± 0.59 bits/spike, n = 67 units, with one unit excluded due to lack of firing outside of immobility) and awake immobility periods (lower plot, 1.17 ± 0.58 bits/spike, n = 68 units). In both conditions, data during SWR periods were excluded. Spatial information was calculated in the rest epoch in which the unit had the highest mean firing rate during awake periods. As in the task environment, N units exhibited spatially specific firing during immobility. Notably, the rest environment is an additional condition in which N units signaled location, moreover in the absence of material reward (analysis of non-reward locations in the task maze in **Extended Data Fig. 5b-d**).
i, Correlation (Pearson's r) of N unit spatial maps between awake immobility periods and awake non-immobility periods in the rest environment. The correlation was calculated from unsmoothed occupancy-normalized firing maps, specifically for spatial bins in which the subject was immobile. Out of 67 units, 35 showed significant correlation (p < 0.05; 0.53 ± 0.03, mean ± s.e.m.), with no negative correlations observed. Correlations were calculated in the rest epoch in which the unit had the highest mean firing rate during awake periods. These positive correlations indicate that N units retained their spatial specificity into immobility periods.
j, Comparison of firing rates across SIA-nesting conditions. Statistical tests (signed-rank, comparison of Nest OUT vs. IN): CA1, SIA ON (n = 18 units), p = 0.014; CA1, SIA OFF (n = 92), $p < 10^{-5}$; CA3, SIA ON (n = 19), p = 0.60; CA3, SIA OFF (n = 58), p = 0.26; CA2 P, SIA ON (n = 15), p = 0.11; CA2 P, SIA OFF (n = 65), p = 0.0027; CA2 N, SIA ON (n = 18), p = 0.022; CA2 N, SIA OFF (n = 57), p = 0.027. As in the evaluation of the nesting position specificity index (**Fig. 5f**), these comparisons show that the CA1 and CA2 N unit populations met dual criteria (description in Supplementary Methods) for nesting position coding, while the CA3 unit population did not. Asterisks: *, p < 0.05; **, p < 0.01; ***, p < 0.001; n.s., not significant at p < 0.05.

k, SIA firing rate vs. nesting position specificity index for all detected unit-sleep period samples. Here, if data was available for a unit (in the rest unit set) during a detected sleep period, then the unit's SIA firing rate during the sleep period was measured and its nesting position specificity index was calculated with respect to that sleep period's nesting position; this sample is then represented by a scatter point. In this approach, an individual unit can contribute more than one sample. CA1 (n = 312 samples from 94 units): Spearman's ρ: 0.55, p < 10^{-25}. CA3 (n = 223 samples from 62 units): Spearman's ρ: 0.12, p = 0.065. CA2 P (n = 263 samples from 65 units): Spearman's ρ: 0.37, p < 10^{-9}. CA2 N (n = 256 samples from 60 units): Spearman's ρ: 0.33, p < 10^{-7}.

l, CA2 P unit distribution of nesting position specificity indices. Mean ± s.e.m.: SIA ON (n = 15): 0.22 ± 0.09, p = 0.048, signed-rank; SIA OFF (n = 65): -0.16 ± 0.04, p < 0.001, signed-rank. Asterisks: *, p < 0.05; ***, p < 0.001.

m, STA class proportions across conditions. In addition to STAs calculated from non-SWR immobility in task epochs (TASK, presented in **Fig. 4** and **Extended Data Figs. 7, 8, 9**), STAs were also calculated from non-SWR immobility during awake periods in rest epochs (REST). For REST STAs, as in TASK STAs, a minimum of 100 spikes outside of SWRs during awake immobility and valid LFP reference sites were required, and units with STAs with mixed features were left unclassified (LFP reference site and unclassified STA criteria in Supplementary Methods; unclassified unit counts: CA1: 8 out of 83, CA3: 4 out of 51, CA2 N: 10 out of 58). As in TASK, N wave-coupled units in REST were detected in substantial proportions. In diagrams, STA positive (N wave-coupled) is in light orange, with a darker orange corresponding to significance in the STA voltage at t = 0 (p < 0.05, signed-rank). STA negative is in grey, with black corresponding to significance. Left (pie charts): proportions (%) of units in each of STA classes. Total unit counts (number of units with classified STAs) are reported at bottom right. Percentages are rounded to nearest whole number. Upper right: unit counts in each (non-overlapping) category (* denotes units with STAs with significance at p < 0.05). Lower right: contingency table for CA1 and CA3 units found active in both task and rest epochs (fired >100 spikes outside of SWRs during immobility in at least one task recording epoch and during awake immobility in at least one rest recording epoch) and with classifiable STAs (positive vs. negative). Notably, no units were observed that were STA positive in both conditions, suggesting that N wave-coupling for a given CA1/CA3 neuron is not a static property. In contrast, the majority of classifiable CA2 N units in both TASK (53/57, or 93%) and REST (38/48, or 79%) were N wave-coupled.

Chapter 2:

High frequency network activation marks switch in neural code for space

High frequency network activation
marks switch in neural code for space

Abstract

In the mammalian brain, the hippocampus constructs an internal map of space understood to be required for cognitive functions such as spatial navigation and episodic memory[1-3]. Recently, it has been shown that an anatomically and physiologically distinct set of hippocampal neurons codes for space specifically when subjects are immobile, in contrast to the classic hippocampal spatial code active during movement[4]. This finding indicates that the hippocampus activates fundamentally different spatial representations at different times. However, neither the timing nor the mechanisms of switching between these representations is known. Here we report that distinct non-classical spatial representations in the hippocampus can reliably activate within hundreds of milliseconds, and that this activation occurs at the time of an equivalently fast activation of a high frequency network pattern detectable in the CA3 and DG subregions. This network pattern was moreover found to entrain neural firing throughout the hippocampus. These results indicate that multiple distinct hippocampal neural codes for space are rapidly regulated, and also identify region-specific circuit mechanisms that may mediate this regulation. We propose that precise temporal segregation of distinct hippocampal spatial representations is critical to their respective functions.

Fig. 1. Non-classical hippocampal firing during behavioral transitions.

Fig. 2. Transient activation of a high frequency hippocampal rhythm at CA3 and DG.

Fig. 3. A transient signature of high frequency activation in CA3 and DG.

Fig. 4. Widespread high frequency synchronization of the hippocampus.

Fig. 5. Anatomical profile of wave gamma.

Fig. S1. Behavioral paradigm and recording sites.

Fig. S2. Transitional firing: non-classical hippocampal spatial coding.

Fig. S3. Identification of a 65-140 Hz rhythm in CA3 and DG.

Fig. S4. Rapid activation of a high frequency rhythm.

Introduction

The hippocampus has a vital role in cognition, yet our understanding of how hippocampal neural activity performs cognitive functions remains incomplete. Traditional approaches have focused on the classic hippocampal place code, defined by the firing of hippocampal neurons in discrete locations as subjects move through an environment[1,5,6]. More recently, it has become clear that when subjects stop moving, the hippocampus generates a radically different neural code in which hippocampal neurons represent past and even possible future spatial experience[7-13]. The elucidation of this neural code (conventionally termed hippocampal "replay"), which occurs in conjunction with a massively synchronous hippocampal network pattern known as the sharp wave-ripple[14,15] (SWR), has begun to clarify how the cognitive functions of the hippocampus are neurally implemented, thereby establishing neural coding state in the hippocampus as a matter of fundamental importance.

Experimental results from a recent study have raised this matter anew. In specific, it was found that a distinct population of hippocampal neurons codes for location not only when subjects stop moving but also in the absence of SWRs, thus establishing a hippocampal neural code distinct from both classic place and SWR coding[4]. However, it remains unclear when and by what mechanisms the hippocampus changes neural coding states: knowledge necessary for an adequate understanding of what the hippocampus represents and therefore of hippocampal function[16]. In light of the well-documented widespread capacity of hippocampal neurons to fire synchronously at the timescale of milliseconds (respectively within the classic place and SWR coding states)[17-22], we hypothesized that transitions between coding states might also occur with high temporal precision, and possibly involve comparably precise network mechanisms.

Non-classical spatial coding during behavioral transitions

We recorded neural activity in the hippocampus of rats engaged in a navigational task[4,9,23-25] (**Fig. 1a, Fig. S1**). In the task, subjects were trained to alternate between each of three locations (reward wells) in a W-shaped maze. Importantly, execution of the task regularly elicits each of the three known hippocampal coding states[4,9,26], enabling study of transitions between them. We began by examining single neuron (unit) firing when subjects entered and exited the maze reward wells, as these behavioral events occurred regularly and were associated with transitions between the immobility-associated (IA) spatial code and the movement-associated classic place (CP) code.

Unexpectedly, we found that a subset of units showed transient increases in firing (lasting <1 s) upon well entry/exit, an activity pattern characteristic of neither CP nor IA coding (**Fig. 1b, c**, **Fig. S2**) (60 unit-well samples, 40 entry and 20 exit, from 54 units, using 20 Hz/s threshold for firing rate changes; 26 unit-well samples, 19 entry and 7 exit, from 25 units at a 30 Hz/s threshold; 440 candidate units evaluated; see Methods for detection procedure). The transient firing pattern was distinguishable from firing associated with CP coding since there was only

minimal change in position immediately after well entry or immediately prior to well exit; furthermore, this firing was distinguishable from firing associated with IA coding since (1) the transient firing was not necessarily accompanied by firing in the periods of immobility following or preceding the entry/exit, (2) IA firing units did not necessarily show transient firing upon well entry/exit (**Fig. 1d**). In light of these findings, we termed the firing pattern transitional firing (TF), defined by precise temporal association with behavioral transitions between movement and immobility. Critically, TF was location-specific, characteristically occurring at specific reward wells despite the similar behavior of subjects at reward wells (**Fig. S2**). Thus TF, in addition to the IA code[4], represents a non-classical spatial code in the hippocampus.

To measure the rate at which these non-classical neural codes could become active or inactive, we first categorized instances of non-classical firing as unit-well samples showing proportionally higher firing rates during either transitional periods (-100 to +1000 ms for well entry, -1000 to +100 ms for well exit) or during immobility at the well. Scatter plots of firing rates (**Fig. 1d**) indicated that units predominantly fired either during periods of movement near well entry/exit, transitional periods at the time of well entry/exit, or during immobility at the well (Movement, Transitional, Immobility axes, respectively). Subsequent analysis of unit-well PETHs disclosed similar firing rate changes (firing rate slope magnitude) between non-classical and classical groups (non-classical well entry, n = 72 slopes from 72 units: median: 26 Hz/s, mean ± SEM: 32 ± 2.8 Hz; classical well entry, n = 100 slopes from 98 units: median: 30 Hz/s, mean ± SEM: 34 ± 2.2 Hz; non-classical well exit, n = 109 slopes from 104 units: median: 18 Hz/s, mean ± SEM: 20 ± 1.3 Hz; classical well exit, n = 148 slopes from 141 units: median: 19 Hz/s, mean ± SEM: 25 ± 1.8 Hz/s; distribution of slope values shown in **Fig. 1f**). These results indicate that the hippocampus regulates non-classical and classical spatial firing patterns at equivalent timescales.

A transiently activated hippocampal rhythm

We hypothesized that the precise regulation of distinct coding patterns we observed might involve broad changes in hippocampal activity. Critically, past work has shown that the CP, IA, and SWR coding states are each marked by distinct non-spiking patterns of hippocampal neural activity (theta[27-29], N wave[4], and SWR[15], respectively) expressed in the local field potential (LFP). Moreover, the participation of neurons in these patterns has been shown to vary by hippocampal subregion[4,28-36], underscoring the integral role of hippocampal anatomical structure in the activation of these patterns. Therefore, to detect wider changes in hippocampal activity during transitions between neural firing patterns, we examined the LFP in multiple hippocampal subregions (CA1, CA3, and DG) at the time of well entry/exit.

We discovered abrupt activation of an unorthodox LFP pattern at CA3 and DG recording sites (**Fig. 2**). CA3 and DG LFP aligned to the time of well entry showed a prominent high frequency fluctuation precisely aligned to the time of entry (**Fig. 2a**). Spectral analyses showed a rapid increase in power at frequencies conventionally classified as gamma (30-80 Hz) and higher,

with an unexpected distinct peak at ~100 Hz (**Fig. 2b, c**). Surprisingly, high frequency activation was weaker in CA1, suggesting predominant influence of the pattern in CA3 and DG.

Additional spectral analyses identified a discrete rhythmic pattern. In specific, cross-frequency analysis identified the 65-140 Hz band in the CA3 and DG LFP as a discrete bandwidth extremely strongly coupled to the phase of the 1-4 Hz band (**Fig. 2d**). This unexpected relationship was present across behavioral states (including NREM sleep, **Fig. S3**), raising the possibility of an underlying neural activity pattern influencing hippocampal neural activity at all times. We then directly analyzed the 65-140 Hz rhythm in CA3 and DG LFP at the time of well entry/exit, confirming a rapid transient increase in power at the time of well entry in CA3 and DG (**Fig. 2e**, **f**, **Fig. S4**).

A widespread hippocampal network pattern

We next determined whether the high frequency rhythm in CA3 and DG broadly influenced neural activity in the hippocampus. Specifically, we evaluated relationships with the 1-4 Hz LFP bandwidth (**Fig. 3**), neural firing (**Fig. 4**), and hippocampal dendritic layers (**Fig. 5**).

Examination of the high frequency rhythm in relation to wide-band LFP revealed that high power rhythmic episodes (2 SD) were associated with a ~200 ms transient positive wave (**Fig. 3a, b**), a relationship consistent with the prominent 1-4 Hz coupling observed previously (**Fig. 2e**). Subsequent analysis demonstrated strong coupling to the positive phase of 1-4 Hz LFP at CA3/DG (**Fig. 3c**). This relationship was opposite to that of SWRs, which were consistently coupled to the negative phase of 1-4 Hz at CA3/DG, a finding consistent with previous work[4,14,31]. These phase-amplitude relationships were moreover seen across behavioral states, indicating that the ~200 ms wave pattern was a consistent signature of activation of the 65-140 Hz rhythm in CA3 and DG. We therefore termed the high frequency rhythm "wave gamma" (WG).

Hippocampal neural firing was widely synchronized by WG (**Fig. 4**). All detected interneuronal units in CA1, CA2, CA3, and DG were found to be significantly modulated by the phase of WG (as measured at a recording site > or >>300 μm from the unit recording site; CA1: 33/33 units, CA2: 11/11, CA3: 19/19, DG: 6/6; Rayleigh tests at p < 0.05). Moreover, a substantial proportion of CA1 units (104/453 units, 23%) was entrained by WG, in addition to a majority of putative principal units recorded at CA2 (148/209, 71%) and CA3 (229/256, 89%). These results indicate that WG is a network pattern with a widespread influence on the temporal organization of hippocampal neural firing.

Lastly, we found that WG was associated with a distinct pattern of activity across hippocampal dendritic layers (**Fig. 4**). In this set of experiments, LFP recording probes with linearly spaced sites were targeted perpendicularly to the CA1 cell layer and advanced to DG, and subjects recorded under the same behavioral paradigm as before. Average LFPs and current source densities (CSDs) of WG episodes and SWRs indicated that these hippocampal network patterns had qualitatively different patterns of synaptic activation. Interestingly, the profile of WG

was similar to that of dentate spikes, a hippocampal network pattern proposed in previous work to result from synaptic drive originating in entorhinal cortex[34,37]. These findings suggest that the activation of WG is primarily the result of extra-hippocampal excitatory drive from entorhinal cortex, though local mechanisms are more likely responsible for the high frequency component[38].

Discussion

We investigated hippocampal activity at the time of behavioral transitions between movement and rest, finding (1) a novel firing pattern (TF) that was transient and spatially specific, (2) temporally precise regulation of non-classical spatial firing patterns (TF and IA), and (3) temporally precise activation of a novel high frequency hippocampal network pattern (WG) detectable in CA3 and DG. These findings indicate that the hippocampal neural circuit is adapted to coordinate multiple distinct hippocampal neural codes (CP, TF, and IA) at the time of behavioral transitions.

Remarkably, these findings recall the past observation of IA coding neurons (CA2 N units) that often show an abrupt decrease in firing at the time of SWRs[4]. This previous result indicates temporally precise switching between IA and SWR coding, therefore representing an analogous scenario to the transitions, described here, between classical (CP) and non-classical (TF/IA) coding. In light of this similarity, we propose that the respective functions of the distinct hippocampal neural codes (CP, IA, TF, and SWR codes) are dependent on adequate segregation in time.

In addition, we note that the lack of a specific overt behavior that matches the rapid time course of the coding transitions (either between IA and SWR codes or between CP to TF/IA codes) suggests that the coding transitions occur on the basis of variables intrinsic to neural circuits rather than on variables related in a simple way to sensory or motor input. Notably, this view has been proposed before in the context of the CP and SWR codes, in that these neural codes appear to be internally consistent abstract representations[1,6,39]. Here, we extend this line of thinking to include neural activity in the hippocampus during transitional periods. Together with the observation that the hippocampus regulates non-classical coding as rapidly as classical coding, these findings suggest that, under naturalistic conditions, the hippocampus makes a critical functional distinction between periods of movement versus rest.

Lastly, we identified a rhythmic hippocampal network pattern (WG) that increased in power precisely at the time of behavioral transitions. This finding suggests possible network-level mechanisms mediating the transition between hippocampal coding patterns. Notably, WG entrained unit firing throughout the hippocampus, suggesting the existence of a circuit mechanism capable of influencing large ensembles of hippocampal neurons. Furthermore, WG was only readily detectable in CA3 and DG, and not CA1, thus localizing a putative circuit mechanism to hippocampal structures synaptically upstream of CA1, which has been conceptualized as the output subregion of the hippocampus[40]. Interestingly, theoretical and experimental studies have

argued that the CA3 and DG networks each have quintessential roles in the selection of behaviorally appropriate neural representations[41-45]. However, these studies have focused on representations assessed at the timescale of minutes: here we raise the possibility of a role for the CA3 and DG networks in inducing radical circuit-wide representational changes at the subsecond timescale.

References

1   O'Keefe, J. & Nadel, L. The hippocampus as a cognitive map. (Oxford University Press, 1978).

2   Buzsaki, G. & Moser, E. I. Memory, navigation and theta rhythm in the hippocampal-entorhinal system. Nat Neurosci 16, 130-138 (2013).

3   Eichenbaum, H. & Cohen, N. J. Can we reconcile the declarative memory and spatial navigation views on hippocampal function? Neuron 83, 764-770 (2014).

4   Kay, K. *et al.* A hippocampal network for spatial coding during immobility and sleep. Nature 531, 185-190 (2016).

5   Wilson, M. A. & McNaughton, B. L. Dynamics of the hippocampal ensemble code for space. Science 261, 1055-1058 (1993).

6   Moser, E. I., Kropff, E. & Moser, M. B. Place Cells, Grid Cells, and the Brain's Spatial Representation System. Annu Rev Neurosci 19 (2008).

7   Foster, D. J. & Wilson, M. A. Reverse replay of behavioural sequences in hippocampal place cells during the awake state. Nature 440, 680-683 (2006).

8   Diba, K. & Buzsaki, G. Forward and reverse hippocampal place-cell sequences during ripples. Nat Neurosci 10, 1241-1242 (2007).

9   Karlsson, M. P. & Frank, L. M. Awake replay of remote experiences in the hippocampus. Nat Neurosci 12, 913-918 (2009).

10   Davidson, T. J., Kloosterman, F. & Wilson, M. A. Hippocampal replay of extended experience. Neuron 63, 497-507 (2009).

11   Gupta, A. S., van der Meer, M. A., Touretzky, D. S. & Redish, A. D. Hippocampal replay is not a simple function of experience. Neuron 65, 695-705 (2010).

12   Carr, M. F., Jadhav, S. P. & Frank, L. M. Hippocampal replay in the awake state: a potential substrate for memory consolidation and retrieval. Nat Neurosci 14, 147-153 (2011).

13   Pfeiffer, B. E. & Foster, D. J. Hippocampal place-cell sequences depict future paths to remembered goals. Nature 497, 74-79 (2013).

14   Buzsaki, G., Horvath, Z., Urioste, R., Hetke, J. & Wise, K. High-frequency network oscillation in the hippocampus. Science 256, 1025-1027 (1992).

15   Buzsaki, G. Hippocampal sharp wave-ripple: A cognitive biomarker for episodic memory and planning. Hippocampus 25, 1073-1188 (2015).

16   Gallistel, C. R. The organization of learning. (MIT Press, 1990).

17   Harris, K. D., Csicsvari, J., Hirase, H., Dragoi, G. & Buzsaki, G. Organization of cell assemblies in the hippocampus. Nature 424, 552-556 (2003).

18   Dragoi, G. & Buzsaki, G. Temporal encoding of place sequences by hippocampal cell assemblies. Neuron 50, 145-157 (2006).

19   Foster, D. J. & Wilson, M. A. Hippocampal theta sequences. Hippocampus 17, 1093-1099 (2007).

20   Diba, K., Amarasingham, A., Mizuseki, K. & Buzsaki, G. Millisecond timescale synchrony among hippocampal neurons. J Neurosci 34, 14984-14994 (2014).

21   Pfeiffer, B. E. & Foster, D. J. Autoassociative dynamics in the generation of sequences of hippocampal place cells. Science 349, 180-183 (2015).

22   Feng, T., Silva, D. & Foster, D. J. Dissociation between the experience-dependent development of hippocampal theta sequences and single-trial phase precession. J Neurosci 35, 4890-4902 (2015).

23   Frank, L. M., Brown, E. N. & Wilson, M. A. Trajectory encoding in the hippocampus and entorhinal cortex. Neuron 27, 169-178 (2000).

24   Kim, S. M. & Frank, L. M. Hippocampal lesions impair rapid learning of a continuous spatial alternation task. PLoS ONE 4, e5494 (2009).

25   Jadhav, S. P., Kemere, C., German, P. W. & Frank, L. M. Awake hippocampal sharp-wave ripples support spatial memory. Science 336, 1454-1458 (2012).

26   Carr, M. F., Karlsson, M. P. & Frank, L. M. Transient slow gamma synchrony underlies hippocampal memory replay. Neuron 75, 700-713 (2012).

27   O'Keefe, J. & Recce, M. L. Phase relationship between hippocampal place units and the EEG theta rhythm. Hippocampus 3, 317-330 (1993).

28   Skaggs, W. E., McNaughton, B. L., Wilson, M. A. & Barnes, C. A. Theta phase precession in hippocampal neuronal populations and the compression of temporal sequences. Hippocampus 6, 149-172 (1996).

29   Mizuseki, K., Sirota, A., Pastalkova, E. & Buzsaki, G. Theta oscillations provide temporal windows for local circuit computation in the entorhinal-hippocampal loop. Neuron 64, 267-280 (2009).

30   Buzsaki, G., Leung, L. W. & Vanderwolf, C. H. Cellular bases of hippocampal EEG in the behaving rat. Brain Res 287, 139-171 (1983).

31   Csicsvari, J., Hirase, H., Czurko, A., Mamiya, A. & Buzsaki, G. Fast Network Oscillations in the Hippocampal CA1 Region of the Behaving Rat. J Neurosci 19, RC20 (1999).

32   Csicsvari, J., Hirase, H., Mamiya, A. & Buzsaki, G. Ensemble patterns of hippocampal CA3-CA1 neurons during sharp wave-associated population events. Neuron 28, 585-594 (2000).

33   Sullivan, D. *et al.* Relationships between Hippocampal Sharp Waves, Ripples, and Fast Gamma Oscillation: Influence of Dentate and Entorhinal Cortical Activity. J Neurosci 31, 8605-8616 (2011).

34   Penttonen, M., Kamondi, A., Sik, A., Acsady, L. & Buzsaki, G. Feed-forward and feed-back activation of the dentate gyrus in vivo during dentate spikes and sharp wave bursts. Hippocampus 7, 437-450 (1997).

35   Mizuseki, K., Royer, S., Diba, K. & Buzsaki, G. Activity dynamics and behavioral correlates of CA3 and CA1 hippocampal pyramidal neurons. Hippocampus 22, 1659-1680 (2012).

36   Valero, M. *et al.* Determinants of different deep and superficial CA1 pyramidal cell dynamics during sharp-wave ripples. Nat Neurosci 18, 1281-1290 (2015).

37   Bragin, A., Jando, G., Nadasdy, Z., van Landeghem, M. & Buzsaki, G. Dentate EEG spikes and associated interneuronal population bursts in the hippocampal hilar region of the rat. J Neurophysiol 73, 1691-1705 (1995).

38   Schomburg, E. W. *et al.* Theta phase segregation of input-specific gamma patterns in entorhinal-hippocampal networks. Neuron 84, 470-485 (2014).

39   McNaughton, B. L., Battaglia, F. P., Jensen, O., Moser, E. I. & Moser, M. B. Path integration and the neural basis of the 'cognitive map'. Nat Rev Neurosci 7, 663-678 (2006).

40   Andersen, P. in The Hippocampus Book (eds P. Andersen *et al.*) 37-114 (Oxford Univ. Press, 2007).

41   Marr, D. Simple memory: a theory for archicortex. Philos Trans R Soc Lond B Biol Sci 262, 23-81 (1971).

42   McNaughton, B. L. & Morris, R. G. Hippocampal synaptic enhancement and information storage within a distributed memory system. Trends Neurosci 10, 408-415 (1987).

43   Rolls, E. T. & Kesner, R. P. A computational theory of hippocampal function, and empirical tests of the theory. Prog Neurobiol 79, 1-48 (2006).

44   Leutgeb, J. K., Leutgeb, S., Moser, M. B. & Moser, E. I. Pattern separation in the dentate gyrus and CA3 of the hippocampus. Science 315, 961-966 (2007).

45   Lee, H., Wang, C., Deshmukh, S. S. & Knierim, J. J. Neural Population Evidence of Functional Heterogeneity along the CA3 Transverse Axis: Pattern Completion versus Pattern Separation. Neuron 87, 1093-1105 (2015).

46   Potter, G. B. *et al.* Generation of Cre-transgenic mice using Dlx1/Dlx2 enhancers and their characterization in GABAergic interneurons. Mol Cell Neurosci 40, 167-186 (2009).

47   Neunuebel, J. P. & Knierim, J. J. Spatial firing correlates of physiologically distinct cell types of the rat dentate gyrus. J Neurosci 32, 3848-3858 (2012).

48   Lorente de Nó, R. Studies on the structure of the cerebral cortex. II. Continuation of the study of the ammonic system. J Psychol Neurol 46, 113-177 (1934).

49   Dudek, S. M., Alexander, G. M. & Farris, S. Rediscovering area CA2: unique properties and functions. Nat Rev Neurosci 17, 89-102 (2016).

50   Tort, A. B., Komorowski, R., Eichenbaum, H. & Kopell, N. Measuring phase-amplitude coupling between neuronal oscillations of different frequencies. J Neurophysiol 104, 1195-1210 (2010).

51   Mitzdorf, U. Current source-density method and application in cat cerebral cortex: investigation of evoked potentials and EEG phenomena. Physiol Rev 65, 37-100 (1985).

52   Mizuseki, K., Diba, K., Pastalkova, E. & Buzsaki, G. Hippocampal CA1 pyramidal cells form functionally distinct sublayers. Nat Neurosci 14, 1174-1181 (2011).

53   Frank, L. M., Brown, E. N. & Wilson, M. Trajectory encoding in the hippocampus and entorhinal cortex. Neuron 27, 169-178 (2000).

Methods

Subjects, neural recordings, and behavioral task. Eleven male Long-Evans rats 4 to 9 months old (500–600 g) were food deprived to 85% of their baseline weight and pre-trained to run on a 1-m linear track for liquid reward (sweetened evaporated milk). After subjects alternated reliably, eight were implanted with microdrives containing 14 (two subjects), 21 (three subjects), or 30 (three subjects) independently movable four-wire electrodes (tetrodes) targeting dorsal hippocampus (all rats) and medial entorhinal cortex (one rat); three were implanted with polymer probes with 18 linearly spaced platinum contacts (20 μm contact size, 90 μm edge-to-edge spacing, Lawrence Livermore National Laboratory) targeting dorsal hippocampus. Voltage amplitudes were generally lower in polymer probe recordings than in tetrode recordings. than Subjects were implanted with recording devices in accordance with University of California San Francisco Institutional Animal Care and Use Committee and US National Institutes of Health guidelines. The minimum number of subjects was established beforehand as four or more, as this is considered to be the minimum necessary to yield data with sufficient statistical power to evaluate the type of effects investigated in this study.

In two microdrive subjects, right and left dorsal hippocampus were targeted at AP: -3.7 mm, ML: ±3.7 mm. In one microdrive subject, dorsal hippocampus was targeted at AP: -3.6 mm, ML: +2.2 mm, in addition to medial entorhinal cortex at AP: -9.1, ML: 5.6, at a 10 degree angle in the sagittal plane. Data from these several subjects have been reported in earlier studies[4,9,26]. In five microdrive subjects, right dorsal hippocampus was targeted at AP: -3.3 to -4.0 mm, ML: +3.5 to +3.9 mm, moreover, in two of these subjects, the septal pole of right hippocampus was targeted with an additional six tetrodes targeted to AP: -2.3 mm, ML: +1.1 mm. Targeting locations were used to position stainless steel cannulae containing 6, 14, 15, or 21 independently driveable tetrodes. The cannulae were circular except in four cases targeting dorsal hippocampus in which they were elongated into ovals (major axis ~2.5 mm, minor axis ~1.5 mm; two subjects with major axis 45° relative to midline, along the transverse axis of dorsal hippocampus; two subjects with major axis 135° relative to midline, along the longitudinal axis of dorsal hippocampus). In the three polymer probe subjects, right dorsal hippocampus was targeted at AP: -3.8 mm, ML: +2.65 mm, and DV: -3.8 to -4.15 mm. Data exclusively from right dorsal hippocampus were analyzed in this study.

In five microdrive subjects, viral vectors with optogenetic transgenes were targeted to either right dorsal CA2 (three subjects, AAV2/5-CaMKII-hChR2(H134R)-EYFP, UNC Vector Core,

135 nl at AP: -3.6 mm, ML: +4.2 mm, DV: -4.5 mm), dorsal DG (one subject, AAV2/5-I12B[46]-ChR2-GFP, 225 nl at AP: -3.75 mm, ML: +2.2 mm, DV: 3.9 mm and AP: -3.75 mm, ML: +1.8 mm, DV: -4.5 mm), or right supramammilary nucleus (one subject, AAV2/5-hSyn-ChETA-EYFP, Penn Vector Core, 135 nl at AP: -4.3 mm, ML: +1.8 mm, and -8.9 mm along a trajectory angled at 6° in the coronal plane). Viruses were delivered during the implant surgery using a glass micropipette (tip manually cut to ~25 um diameter) attached to an injector (Nanoject, Drummond Scientific). In addition, a driveable optical fiber (62.5/125 µm core/cladding) was integrated in the tetrode microdrive assembly to enable light delivery to hippocampus. This fiber was advanced to its final depth (2.5-3 mm) within 7 days of implantation. Data reported in this study were collected prior to light stimulation. No overt differences in neural activity were observed in subjects that received virus. In particular, CA2 recording sites reporting CA2 N units were found in subjects either receiving or free of viral vectors.

Over the course of two weeks following implantation, the tetrodes were advanced to the principal cell layers of CA1 (all subjects), CA2 (5 subjects), CA3 (all subjects), and DG (3 subjects). For DG, tetrodes were advanced to the cell layer using a previously described protocol in which the tetrodes were slowly advanced within DG (~10 µm increments) and unit activity monitored over long periods of rest[47]. DG cell layer was identified by the presence of highly sparsely firing putative principal units. In several subjects, tetrodes were also left in cortex overlying dorsal hippocampus. Neural signals were recorded relative to a reference (REF) tetrode positioned in corpus callosum above right dorsal hippocampus. The REF tetrode reported voltage relative to a ground screw installed in skull overlying cerebellum, and local field potential (LFP) from this tetrode was also recorded. All tetrode final locations were histologically verified (see below).

After 5-7 days of recovery after surgery, subjects were once again food deprived to 85% of their baseline weight, and again pre-trained to run on a linear track for liquid reward. At ~14 days after surgery, six subjects were then introduced to one task W-maze (**--**) and recorded for 3 to 6 days before being introduced to a second task W-maze, located in a separate part of the recording room and rotated 90° relative to the first. On recording days in which the second task W-maze was used, recordings were also conducted in the first task W-maze. In two subjects, recordings were conducted in both task W-mazes on every recording day. The W-mazes were 76 x 76 cm with 7-cm-wide track sections. The two task W-mazes were separated by an opaque barrier.

In each W-maze, subjects were rewarded for performing a hippocampus-dependent continuous alternation task (**Fig. S1**). Liquid reward (sweetened evaporated milk) was dispensed via plastic tubing connected to a hole at the bottom of each of the three reward wells (wells A, B, and C), miniature bowls 3 cm in diameter. In three subjects, reward was dispensed via syringes operated manually by an experimenter who was located in a separate part of the recording room. In five subjects, entry of subjects' head into reward well was sensed by an infrared beam break

circuit attached to the well, and reward was automatically delivered by syringe pumps (OEM syringe pumps, Braintree Scientific) either immediately or after an imposed delay lasting from 0.5 to 2 s. In these subjects, digital time stamps corresponding to well entry and reward delivery were recorded, but were otherwise not used in determining entry times or occupancy of the subjects at the wells. Task epochs lasting ~15 minutes were preceded and followed by rest epochs lasting ~20 minutes in a high-walled black box (floor edges 25-35 cm and height 50 cm), during which rats often groomed, quietly waited, and slept. Two subjects also ran in an open field environment for scattered food (grated cheese) after W-maze recordings, with additional interleaved rest epochs. Tetrode positions were adjusted after each day's recordings.

Data were collected using the NSpike data acquisition system (Loren Frank and James MacArthur, Harvard Instrumentation Design Laboratory). During recording, an infrared diode array with a large and a small cluster of diodes was affixed to headstage preamps to enable tracking of head position and head direction. Following recording, position and direction were reconstructed using a semi-automated analysis of digital video (30 Hz) of the experiment. Spike data were recorded relative to the REF tetrode, sampled at 30 kHz, digitally filtered between 600 Hz and 6 kHz (2-pole Bessel for high- and low-pass), and threshold crossing events were saved to disk. Local field potentials (LFPs) were sampled at 1.5 kHz and digitally filtered between 0.5 Hz and 400 Hz. LFPs analyzed were relative to the REF tetrode except where otherwise indicated.

Individual units (putative single neurons) were identified by clustering spikes using peak amplitude, principal components, and spike width as variables (MatClust, Mattias Karlsson). Only well-isolated neurons with stable spike waveform amplitudes were clustered. A single set of cluster bounds defined in amplitude and width space could often isolate units across an entire recording session. In cases where there was a shift in amplitudes across time, units were clustered only when that shift was coherent across multiple clusters and when plots of amplitude versus time showed a smooth shift. No units were clustered in which part of the cluster was cut off at spike threshold.

Histology and recording site assignment. After recordings, subjects implanted with microdrives were anesthetized with isoflurane, electrolytically lesioned at each tetrode (30 µA of positive current for 3 s applied to two channels of each tetrode), and allowed to recover overnight. In one subject, no electrolytic lesions were made, and tetrode tracks rather than lesions were used to identify recording sites. Subjects implanted with linear probes were similarly electrolytically lesioned at two deepest recording sites. After recovery, all subjects were euthanized with pentobarbital and were perfused intracardially with PBS followed by 4% paraformaldehyde in PBS. The brain was post-fixed *in situ* overnight, after which the tetrodes or probes were retracted and the brain removed, cryo-protected (30% sucrose in PBS), and embedded in OCT compound. Coronal (7 subjects) and sagittal (1 subject) sections (50 µm) were taken with a cryostat. Sections were either Nissl-stained with cresyl violet or stained with the fluorescent Nissl reagent NeuroTrace Blue (1:200) (Life Technologies, N-21479). CA2 recording

sites were designated as those in which the electrolytic lesion or end of tetrode track overlapped with the dispersed cytoarchitectural zone characteristic of CA2[48,49]. This strategy was deliberately inclusive to maximize detection of putative CA2 neurons with novel physiological responses (N units[4]). It is important to note that CA2 sites defined in this way include recording locations that have been designated in previous studies as "CA3a."

Data Analysis. All analyses were carried out using custom software written in Matlab (Mathworks).

Principal vs. interneuronal unit classification. For all units detected, scatter plots of firing rate, spike width, and autocorrelation function mean (calculated from 0 to 40 ms; low values indicating burst firing) showed two distinct clusters (example plot in Chapter 1, **Fig. 1c**). Putative principal units corresponded with the low firing rate (<4 Hz), large spike width, low autocorrelation mean cluster, while putative interneuronal units corresponded to the cluster characterized by high firing rate, small spike width, and high autocorrelation mean. Twenty-one units with ambiguous features were left unclassified.

Unit inclusion. Two unit sets were analyzed in this study. The first, analyzed in **Fig. 1** and in **Fig. 4**, was the set of putative principal units (n = 975; CA1: 478, CA2 N: 84, CA2 P: 142, and CA3: 271) that fired at least 100 spikes outside of sharp wave-ripples (SWRs) in at least one task epoch. These units were the same as the "task unit set" in Chapter 1. The second was the set of all interneuronal units (n = 63) detected in CA1, CA2, CA3, and DG, analyzed in **Fig. 4**.

Behavioral state. Periods of movement were defined as times when head speed was >4 cm/s. Periods of high speed were times when the head speed was >20 cm/s. Periods of immobility were times when head speed was <4 cm/s separated from periods of movement by 2 s buffer intervals (preceding and following). Thus brief interruptions in movement did not qualify as formally detected periods of immobility.

Well visits and well exit/entry. To determine when subjects were located at reward wells, 2D position data (corresponding to subjects' head location) for all subjects was first converted to linear position. Linear position was measured as the distance from the center reward well along the linear arms of the W-shaped task maze, with the minimal and maximal positions corresponding to the center of respective reward wells.

Well periods were defined as times when the subject's linear position matched that of the reward well (<2 cm separation). Well visits were defined as well periods that lasted at least 2 s and were preceded earlier in the recording epoch by a well period at a different well. In instances in which subjects re-visited the well they departed from before visiting another well, a well visit was only registered after an exclusion period of 5 s. Well entry and exit times were defined as the beginning and end of well visits, respectively.

Well firing and transitional firing (TF). For hippocampal principal units, firing was analyzed at the time of well entry/exit for each of the three wells of the task. Thus each unit contributed up to six unit-well samples, depending on subsequent acceptance criteria. Unit-well samples were

analyzed in the latest task 15-minute recording epoch in the recording day. On recording days in which two W-mazes were used (see above), both W-mazes were analyzed. Furthermore, at least 10 well entry/exit trials were required for analysis, and initial firing rate analysis was restricted to the final 10 well entry/exit trials, at the specific well, in the task recording epoch.

For each unit-well sample, mean firing rates were calculated in three period types that were defined relative to the time of well entry/exit (t = 0): Baseline, Transitional, and Immobility (**Fig. 1d**). For well entry, Baseline was defined as -500 to -100 ms, Transitional as -100 to 1000 ms, and Immobility as the periods of behaviorally defined immobility (see above) while located at the well. For well exit, Baseline was defined as +100 to +500 ms, Transitional as -1000 to 100 ms, and Immobility as the periods of behaviorally defined immobility while located at the well.

Next, peri-event time histograms (PETHs, 1-ms bins) were generated for each unit-well sample and subsequently smoothed with a Gaussian window (SD = 100 ms). In addition, the first-order derivative of the PETH was calculated and then smoothed with a Gaussian window (SD = 5 ms) to obtain the firing rate slope function of the unit-well sample (Fr slope; **Fig. 1b, c**). The firing rate slope during well exit/entry (**Fig. 1f**) was then estimated as follows: within the Transitional window, the positive peaks and negative troughs in the firing rate slope function were identified. Then from among these times, the time corresponding to the largest magnitude slope was identified. The signed value of the slope function at this time was defined as the firing rate slope.

Transitional firing (TF) was then evaluated for unit-well samples that had PETHs exhibiting a >2 Hz rate at times in the Transitional window. To do so, positive local extrema (peaks) and negative local extrema (troughs) were detected in the Fr slope during the Transitional window. A unit-well sample was classified as expressing TF if a positive peak value exceeding the detection threshold magnitude (20 or 30 Hz/s) was followed by a negative trough value also exceeding the detection threshold in magnitude.

The spatial specificity of units expressing TF (**Fig. S2c**) was measured using the well specificity index[4] (WSI). The WSI was only calculated for units with unit-well samples expressing TF and in cases where there were at least five well visits for each well in the epoch in which TF was detected. To calculate the well specificity index (WSI), the mean firing rate during Transitional periods at each of the three wells of the maze was first determined. Next, each of the three well firing rates was divided by the numerical sum of the three well firing rates (normalization) to create a three-category (well A vs. B vs. C) probability distribution of firing activity. This probability distribution was subsequently treated as a circular distribution with a vector whose length corresponded to the probability mass for well A placed at 0°, a vector for well B at 120°, and a vector for well C at 240°. The WSI was the magnitude of the vector sum (resultant). The WSI directly reflects specificity of firing: a WSI = 0 corresponds to equal firing at all three wells (completely non-specific), WSI = 0.5 corresponds to firing at two wells, and WSI = 1 corresponds to firing at one well.

Spectrograms and power spectra at well entry. LFP from recording sites in the cell layer of

CA1, CA3, and DG were aligned to the time of well entry and transformed to the frequency domain. In specific, spectrograms (**Fig. 2b**) for each well entry were calculated for LFP in non-overlapping 100-ms windows using spectrogram (Matlab Signal Processing Toolbox). In addition, power spectra for each well entry were calculated for LFP in the 200-ms window prior to (pre) and after (post) well entry using mtspectrumtrigc (Chronux toolbox; http://chronux.org). These spectra were then smoothed with a Gaussian window (SD = 8 Hz). The ratio of the post spectrum to the pre spectrum was defined as the entry power ratio (**Fig. 2c**).

Modulation index. Phase-amplitude relationships in hippocampal LFP were detected using the modulation index[50] (MI). The MI is a measure of the non-uniformity of the distribution of LFP amplitude at a certain frequency (f_a) as a function of the LFP phase at another frequency (f_p). MI was calculated for f_p in 2-Hz steps with 4-Hz bandwidths (0 to 12 Hz), and f_a (10-250 Hz) at 5-Hz steps at 10-Hz bandwidths.

Continuous rhythmic power. LFP was only analyzed when at least three CA1 recordings and at least two CA3 or DG recordings were available. LFPs were segregated into two group types: group 1 was from CA1 cell layer recording sites, filtered at 150-250 Hz, used for SWR analysis; group 2 was from CA3 and DG recording sites, filtered at 65-140 Hz, used for WG analysis. Offline, filtered LFPs from each group type were squared, smoothed with a Gaussian kernel (group 1 LFP, SD = 10 ms; group 2 LFP, SD = 25 ms; for analysis at top in **Fig. 2e** and **Fig. 5b**, SD = 4 ms), and averaged across group recording sites. The square root of this average was then z-scored to obtain the amplitude trace (**Fig. 3**).

SWR and gamma episode detection. SWRs were detected when the group 1 LFP amplitude trace exceeded 2 SD for at least 30 ms. SWR periods were then defined as the periods, containing the times of threshold crossing, in which the amplitude trace exceeded the mean value. Detection of SWRs was performed only when subjects' head speed was <4 cm/s. WG episodes were detected when the group 2 LFP amplitude trace exceeded 2 SD for at least 40 ms. WG episode start and end times were then defined as the periods in which the amplitude trace exceeded the mean value. WG episodes were detected at all movement speeds. For the analyses in **Fig. 2e** and **Fig. 5b**, 2 SD periods were detected using a minimum threshold crossing duration of 15 ms.

LFP averages of rhythmic events. LFP averages of rhythmic events (SWRs and WG episodes; **Fig. 3b**) were calculated in task epochs. For WG, averages were calculated for two types of behaviorally defined periods: movement and immobility (see above). In each subject, the recording electrodes used to calculate LFP averages in each hippocampal subregion (CA1, CA3, and DG) were kept constant across recording days. Each LFP recording site either reported principal units for its correspondent region (if CA2, CA3, DG) or was within 60 µm of the depth range at which principal units were detected, as determined from records of electrode adjustment depths.

73

Low frequency (1-4 Hz) entrainment of rhythmic events. To estimate the phase of the low frequency bandwidth (identified in **Fig. 2d** and apparent in **Fig. 3a**), LFP from a recording site (kept constant over days) in the principal cell layer of CA3 was filtered at 1-4 Hz. The phase of the Hilbert transform of the filtered LFP was then designated as the low frequency phase. Next, for detected 2 SD rhythmic events (see above), the time of the peak power for each individual event was determined from the amplitude trace of the respective event type. These times were then converted into 1-4 Hz phases and histogrammed (15° bins). Four recording days from a single subject were excluded due to artifacts in the 1-4 Hz range; otherwise plotted data are from all recording sessions for all 8 subjects (microdrive tetrode experiments).

Wave gamma (WG) entrainment. To estimate the phase of WG, LFP from a recording site (kept constant over days) in the principal cell layer of CA3 was filtered at 65-140 Hz (WG). The phase of the Hilbert transform of the filtered LFP was then designated as the gamma phase. For a given unit, gamma phase locking analysis was performed for all spikes in all available recording epochs, with spike times converted into gamma phase.

Current source density (CSD). CSD traces were calculated as the second-order spatial derivative[51] of linear probe LFP.

Sleep state identification. Non-REM sleep periods were identified for phase-amplitude analysis (**Fig. S3**). First, in rest recording epochs, awake periods were identified as times in which head speed was >4 cm/s in addition to times <4 cm/s within 7 s of a previous movement >4 cm/s.

Candidate sleep periods were identified as times <4 cm/s preceded by 60 s with no movement >4 cm/s. REM periods within candidate sleep times were identified following an established procedure[52]. Specifically, the ratio of Hilbert amplitudes (smoothed with a Gaussian kernel, $\sigma = 1$ s) of theta (5-11 Hz) to delta (1-4 Hz) filtered LFP was calculated for all available CA1 tetrodes (referenced to cerebellar ground), and the mean taken over tetrodes. For each rest epoch, a threshold (range: 1.2-1.8) was manually set to capture sustained periods (10 s minimum duration) in which the theta:delta ratio was elevated. LFP and position data from each detected REM period were visually inspected.

For a given day's set of candidate sleep times outside of REM periods, LFP from each available CA1, CA3, and DG recording site was squared then smoothed with a Gaussian kernel ($\sigma = 300$ ms). The square root of the smoothed signal was then z-scored and summed across sites. The sum trace was in turn z-scored to obtain an aggregate hippocampal LFP amplitude. For each rest epoch, the distribution of aggregate LFP amplitudes was plotted (example trace and distribution in Chapter 1, **Fig. 5a**). From a rest epoch in which bimodality was observed, the value at the local minimum separating the two modes was chosen as the SIA (small-irregular activity, see Chapter 1 for description) z-score threshold for the day. SIA periods were defined as non-REM times in which the aggregate LFP amplitude was below the threshold, and LIA (large-irregular activity) otherwise. In a minority of cases, a threshold was chosen to isolate a heavy left tail of the distribution, later verified in the LFP to correspond to SIA periods. SIA thresholds across

all recording days (n = 73 days) were -0.67 ± 0.24 (z-score, mean ± s.d.), and median period durations were SIA: 1.20 s; LIA: 2.48 s; REM: 27 s.

Sleep periods were candidate sleep periods at least 90 s in duration and containing extended (>5 s) continuous LIA periods. Across all recording days, 465 sleep periods (median duration: 218 s) were identified. Non-REM periods were all sleep period times outside of REM periods.
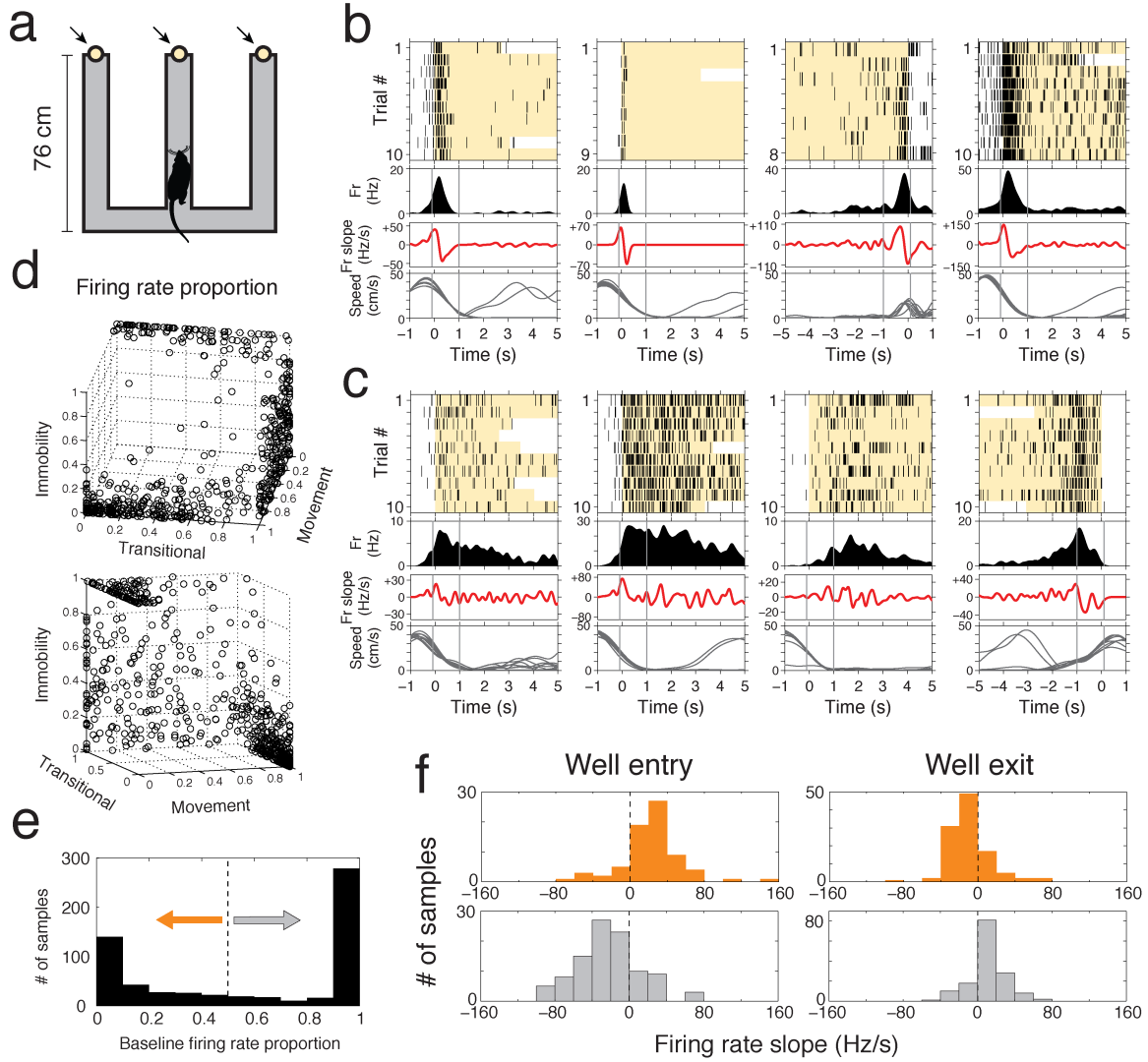
Figure 1

Fig. 1. Non-classical hippocampal firing during behavioral transitions.
a, Diagram of the task maze. Arrows indicate the locations of reward wells. Description of the task is provided in **Fig. S1**.
b, Four examples of units expressing transitional firing (TF). Plots show neural activity and behavior aligned to the time of well entry/exit (t = 0). Each column shows data from one of three reward wells in the task for the final 10 trials, where available, in a task recording epoch. First row: spike rasters. Yellow zones indicate times when the subject was at the well. Second row: peri-event time histogram (PETH). Spike trains were binned in 1-ms vectors and smoothed with a Gaussian (SD: 100 ms) to estimate firing rate (Fr). Third row: firing rate slope, calculated as the first-order differential of the PETH. Fourth row: head speed of the animal. Additional examples and spatial measurement provided in **Fig. S2**.
c, Four examples of units expressing immobility-associated (IA) coding. Plotting conventions are the same as in **b**. Plotted are data from the well for which the unit showed preferential firing. Not shown is firing activity at other wells, which was relatively low[4].
d, Scatter plot of normalized mean firing rates for time periods related to the time of well entry and exit (t = 0). Shown are 614 unit-well samples from 366 units. For well entry, Baseline periods were defined as times -500 to -100 ms, Transitional periods -100 to +1000; for well exit, Baseline periods were +100 to +500 ms, Transitional periods as -1000 to +100. Immobility periods were defined as time periods spent at the well and separated from movements >4 cm/s. For each unit at each well, mean firing rates for each of these time periods were calculated. The firing rate proportion was obtained by normalizing to the highest mean rate in any period type. Only unit-well samples that exceeded a mean rate of 2 Hz in at least one period type were plotted.
e, Histogram of baseline firing rate proportions for hippocampal principal units (n = 614 unit-well samples from 366 units). Baseline period mean firing rate proportions were calculated as in panel **d**. Arrows indicate how unit-well samples were categorized: samples with values <0.5 were classified as non-classical (orange) and classical (grey) otherwise.
f, Histogram of Transitional period firing rate slopes among non-classical (orange) and classical (grey) unit-well samples. Firing rate slope for a unit-well sample was the slope value with the largest magnitude in the well entry/exit transitional period (see Methods for full procedure).
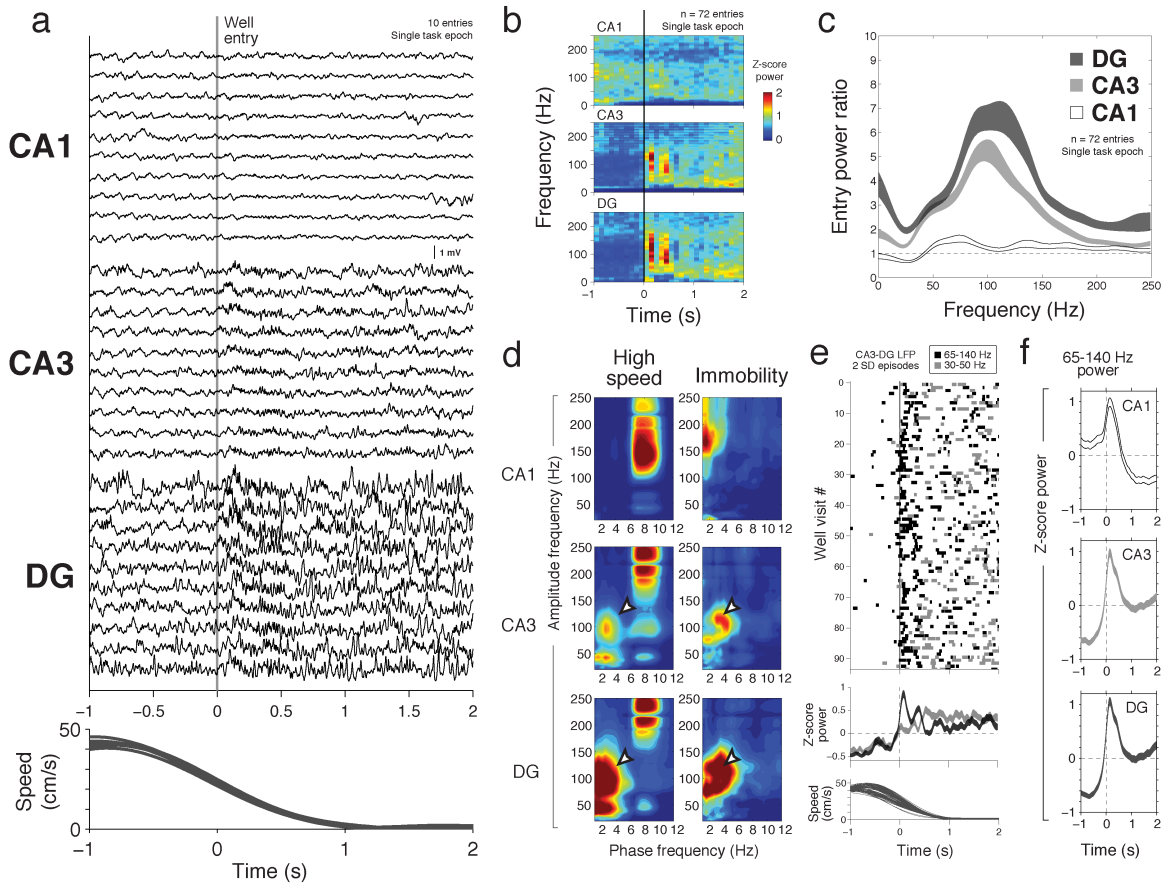
Figure 2

Fig. 2. Transient activation of a high frequency hippocampal rhythm.
Data in **a-c** were from a single 15-minute task recording epoch.
a, Example hippocampal LFP traces at time of well entry. Shown are data from ten consecutive entries at a single well. Recording sites were located in the principal cell layer of the indicated hippocampal subregion. Traces are aligned in consecutive order (top to bottom) within each respective recording site region. At bottom is the head speed of the subject for all ten trials.
b, Spectrogram of LFP at time of well entry. Z-scores were calculated relative to the entire task recording epoch. Individual spectra were calculated in 100-ms non-overlapping windows.
c, Power spectra of LFP at time of well entry. Spectra were calculated for the window immediately prior to (pre, -200 to 0 ms) and after (post, 0 to +200 ms) well entry. Individual spectra were smoothed with a Gaussian window (SD: 8 Hz). Plotted is the mean ratio of post to pre spectra across well entries. Width indicates ± SEM (n = 72 well entries).
d, Cross-frequency coupling in LFP across hippocampal subregions. The modulation index[50] (MI) was used to measure phase-amplitude coupling in the LFP, either for times in which the subject was moving at high speed (>20 cm/s) or immobile (<4 cm/s periods separated 2 s from periods >4cm/s). Data shown is from a single task recording epoch. Arrowheads indicate a distinct high frequency bandwidth (65-140 Hz) in both CA3 and DG. See **Fig. S2** for additional comparison with non-REM sleep.
e, Rhythmic episodes in CA3-DG LFP at time of well entry. Power in LFP filtered at the frequencies indicated was smoothed then averaged across CA3 and DG recording sites. The signal was the z-scored (1 Z = 1 SD) for all times in task recording epochs. Top: rhythmic episodes (2 SD, from power traces smoothed using Gaussian with SD = 4 ms) across trials at a single well. Filled zones indicate times of episodes for either the 65-140 Hz (black) or 30-50 Hz (grey) bandwidths. Middle: z-scored CA3-DG multisite power in each band. Power traces from individual trials were smoothed with a Gaussian window (SD = 40 ms). Bottom: head speed across all trials.
f, LFP power at 65-140 Hz at the time of well entry (t=0) for CA1 (n = 4851 entries), CA3 (n = 4851), and DG (n = 4726) LFP. Data shown are from three subjects with available data in all three subregions. Width of trace indicates ± 5 * SEM. In CA3 and DG, an increase in power in the window -100 to 0 ms versus 0 to +100 ms was extremely significant (p < 10^{-10}, sign-rank). See **Fig. S4** for additional subjects.
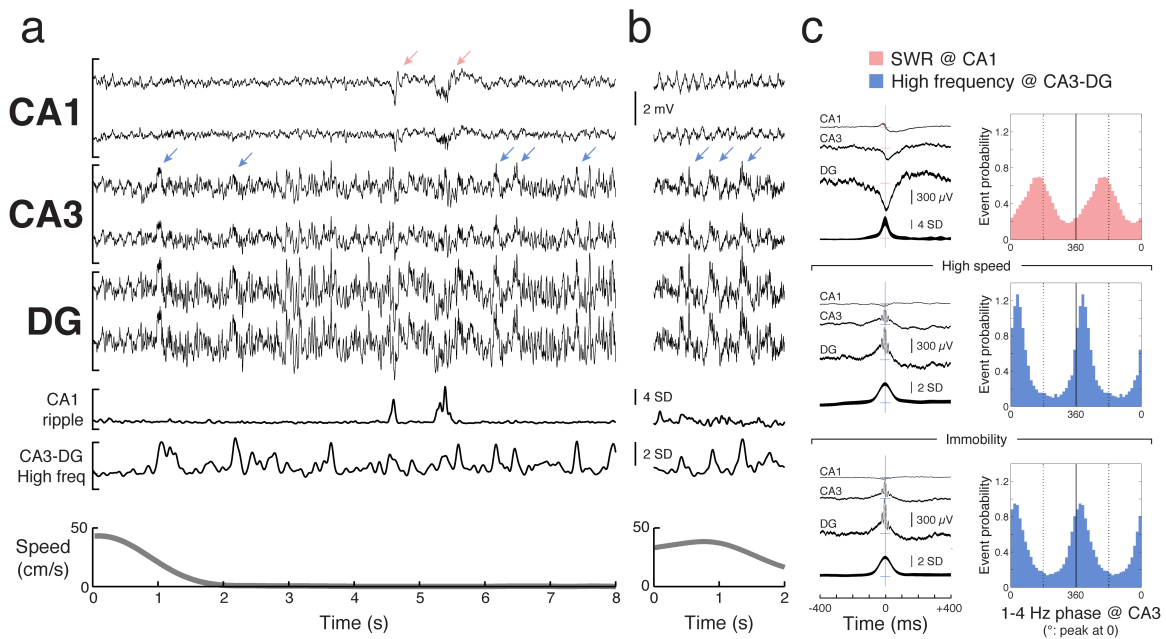
Figure 3

Fig. 3. A transient signature of high frequency activation in CA3 and DG.
a, Example hippocampal LFP during the task. Upper plots: LFP from two distinct recording sites from each hippocampal region. Middle plots: power traces for the ripple band (150-250 Hz) at CA1 recording sites and the high frequency band (65-140 Hz) at CA3-DG recording sites. Lower plot: head speed of the subject. Note slower fluctuations coincident with activation of the higher frequency rhythms (highlighted with arrows: SWRs in pink and high frequency episodes in CA3-DG in blue).
b, Example hippocampal LFP from an extended period of high speed movement. Plotting conventions are the same as in a. Note the presence of similar activity patterns as seen in **a**.
c, Coupling of high frequency rhythms to low frequency waves. Left column: SWR- (top row) and high frequency (65-140 Hz, second and third rows) episode-triggered averages (width indicates ± SEM) of hippocampal LFP. A horizontal bar (60 ms in length) indicates the 0 μV level for each respective LFP average. Below the LFP averages in each group is an averaged power trace (width indicates ± 5 * SEM). Data plotted are from task epochs from a single recording day. Right column, 1-4 Hz phase histogram of SWRs and high frequency episodes. Phase estimated from 1-4 Hz LFP from CA3 LFP. SWRs occurred near troughs (180°) of the low frequency LFP while high frequency episodes occurred near peaks (0° and 360°).

Figure 4
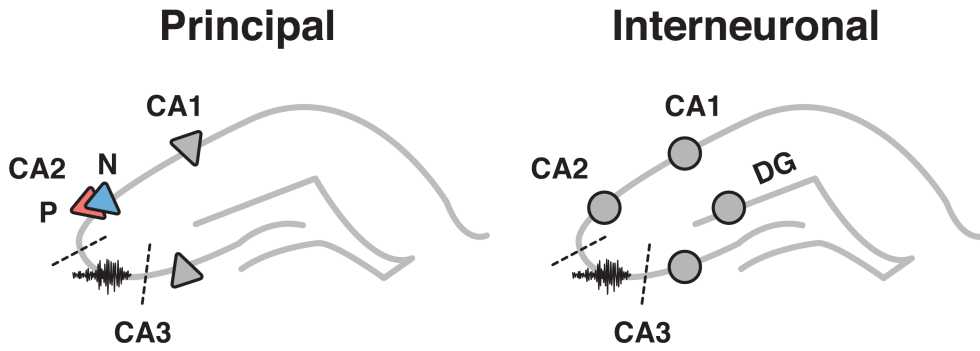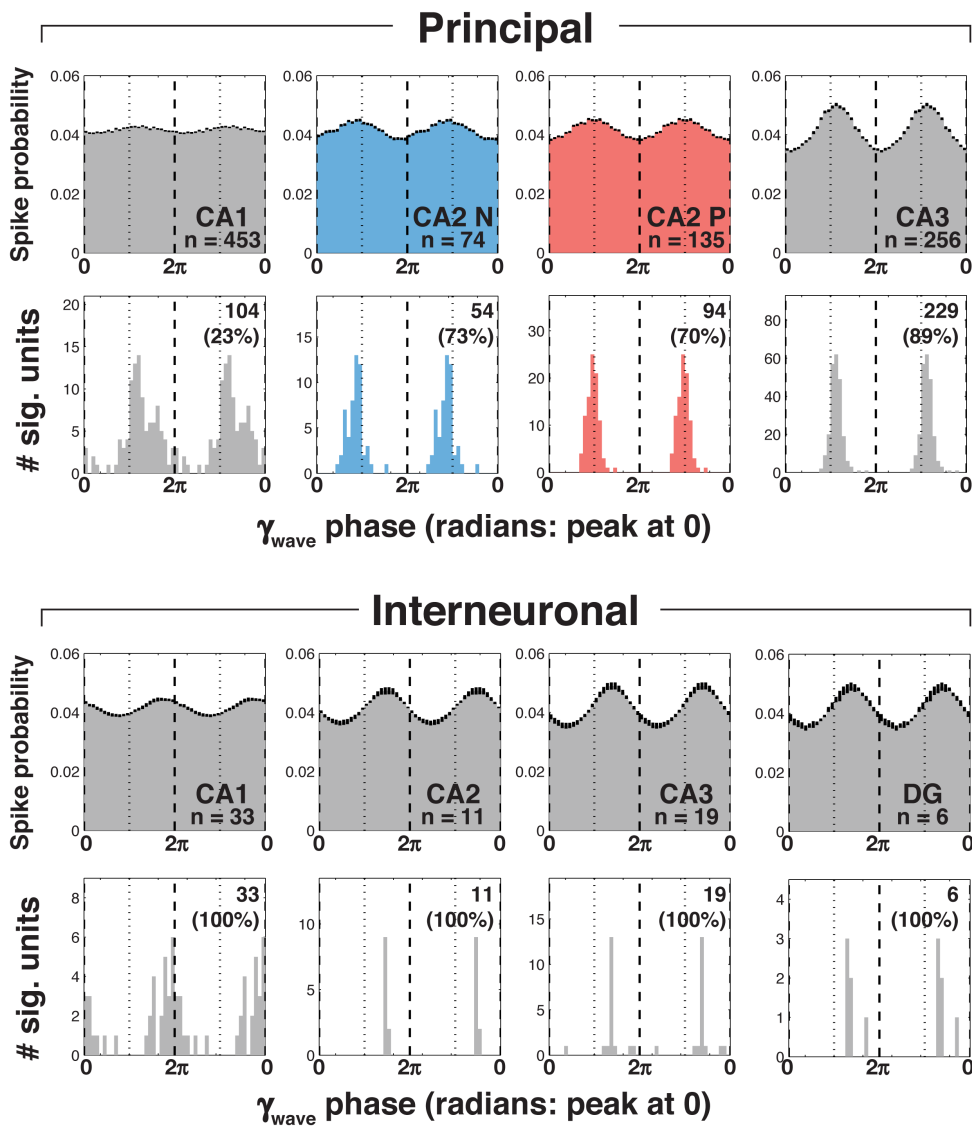
Fig. 4. Widespread high frequency synchronization of the hippocampus.
a, Diagram of the configuration for gamma entrainment analysis. Triangular symbols: putative principal units. Blue and red coloring indicate two CA2 unit types identified in previous work[4]. Circular symbols: interneuronal units. Wave gamma (WG, 65-140 Hz; indicated by trace symbol) phase was estimated from a recording site in CA3 that was spatially separate (> or >> 300 μm) from unit recording sites.
b, Widespread entrainment of hippocampal unit firing by WG. In each group, the first row corresponds to WG phase histograms for unit spiking averaged across units in each unit population (total numbers of units averaged is indicated), while the second row corresponds to mean phases of significantly modulated units (Rayleigh tests, $p < 0.05$; total # of significantly modulated units shown, in addition to the % of units significantly modulated). All spikes in all behavioral states from both task and rest recording epochs were included in the analysis.

Figure 5
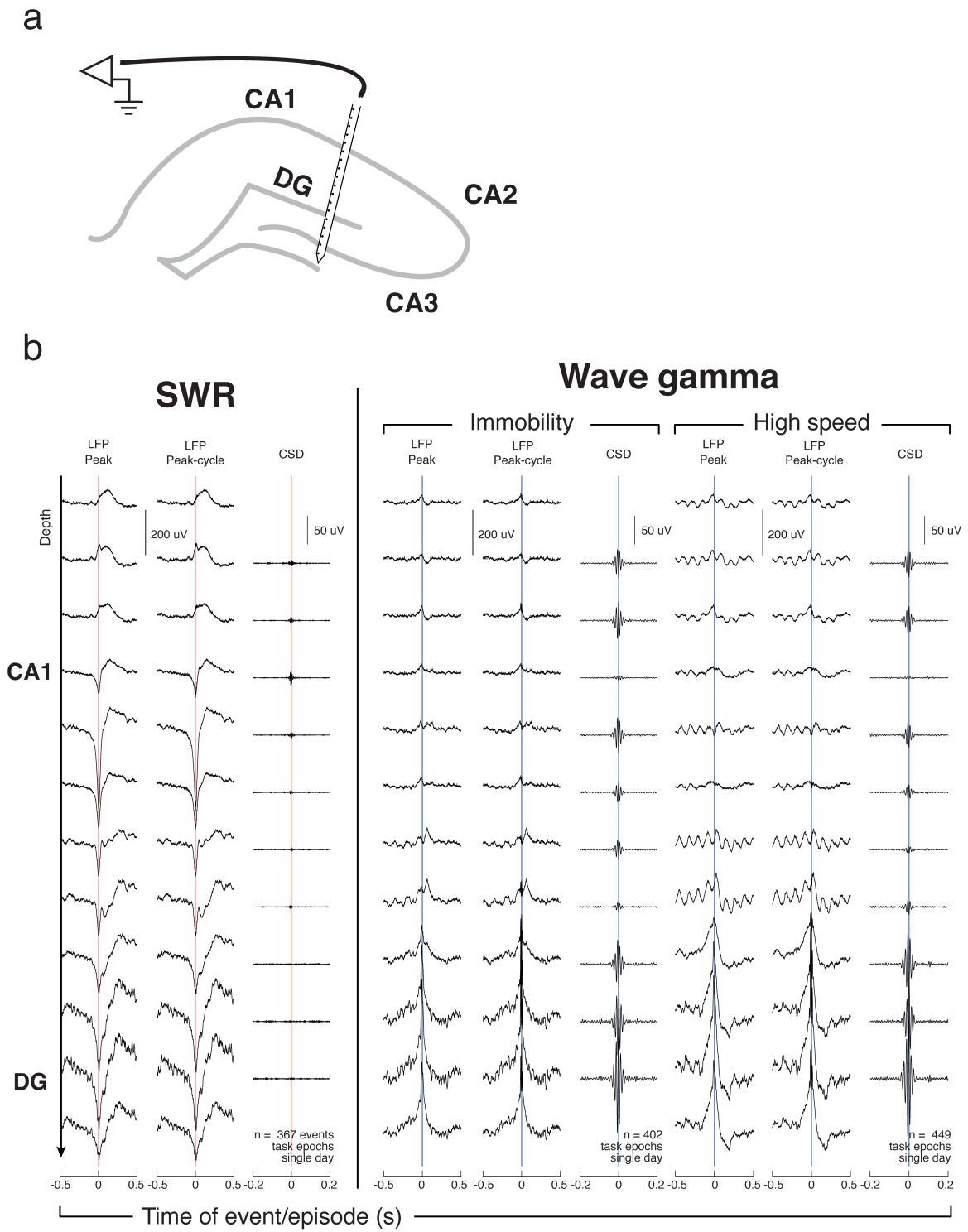
Fig. 5. Anatomical profile of wave gamma.
a, Diagram of recording configuration. LFP was recorded using probes with linearly spaced recording sites (100 μm).
b, SWRs vs. WG activation across hippocampal dendritic layers. Shown are LFP and CSD averages for 2 SD SWRs and WG episodes from task epochs from a single day. Hippocampal subregion indicated at left, next to recording site nearest the principal cell layer of the indicated region. LFP averages were aligned either to the time of peak power ("Peak") of the filtered LFP (SWR: 150-250 Hz at CA1; WG: 65-140 Hz at DG) or time of the trough in filtered LFP nearest the time of peak power ("Peak-cycle"). CSDs were calculated from the center-cycle LFP averages, specifically from filtered LFP. SWRs and WG episodes showed markedly different patterns of activation across dendritic layers.

Figure S1

a

b

c
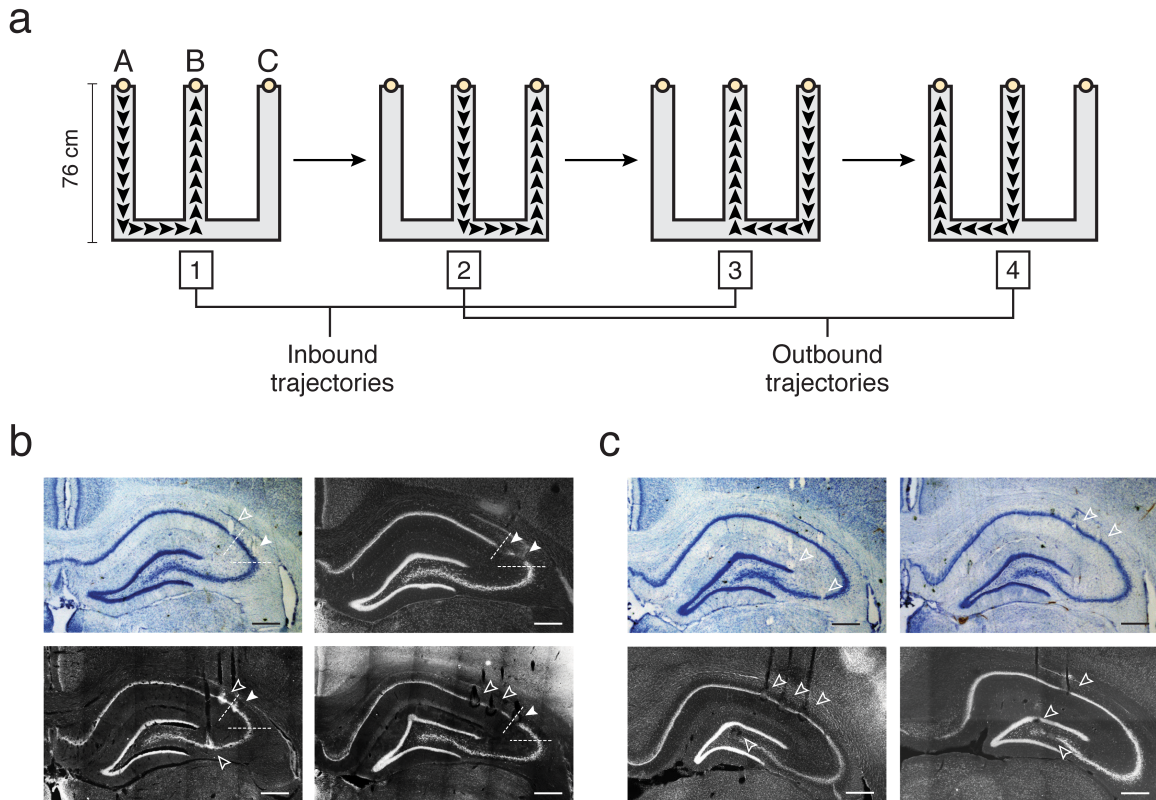
Fig. S1. Behavioral paradigm and recording sites.
a, Continuous spatial alternation task[9,24,53]. The task environment is a W-shaped maze with a center arm and two outer arms. Reward (~0.3 mL of sweetened evaporated milk) is dispensed through 3-cm diameter wells (designated "A," "B," and "C" for reference in data plots), located at the end of each arm. Rats are rewarded for performing the trajectory sequence shown, in which the correct destination after visiting the center well is the less recently visited outer well. All subjects stopped locomoting upon reaching the reward wells to check for (by licking) and consume reward. Subjects also stopped intermittently elsewhere on the track (most frequently at maze junctions), particularly in earlier exposures to the task.
b, **c,** Example hippocampal histological sections showing tetrode tracks and electrolytic lesions in CA1, CA2, CA3, and DG. Nissl-stained sections show neuronal cell bodies in dark blue, while sections stained with Neurotrace show neuronal cell bodies in light grey. Panel **b** shows example sections with sites overlapping with the CA2 cytoarchitectural locus[48,49] (enclosed by dotted lines; characterized by dispersion of the hippocampal cell layer in the region between CA1 and CA3). Filled arrowheads indicate sites overlapping with CA2, while empty arrowheads indicate non-CA2 recording sites. The CA2 site assignment was deliberately inclusive to maximize detection of units at CA2 with distinct physiological responses (N units[4]). Scale bars: 500 μm.

Figure S2

a

b

Example unit 4   Example unit 5   Example unit 6

Well visit #

Firing rate (Hz)

C

Well entry

Well exit
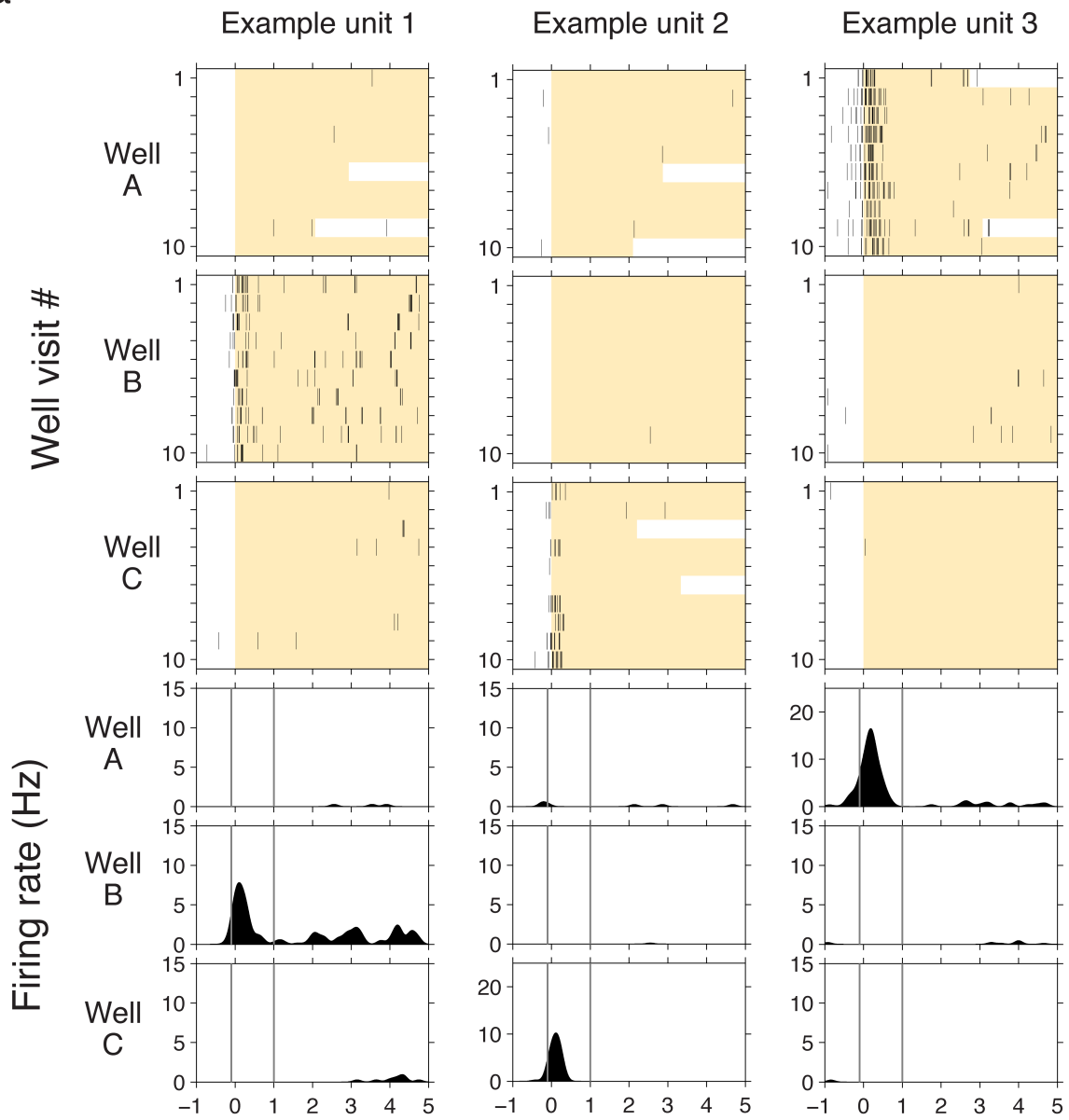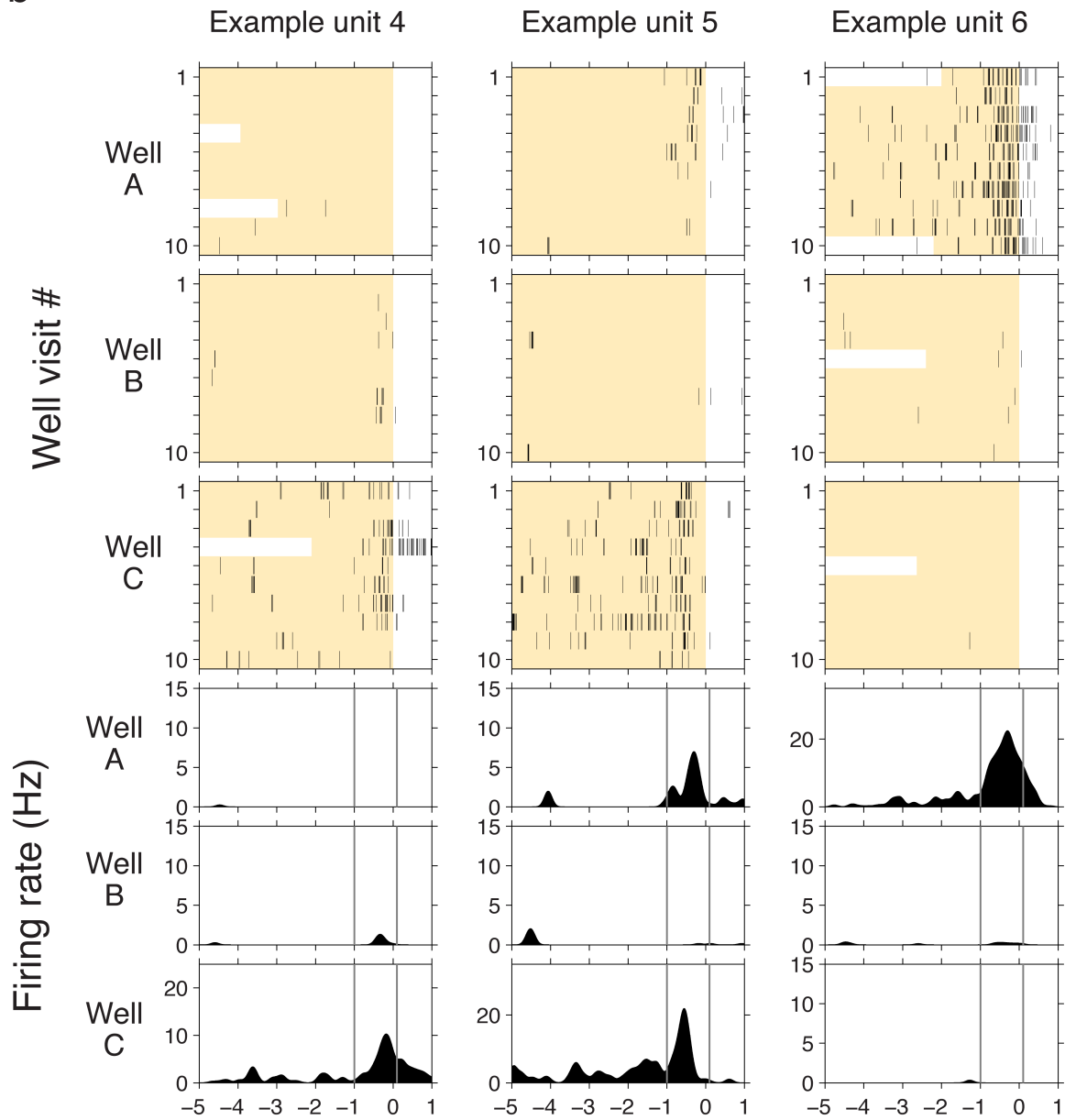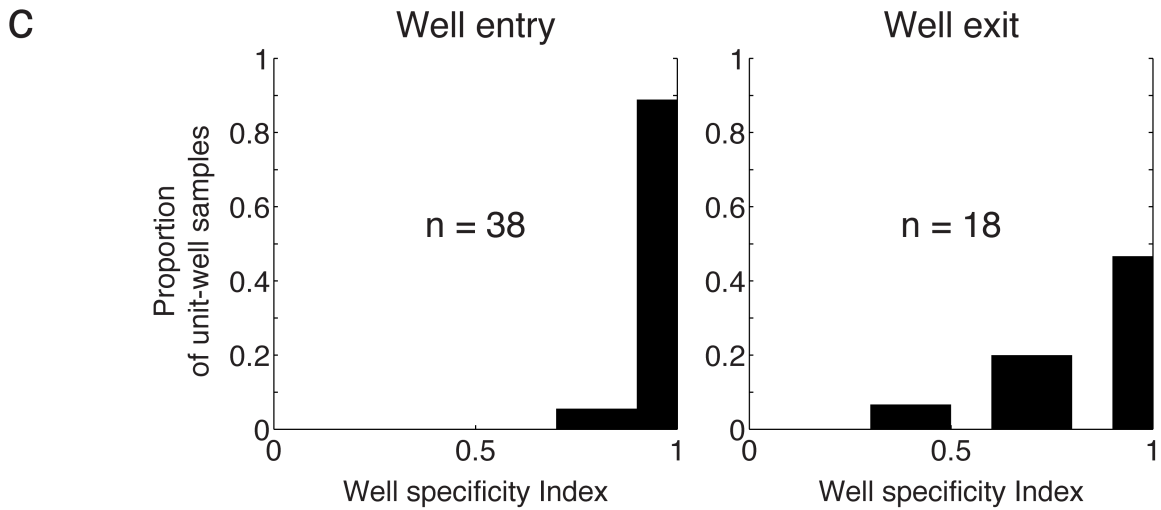
Fig. S2. Transitional firing: non-classical hippocampal spatial coding.
a, Examples of units expressing transitional firing (TF) at well entry (t = 0). Each column corresponds to a unit data from the final 10 trials in a 15-minute task recording epoch. Upper plots: spike rasters. Yellow zones indicate times when the subject was at the well. Lower plots: peri-event time histograms (PETHs). Spike trains were binned in 1-ms vectors and smoothed with a Gaussian window (SD: 100 ms).
b, Examples of units expressing transitional firing (TF) at well exit (t = 0). Plotting conventions are the same as in **a**.
c, Spatial specificity of TF. Well specificity index was calculated as a measure of spatial specificity. See Methods for description.

Figure S3
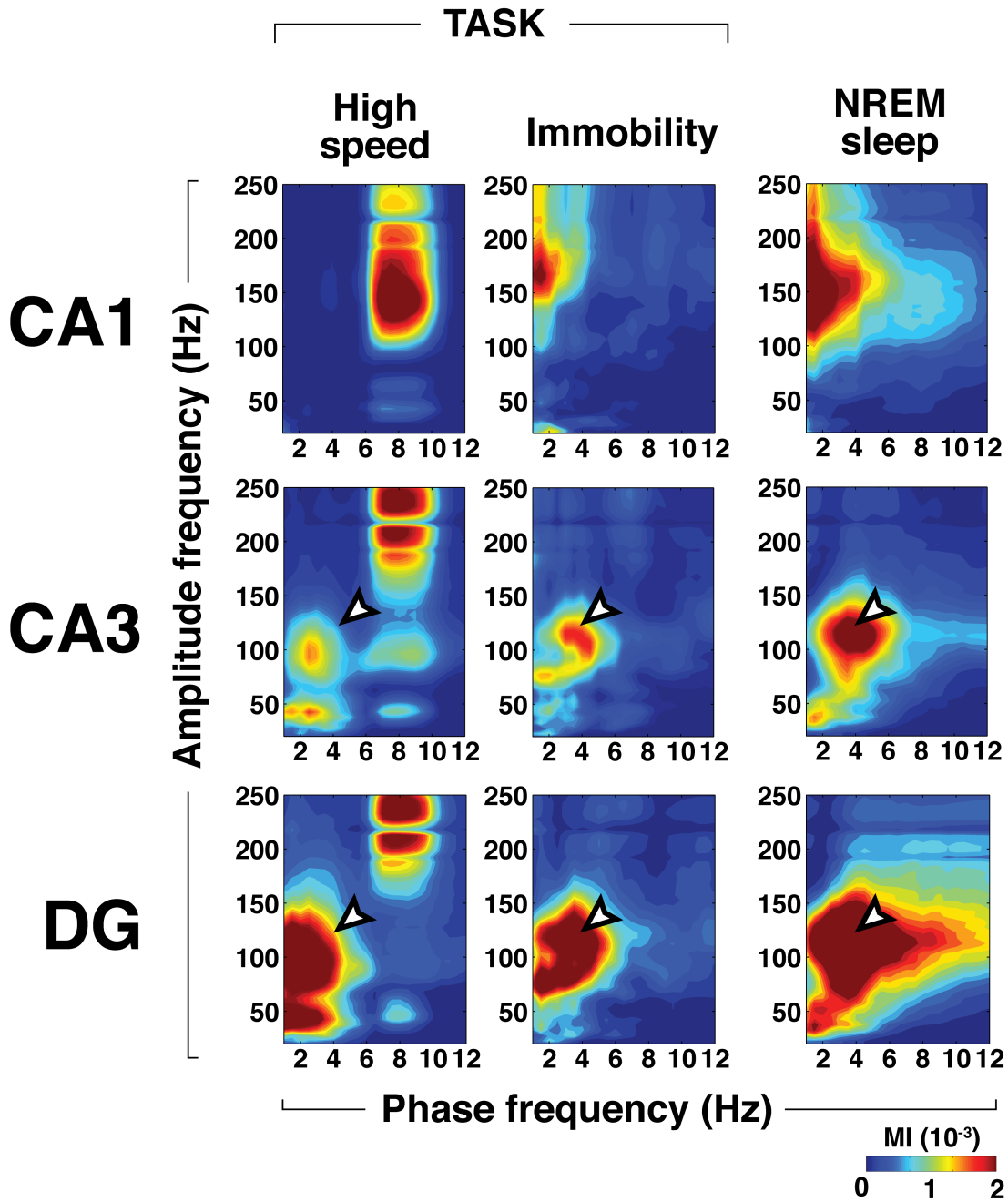
Fig. S3. Identification of a discrete 65-140 Hz rhythm in CA3 and DG.
Cross-frequency coupling in LFP across hippocampal subregions. The modulation index (MI) was used to measure phase-amplitude coupling in the LFP (see Methods). Data analyzed were either in waking behavioral periods (High speed: periods >20 cm/s; Immobility: periods <4 cm/s separated 2 s from periods >4 cm/s) in task epochs (TASK) or non-REM sleep in rest epochs. Arrows indicate a distinct high frequency bandwidth (65-140 Hz) present in LFP in both CA3 and DG, but not CA1.

Figure S4
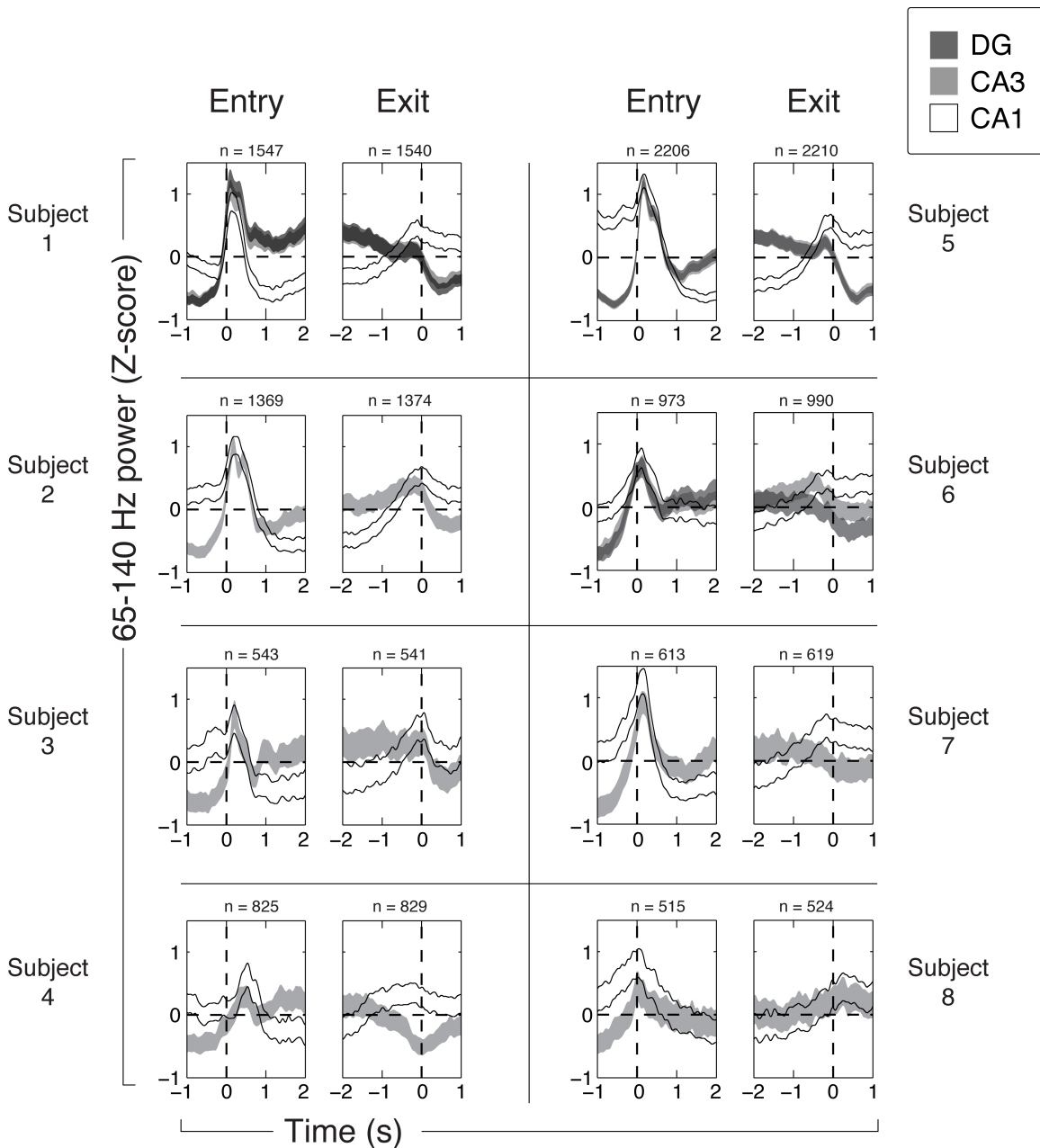
Fig. S4. Rapid activation of a high frequency rhythm.
High frequency (65-140 Hz) power in CA1, CA3, and DG at the time of well entry (first column) and exit (second column) for eight subjects from main study. Width indicates ± 5 * SEM. For well entry, note rapid power increase from below baseline for power in CA3 and DG, but not in CA1.

Chapter 3:
Discussion

Summary of Findings

To investigate the biological basis of cognition, we recorded neural activity in the hippocampus of rats behaving under naturalistic conditions. These were the main findings:

Chapter 1: A hippocampal network for spatial coding during immobility and sleep

1. A distinct population of hippocampal neurons in subregion CA2. These neurons, termed CA2 N units, were defined by an unexpected activity pattern given prior work, namely, a consistent lack of firing during sharp wave-ripples (SWR).

2. Spatially specific neural firing that was more active at rest than during movement. This pattern of activity, expressed by CA2 N units, was unexpected given prior work showing that CA1 and CA3 place cells fire more during movement.

3. The N wave: a ~200 ms hippocampal network pattern detectable in CA3/DG and associated with spatially specific firing during immobility in CA1, CA2, and CA3.

4. Hippocampal coding of sleeping location during sleep. CA1 and CA2 N units were found to signal sleeping location during micro-arousal periods (termed small-irregular activity in the hippocampal literature) that occur during natural sleep. CA3 units surprisingly were not found to code for sleeping location. These findings extend prior work that focused on CA1.

Chapter 2: High frequency network activation marks switch in neural code for space

5. Transitional firing (TF): a spatially specific transient burst of firing at the time of transitions between movement and rest. This firing pattern was distinct from previously characterized forms of hippocampal spatial firing.

6. TF and spatial firing during immobility showed regulation of firing rates that was as rapid as classic hippocampal place firing.

7. Wave gamma (WG): a high frequency network pattern (65-140 Hz) detected in CA3/DG showing precise activation at the time of transitions between movement and rest. WG was characteristically coupled to a transient positive LFP pattern (a ~200 ms "wave").

8. Anatomically widespread entrainment of hippocampal neural firing by WG.
First, all recorded interneuronal units (CA1: 33, CA2: 11, CA3: 19, DG: 6) were found to be entrained by the phase of WG. Second, most putative principal units in CA2 (>70%) and principal units in CA3 (89%) were found to be entrained by the phase of WG. A smaller proportion of CA1 principal units (23%) was entrained.

9. WG showed an anatomical profile of activation suggestive of entorhinal synaptic input to the hippocampus[1,2], in contrast to SWRs, which showed an anatomical profile reflecting primarily CA3 synaptic input[3,4].

On the basis of these experimental findings, we came to these four main conclusions:

1. The hippocampus represents location when subjects are at rest.
2. The hippocampal representation of location at rest is fundamentally different from the hippocampal spatial representation active during movement.
3. The hippocampus precisely coordinates when these distinct spatial representations begin and cease to be active.
4. A distinct network activity pattern originating in CA3 and DG likely mediates this temporally precise regulation of spatial representations.

Below we discuss the implications of these results.

Discussion sections
A. Multiple hippocampal neural codes
B. A distinct mechanism for switching neural codes
C. A neural code for location at rest
D. A neural code for location during sleep
E. Essential input for hippocampal spatial coding
F. Multiple spatial maps in the hippocampus
G. Hippocampal replay
H. Hippocampal sharp wave-ripples
I. Hippocampal gamma
J. Hippocampal subregion CA2
K. Limitations of study

A. Multiple hippocampal neural codes

One of the most remarkable features of the hippocampal neural code is that it fundamentally changes from moment to moment. This fact has been made clear in studies showing that replay events, which code for space radically differently from classic place activity, often occur within seconds of classic place activity[5-9].

In Chapter 1 we show that there exists a hippocampal neural code distinct from both the classic place and replay codes. This claim rests on the properties of a distinct hippocampal neuron population we identified and subsequently termed N units: (1) unlike classical place coding neurons, N units consistently fired more at lower movement speeds, (2) N units did not fire more during SWRs, indicating that N unit firing does not contribute directly to the SWR-associated replay events (see additional discussion below), (3) N unit firing was associated with a network pattern (the N wave) that was distinct from the network patterns known to be associated with classic place and replay activity (theta and SWRs, respectively), (4) unlike both classic place and

replay coding neurons, N units were found predominantly at a distinct anatomical locus (CA2), indicating the existence of a privileged structural correlate.

Furthermore, in Chapter 2, we present evidence of an additional coding pattern in the hippocampus: a transient burst of unit firing upon entry or exit from specific reward wells in a maze. The spatiotemporally restricted nature of this firing pattern indicates a fundamental difference from both the classic place code and the immobility-associated spatial code identified in Chapter 1.

These findings indicate that the hippocampus generates a spatial representation of the world at all times, but for reasons that remain unclear does so by employing different neural codes from moment to moment. We refer to the four identified hippocampal neural spatial codes as the classic place (CP), immobility-associated (IA), transitional firing (TF), and sharp wave-ripple (SWR, or replay) codes. While these neural codes become active in different behavioral states under naturalistic conditions, it is more appropriate to view the regulation of these neural codes as dependent on internal variables within the brain.

The following questions arise:
1.   How does the hippocampus switch between these different neural codes?
2.   What inputs are required for their spatial specificity?
3.   Do downstream neural circuits distinguish between them? If so, how?
4.   What circuit- and behavioral-level functions do they perform?

Note that 1 and 2 refer to "permissive" and "instructive" inputs, respectively.

These questions are variously addressed in the following discussion sections.

B. A distinct mechanism for switching neural codes

In Chapter 2 we investigated whether there exist mechanisms for switching between hippocampal neural codes. We identified a high frequency (65-140 Hz) network pattern that was rapidly activated at the time of the transition from the classic place code (inferred by movement of the subject) to the immobility-associated spatial code. This pattern, which we termed wave gamma (WG), (1) was distinct from well-established hippocampal network patterns (theta and sharp wave-ripples), (2) was associated with hippocampus-wide pattern of dendritic activation suggestive of massively synchronous synaptic input from entorhinal cortex, (3) entrained units in all hippocampal subregions, including an exceptionally large proportion (89%) of CA3 principal units. These properties raise the possibility that WG represents a discrete neural mechanism for inducing an anatomically widespread yet coherent change in neural coding in the hippocampus.

A general note: even within the hippocampal field, the issue of distinct neural codes that are competitively engaged is only beginning to be widely recognized as a question of interest, and moreover mainly as a result of the relatively recent elaboration of the replay neural code.

Research has conventionally focused on the classical place representation. As a consequence, transitional periods have largely been ignored or have been viewed as times when the circuit relaxes from a prior active state[10]. Our identification here of a discrete network pattern active during transitions may therefore broadly motivate further investigation.

The finding that WG activation appears to reflect synchronous input (at the ~200 ms timescale) from entorhinal cortex (EC), a brain region upstream of the hippocampus, provides a potentially critical clue regarding the structural and functional correlates of the WG network pattern. Below I point out some specific implications and areas to address in future work.

First, it should be pointed out that studies of neural activity in entorhinal cortex generally do not analyze activity during immobility, much less during behavioral transitions (though a recent report[11] is an important exception). We suggest that both of these periods be expressly studied in future work.

Second, the timescale of the activation of WG in CA3/DG appears to be ~200 ms (1-4 Hz), suggesting organization of entorhinal neural activity at this timescale. To our knowledge, studies of entorhinal neural activity in the awake animal have not analyzed synchrony at this timescale, instead focusing on theta- (5-11 Hz) and gamma- (30-150 Hz) paced activity during movement[12-17]. We hypothesize that analysis of entorhinal activity will reveal prominent activation at slower timescales, and may, upon identification and characterization, provide further clues about the origin of WG in the hippocampal-entorhinal circuit.

Third, it is now well established that neural representations in entorhinal cortex are strikingly different from neural representations in hippocampus[18-23] – specifically, medial entorhinal cortex (MEC) neurons coding for space include grid cells, head direction cells, and conjunctively coding grid-head direction cells, among others, while neural representations in lateral entorhinal cortex relate to specific objects in an environment. If WG represents input from entorhinal cortex, which particular subdivisions, neurons, and representations of entorhinal cortex are relevant?

The fourth point is that synchronous activation of entorhinal principal neurons as an underlying mechanism of WG appears analogous to the synchronous activation of CA3 principal neurons underlying SWRs. This merits special consideration since each network pattern is associated with rapid activation of a specific hippocampal neural code (WG with TF/IA; SWR with replay), thus suggesting a possible link between global transitions in neural coding and acutely high synchronization of principal neuron ensembles.

Lastly, it is worth mentioning that the matter of how globally directed brain states influence neural coding has in parallel been gaining recognition in studies of neocortex, with prominent recent advances[24-30].

C. A neural code for location at rest

Apart from replay, the study of how space is represented in the mammalian brain has conventionally excluded or minimized periods of behavioral immobility. Replay itself only accounts for a small proportion of time spent immobile (<10%), as it occurs intermittently and in brief SWR-associated bursts[31-34]. Yet periods of awake rest are not only extensive in the daily life of an animal – associated, for instance, with feeding and deliberation – but also an intrinsic part of a wide range of behaviors known to rely on the hippocampus, from spatial navigation itself to defensive and anxiety-related behaviors[10,35-40].

Chapter 1 presents experimental findings that together identify a distinct neural code for location at rest (immobility). Why might the hippocampus have such a code?

As a brain region known to required for spatial navigation[10,39,41,42], the hippocampus might be expected to represent location at rest if only because periods of rest have been observed to be intrinsic to spatial navigation in animals[43-47]. For example, rats exploring a novel environment are known to establish a "home base," that is, a location where the rat frequently revisits and spends a disproportionate amount of time immobile. In this behavioral context, exploratory excursions from the home base are punctuated by full stops, with each excursion eventually terminating in a fast and straight return to home base – an instance of path-integrative behavior known to require the hippocampus. Therefore it might be expected that, over the course of a set of exploratory excursions, the hippocampus accesses or itself maintains a representation of location during stopped periods. Particularly in cue-poor scenarios, such as darkness, in which spatial information is more difficult to infer from external sensory input, a representation of current position during immobility would act to store a previously computed estimate of current position. This example illustrates one ethological scenario of navigation – spatial exploration in a novel setting – for which a representation of location during immobility would be useful, if not essential.

In more explicitly goal-directed navigational paradigms[41,48-52], including paradigms in which subjects benefit from taking efficient and novel routes to previously visited goal locations[53,54], we would expect the hippocampus to represent goal locations when learning (encoding) the navigational task[5,55-57] (and, as an aside, also subsequently in route planning). Importantly, under native conditions, goal locations are characteristically places (such as locations of food, conspecifics, or safety) where animals would be expected to spend relatively more time – in other words, places where subjects would be relatively if not altogether immobile. We therefore would expect a spatial navigational system to represent location during immobility.

Second, the hippocampus has been implicated in the storage of memory for events[10,58-64] (episodic memory). One component of event memory is location: in recalling a particular event we can typically recreate the spatial context and spatial relationships originally present in the remembered experience. This observation implicates spatial representation in the encoding of this type of memory, yet, importantly, encoding of episodic memories is not thought to depend upon the movement state of the subject. Therefore we might expect that the hippocampus

accesses or itself maintains a representation of location regardless of movement state, including during periods of immobility, thus enabling location to be integrated into a memory of an event occurring during immobility.

The third point is a broader version of the previous one. The hippocampus has been proposed to be a continuously active monitoring system ("sentinel") whose neurons and synapses always efficiently encode ongoing experience in case something particularly important happens[49,65,66]. In this view, we would expect the hippocampus to encode experience during periods lacking movement – that is, times when important experiences may, as a matter of course, occur. Indeed, outside of conventional place cell experimental paradigms, studies demonstrating behaviorally relevant unit firing in the hippocampus have been conducted under conditions of immobility[67-71], indicating that the hippocampus is capable of encoding experience without requiring movement.

It is important to note that the overall interpretation of a spatial code specific to immobility merits some caution. First, our findings do not rule out the possibility that the specificity of the neural code to immobility is secondary to other variables. For example, the firing we describe might in fact be related to, or even in some sense elicited by, saliency – in one possible scenario (at least in the maze environment), salience independently of immobility might be a important factor for driving a distinct form of spatial firing, and saliency itself would tend to elicit stopping behavior in the subjects. The second major caveat is more explicitly indicated by the data, namely, that we observed preferential firing during immobility in CA2 N units in the task-maze condition, but not when subjects were in a two-dimensional enclosure and unengaged in a navigational task. Notably, this difference echoes previous findings showing that the spatial firing patterns of place cells often entirely depend on behavioral context (e.g. task structure)[72-81] (see additional discussion below). Future work will need to control for different variables that may contribute to the preferential firing during immobility observed in CA2 N units. The third major caveat is that we cannot claim that the neurons (CA2 N units and N wave-coupled units in CA1 and CA3) studied in Chapter 1, much less hippocampal neurons, are the neurons that are generally responsible for the function of spatial representation during rest. For example, it still remains possible that neurons upstream of the hippocampus are sufficient for animals' ability to track location at rest, while hippocampal neurons that code for location during immobility are not necessary to do so. I propose that the first step towards assessing possibilities such as these is explicit analysis of spatial coding during immobility in spatially tuned neurons outside of the hippocampus.

D. A neural code for location during sleep

In Chapter 1, we presented evidence that CA1 and CA2 N units encode sleeping location ("nesting position" in ethological terms). Specifically, we found that when subjects slept in the spatial firing field of a unit of either of these groups, the unit continuously fired during periods of micro-arousal known in the hippocampal field as small-irregular activity (SIA). Conversely, when

subjects slept outside of the unit's spatial firing field, the unit did not continuously fire during SIA. This overall pattern indicates a location-specific neural code active during periods of SIA – we refer to this in shorthand as the SIA spatial code. Here a remark is in order: this neural code was first established in a set of pioneering reports in the early 2000s[82-84], but has not been studied further since then. These reports provide an overview of past work on SIA and emphasize that SIA is the hippocampal manifestation of a global brain state (marked by widespread desynchronization of neural activity) prevalent in and intrinsic to natural sleep. Broadly, we recommend that future study of neural coding and basic neurophysiology detect and expressly analyze SIA/microarousal activity. Below I briefly discuss some specific points of interest.

The results we present in Chapter 1 extend previous work on hippocampal SIA by implicating a specific structural correlate for the SIA spatial code. This comes from the observation that there exists an anatomically localized hippocampal neuron population (CA2 N units) that participates both in the SIA and IA (immobility-associated) spatial codes, thereby suggesting that SIA coding is expressed in a specific group of neurons that, in a broad sense, represent location during immobility. Furthermore, we also observed a lack of SIA coding in CA3 units. This suggests that there are region-specific circuits for SIA coding in the hippocampus and even possibly beyond the hippocampus. Notably, CA2 is known to provide strong synaptic input to CA1, and also receives strong synaptic input from entorhinal cortex[85-87] (in contrast to CA3, for which the synaptic input to CA2 is dominated by inhibition[87]), suggesting that SIA coding in CA1 might rely on instructive input from the neurons corresponding to CA2 N units, and, moreover, that SIA coding in CA2 N units may rely on instructive input from entorhinal cortex. Clearly, much work remains to be done on the determinants of SIA coding. One intriguing possibility that has been raised[83] is that SIA coding reflects a latent memory trace, originating within the brain, rather than a processed signal originating from the sleeping animal's sensorium. This possible scenario could be implemented in the hippocampal-entorhinal circuit in any number of ways. For example, it may be that the highly recurrent CA2 network[88-91] itself stores a latent memory trace encoding location, and is responsible for reinstating the representation of location in downstream CA1 neurons (and possibly elsewhere) during SIA periods and upon waking. While it is not clear how this would be achieved, it is notable that CA2 neurons project not only to CA1[92], but also possibly substantially to CA3[89,90] and entorhinal cortex[93]. Interestingly, CA1 appears to have a population of principal neurons that receives more synaptic input from CA2 than other principal neurons[94] (deep layer population[95-97]), suggesting a scenario where neurons within the hippocampus and possibly elsewhere are specialized to process CA2 representations. More broadly, it is worth pointing out that memory-based encoding of location, here described for sleep, could in the awake state serve to store a previously computed estimate of position under navigational conditions dependent on path integration (e.g. in darkness with few landmarks; discussed above and further below).

What is the function of SIA coding? One possibility is that SIA coding is the means by which a sleeping animal, upon awaking, can quickly recover its bearings after having been unaware or relatively unreceptive to external stimuli (which may in turn be scant in the sleeping environment). For instance, in a dangerous circumstance interrupting sleep, it may be critical to act rapidly and with knowledge of current location. Another possibility, not mutually exclusive with the first, is that SIA coding influences sleep ("offline") processing, which is in fact known to occur with remarkable representational specificity in the hippocampus (sleep re-activation[98,99] and replay[100-102]).

E. Essential input for local spatial coding in the hippocampus

The previous two sections discuss how findings described in Chapter 1 relate to particular behavioral periods. However, these findings might also bear on the more general question of the neural inputs essential for local (self-location) spatial representation in the hippocampus. This question has motivated decades of experimental and theoretical research, both in the hippocampus and more recently in upstream brain regions[103,104]. The resulting body of work has outlined an answer, but at the same time has led to surprising findings indicating that reinterpretation of past findings will be necessary[105-108]. Here I give a very short synopsis of what we do know ("input classes") and of what remains unclear ("input structures"), followed by discussion of what possible insight is afforded by the findings in this thesis.

What we know is that the hippocampal spatial representation is constructed from three different instructive classes of input: (Class 1) external input (e.g. sensory cues in a given environment)[109,110], (Class 2) internally generated input encoding movement (vestibular, motor, and proprioceptive inputs)[80,111-114], and (Class 3) internally generated input sensitive to or encoding behavioral context (e.g. past experiences, task structure, "cognitive factors")[77,81,115]. In addition, it appears that within the hippocampal circuit there are network mechanisms to ensure that spatial representation is coherent across ensembles of hippocampal neurons[116-122]: these internal mechanisms could be conceptualized as a fourth class of input.

What remains unclear is which brain structures or group of neurons provide these respective classes of input. In fact it still remains unclear what brain structures are essential for spatially specific firing in the hippocampus in a general sense: to date, no manipulation of any particular input to the hippocampus has abolished spatially specific firing in the hippocampus. Given the traditional view of the hippocampus as a "trisynaptic" circuit[39,123,124], earlier attempts to address this question targeted upstream hippocampal regions in this processing chain – namely, the dentate gyrus (DG) and CA3 subregions. Perhaps surprisingly, spatially specific firing in CA1 place cells persisted despite lesioning/inactivation of these upstream hippocampal regions[125-127].

This experimental outcome also appears to be the case in studies lesioning/inactivating medial entorhinal cortex[106,107,128,129] (MEC). The MEC is an exceptional target as it not only provides a major source of cortical synaptic input to the hippocampus[39,130], but also exhibits a

variety of striking spatial firing correlates of its own[18,20,22,103,104,131]. This latter property of MEC has led to the view that spatial firing in the hippocampus derives from MEC input[132-135]. Thus the finding[107,128,129] that spatially specific firing persists in the hippocampus despite MEC lesioning/inactivation is surprising. Notably, this finding follows and complements other findings indicating that MEC and MEC-related inputs (grid and theta-paced input) do not have essential roles in generating spatially specific firing in the hippocampus[105,136-142].

      Input classes. In this thesis, we describe hippocampal spatial firing that does not directly rely on internally generated input encoding movement (Class 2). This point is worth highlighting since a prior study found that spatially specific firing in CA1 place cells was eliminated when animals were not permitted to move themselves and instead were passively moved through an environment[143,144]. This result suggested that place cell firing might in fact require motor-related input correspondent with an animal's preparedness to make limb movements that would displace the animal from its current position ("motor set"). Counter to this possible requirement, we describe spatially specific firing (during immobility) in neurons in CA1, CA2, and CA3 when there was no preparedness of subjects to make translational movements. Rather, the spatial firing seen in these neurons points to the contribution of other input classes. In particular, CA2 N unit spatial firing looks to be particularly dependent on internally generated input encoding behavioral context (Class 3), since these neurons expressed a distinctive firing pattern – higher firing at low speeds – that was dependent on subjects' engagement in a navigational task: when animals were left to rest in an empty box, higher firing at low speeds was not observed. Since this firing pattern is not observed in CA1 and CA3 neurons, its expression in CA2 N units is a special instance of context sensitivity.

      In addition to spatial firing during immobility, the spatial firing seen in CA1 and CA2 N units during sleep (nesting position coding during SIA) is also informative in a particular way. First, as with spatial firing during awake rest, it is evident that internally generated input encoding movement (Class 2) is not essential. The second point is that external input (Class 2) may not be essential either. This is because of the possibility that the hippocampus, during sleep, might not be processing input originating from the subject's sensorium, much less processing sensory input in a way that would renew an internal representation of location. This possibility is plausible given a previous study showing that changing the visual field of sleeping rats did not alter the SIA spatial firing pattern active in a given sleep period[83]. The implication is that the hippocampus (or upstream regions representing location in sleep), instead of processing external sensory input during SIA periods, maintains a persistent memory of the location at which the animal fell asleep. This scenario would demonstrate spatially specific hippocampal coding that is essentially dependent on a cognitive faculty (Class 3), namely memory.

      Taken together, the findings above indicate that spatially specific firing in the hippocampus directly requires neither Class 1 nor Class 2 input. It is also worth pointing out that these findings make this case in rodents (here rats) under drug-free conditions.

Input structures. The immobility-associated spatial firing described in this thesis suggests contributions from specific brain structures. While further experimental work is ultimately necessary, here I offer some speculation with regard to upstream input structures essential for CA2 N unit spatial firing.

First, the overall lack of theta during periods of immobility, the positive correlation between theta power and speed, and the coupling of CA2 N unit firing to a non-theta network pattern (the N wave) together argue against an essential or major role of theta-paced input (i.e. input from either medial septum or MEC). Still, retrograde tracing work shows that both medial septum and MEC project to CA2[94,145,146].

Second, given the predominance of inhibition in the CA3 to CA2 synaptic input[87], as well as the fact that CA3 principal neurons do not consistently fire more at lower speeds and immobility[72,147], it also appears unlikely that CA3 neurons play a critical role in CA2 N unit firing.

Third, DG may have an important role given that excitatory afferents from DG to CA2 have been reported[94]. However, other studies do not report DG input to CA2[146,148].

Lastly, lateral entorhinal cortex (LEC) is a strong candidate for instructive spatial input essential for CA2 N unit firing. While early work suggested a lack of spatial firing in LEC compared to MEC[19], more recent work in object-rich settings has established that LEC neurons encode object-location conjunctions[21,23,149]. This information could be processed by downstream hippocampal neurons to produce a spatially specific representation that is not reliant on MEC input.

With this basic scenario as a starting point, one possibility is that LEC input complements MEC input in that LEC provides the hippocampus with input encoding landmarks (Class 1) while MEC provides input required for hippocampal path integration[42,144] (Class 2). In the context of spatial navigation, LEC and LEC-related inputs could therefore serve to correct accumulated error in the hippocampus' estimate of position (resulting from MEC-based path integration mechanisms)[150,151]. This function might be particularly important at environmental locations where MEC spatial representations might be equivocal (e.g. at an isolated landmark within an otherwise empty two-dimensional setting). While this is entirely speculative, perhaps the CA2 N unit spatial code reflects selection of relatively neutral landmark information proffered by LEC. More specifically, the CA2 N population could selectively represent salient and reliable landmarks suitable for path integration in upcoming navigational excursions. Selected landmark representations might also be used in additional functions, for instance serving as a common anchor for different hippocampal replay events (additional discussion below) or encoding object-place information in an event memory. Under this overall view, the relative non-specificity in the LEC representation of landmarks would be analogous to the relative homogeneity of spatial representations in MEC. To evaluate these and other possibilities, it will be essential to record LEC neurons under navigational conditions.

A general caveat: the above discussion regarding major anatomical structures and their respective contributions to hippocampal spatial coding may be somewhat misleading in that it remains possible that there is no single major anatomical structure that is essentially required for spatially specific firing in the hippocampus.

F. Multiple spatial maps in the hippocampus

In addition to the functional and structural types of input outlined in the previous section, there is also a possible classification of inputs to the hippocampus on the basis of distinct frames of reference exhibited by hippocampal place cells[39,110,115]. This view originates in past work in which external cues were systematically varied and place cells subsequently evaluated for changes in their spatial firing patterns. These experimental manipulations demonstrated that spatial firing fields in simultaneously recorded place cells could anchor to different types of external cues.

Ostensibly, these findings concern landmark-based spatial navigation[10,63,76,152] and also the mechanisms by which spatial maps in the brain are stably aligned in a given environment[110,153-155]. More deeply, they demonstrate that different spatial representations – "maps" in shorthand – in the hippocampus are essentially constructed through internal processes (likely related to memory functions[77,81]). These issues are fundamental to understanding what the hippocampus represents, and therefore are of fundamental concern in understanding complex hippocampal functions. What, then, organizes these distinct spatial maps? Here I highlight a few conclusions from past work, then suggest some considerations for future work in light of the experimental findings in this thesis.

To begin with, prior work illustrates a useful distinction between hippocampal spatial maps anchored to "distal" vs. "local" cues (a recent report in bats[156] is an insightful exception to this convention). Next, distinct hippocampal spatial maps appear thus far to be internally consistent (ensemble coherence[157]). In the context of spatial representation, this means that neurons with overlapping spatial firing fields fire together more than neurons with non-overlapping spatial firing fields. This property is important since it indicates that spatial representation is coherent across the hippocampal anatomical structure (place cells are generally recorded at separate sites across the hippocampus) and coherent in time, making it plausible that downstream neural circuits performing functions requiring spatial information can make use of the activity outputted by the hippocampus. Third, recent experiments show that when two distinct hippocampal spatial maps are immediately relevant to the animal[115,117,158,159], these spatial maps are alternately, rather than simultaneously, active. Alternation between spatial maps appears to occur essentially spontaneously (again implicating mechanisms intrinsic to the brain) and can moreover occur as fast as within a single theta cycle (~125 ms).

In Chapter 2, we present results with some similarity to the findings concerning alternating spatial maps. In specific, we found that distinct neural codes for space (CP, TF, IA

codes), defined in part by the movement speed of the subject, can begin or end within ~1 s. It remains unclear what the relationship is between these neural codes and the distinct spatial maps previously described in the hippocampal place cell literature. By convention, the neural firing evaluated in previous studies establishing distinct spatial maps would, by and large, be considered to be conventional place firing (though in past literature the qualifier "classic" has been used to refer to place cell firing anchored to "distal" cues, namely those cues located farther from the subject) – however, what is actually the case may be even more complex.

Here I point out three possibilities that I suggest should be considered in future work. One is that there may be some consistent relationship between the IA code and a specific type of hippocampal spatial map. For instance, perhaps spatially specific firing in the IA code solely participates in a spatial map (or maps) anchored to local cues.

A second possibility is that different hippocampal spatial maps may correspond with structurally distinct subpopulations of hippocampal neurons. The finding that the CA2 subregion contains a representationally distinct population of neurons (CA2 N units) suggests this might be in case in other populations of neurons. For example, it may be informative to reassess whether ensembles of CA1 and CA3 neurons coherently code for location in a single given environment[6,8], or whether groups of neurons of a single hippocampal subregion[94-96,160,161] participate differentially in different spatial maps.

A third possibility is that there yet may be distinct hippocampal spatial maps that are simultaneously, and not primarily alternately, active. For example, we observed that CA2 N units, which might participate in a distinct spatial map that is active during immobility, could also at times show substantial firing when animals were moving. The precision of the temporal segregation observed between hippocampal neural codes (explored in Chapter 2) and between hippocampal spatial maps may for example exhibit a strong dependence on the learning state of the subject[50,51,119,162-164].

G. Hippocampal replay

Hippocampal replay has been proposed to have critical roles in memory and spatial navigation[33,165,166]. This view relies on the specificity of the replay representation, such that a given replay event corresponds to a specific spatial experience of behavioral relevance. Indeed an accumulating number of studies convincingly demonstrate this property. However, it remains essentially unknown how any particular spatial representation at all is specifically activated in a given replay event. This basic problem is even more unusual in that there are also fundamentally different types of replays (forward vs. reverse replays[5,6,9,167]) that thus far lack empirically driven accounts of their neural implementation. We therefore now seek to identify the instructive neural inputs in the generation of the replay code.

One prominent clue to this problem is that replays tend to represent the recent or immediate experience of a subject[6,9,168]. In particular, replay in awake subjects tends to represent

spatial trajectories that begin from the current location of the animal. This finding suggests that some form of neural input representing current location contributes to replay[7,8]. The observation in Chapter 1 of hippocampal neurons showing spatial coding during immobility raises the possibility that neurons within the hippocampus may play this role. In particular, given the apparent generative role of CA3 in hippocampal replay, and projections from CA2 to both CA1[87,94 92] and CA3[88-91], we suggest that neurons coding for immobility in CA2 and CA3 may contribute to the generation of hippocampal replay events depicting a trajectory beginning at subjects' current location.

Currently, little is known about how CA2 neurons may influence activity in CA3, though it has become clear that the CA2 to CA1 projection is efficacious[85-87,94]. Given that the CA2 N unit population either partially overlaps, or is equivalent to, with the CA2 neuron population (see additional discussion below), these findings are consistent with a scenario in which CA2 neurons have a role in determining which neural representations become active during replays. Experimental evidence along these lines would link two major threads in hippocampal research – local spatial representation and replay representation – and implicate a specific hippocampal structural correlate, namely the CA2 subregion. This would inform our understanding of the relationship between the classic place representation and the replay/SWR representation[7,8,32,169].

H. Sharp wave-ripples

It is also worth re-evaluating sharp wave-ripples[33] (SWRs) apart from their connection to replay – that is, as a circuit-level activity pattern whose mechanisms are not yet fully elucidated. In particular, I suggest here that excitatory synaptic input from CA2 neurons may have a crucial role in eliciting SWRs.

Anatomically, since CA2 neurons project to both CA1 and CA3, two hippocampal regions critical to SWR generation, it is plausible that the putative CA2 neuron populations described in Chapter 1 (CA2 N and CA2 P units) contribute to the generation of SWRs.

Physiologically, CA2 N units were observed to be exceptionally active during immobility (when SWRs characteristically occur), and moreover highly active immediately prior to the onset of certain SWRs (Chapter 1, Figure 1c-d). This temporal profile is consistent with a role in generating SWRs.

Notably, prior work on unit firing during SWRs indicates that principal units in the portion of CA3 nearest CA2 tend to be active earlier during SWRs than the portion of CA3 nearest DG, with CA1 active latest[170]. This anatomical sequence across the transverse axis of the hippocampus has moreover been observed to organize other variables: (1) the degree of recurrent synaptic connections in CA3[90,171], (2) hippocampal gamma phase in CA3[172], (3) the direction of propagation of network bursts in disinhibited hippocampal slices[173], and (4) the degree of pattern completion in CA3 place cell representations across different environments[174,175].

I. Hippocampal gamma

In Chapter 2 we describe a rhythmic hippocampal network pattern (~100 Hz peak frequency, 65-140 Hz bandwidth) that was specifically detectable in CA3 and DG. We termed this pattern "wave gamma" (WG) to reflect its consistent association with a ~200 ms "wave" pattern, its expression within the gamma frequency range, and its anatomically widespread entrainment of hippocampal unit firing. Excellent commentaries and reviews concerning gamma rhythms and oscillatory neural activity in the hippocampus and beyond can be found elsewhere[122,176-183]. Here I mention immediate points of interest regarding WG.

The first point is that recent advances in our understanding of hippocampal gamma rhythms have mainly dealt with gamma rhythms in CA1[14,17,120,184-189]. In contrast, WG is not detectable in CA1 LFP using procedures that readily indicate its activation in CA3/DG. Moreover, WG as yet has no obviously direct relationship to gamma rhythms in CA1.

Second, it is not clear whether WG shares mechanisms with previously described subtypes of hippocampal gamma[14,17,190-194]. Prior work indicates that different these subtypes engage different subsets of hippocampal neurons, indicating non-overlapping circuit mechanisms.

Third, the wave component of WG suggests a burst-like mechanism of generation that may be similar to that of SWRs, but unlike that of previously described hippocampal gammas. While other hippocampal gamma oscillations might also show association with a low-frequency (1-4 Hz) transient wave pattern, our analysis of this coupling via the modulation index indicates that only the high frequency bandwidth of WG (65-140 Hz) is exclusively coupled to low-frequency LFP across behavioral states (movement, immobility, and NREM sleep). On the basis of similarity to a previously described hippocampal network pattern termed dentate spikes[1,2], we suggest that this wave component reflects synchronous synaptic input from entorhinal cortex.

Fourth, it is important to stress that while WG activation was most prominent at the time of behavioral transitions from high to low movement speeds, WG activation also occurred during periods of immobility and during otherwise theta-dominated periods of movement.

Fifth, WG, to our knowledge, exhibits the most widespread phase entrainment of hippocampal unit firing of any high frequency hippocampal network pattern[17]. This is particularly distinct from the hippocampal ripple oscillation (150-250 Hz), which is only phase coherent within limited spatial domains in CA1[195-197] (**Illustration 2**).

J. Hippocampal subregion CA2

It is important to note that it is not clear whether CA2 N units are CA2 principal neurons, though several lines of evidence suggest that this is in fact the case. Here I review some relevant points.

The first is cautionary: namely, that for extracellular recordings in CA2, unlike in CA1 and CA3, there exists no standard criterion to classify principal versus interneuronal units. While this

might not be a major reason for additional caution, studies have found that the CA2 region has a significantly higher density of interneurons and also has unique interneuron subtypes[198,199]. These facts are worth keeping in mind since this means further work is necessary before we can conclusively identify extracellularly recorded CA2 units as principal neurons. On the other hand, we found that CA2 N units had largely similar mean firing rates, spike widths, and levels of bursting as CA1 and CA3 principal units, especially as compared to interneuronal units. These properties have long been validated as discriminative of principal vs. interneuronal unit activity in the hippocampus[15,97,200-208].

The second point is general. Simply, it is that CA2 principal neurons have a markedly distinct set of excitatory synaptic inputs and outputs than CA3 and CA1 neurons[87,93,94,146], suggesting a distinct functional role. This fact does not entail, for instance, a particular representational correlate *in vivo,* but rather raises the possibility that the functional correlates (whether physiological, representational, or behavioral) of CA2 may be fundamentally different from those of CA3 and CA1 neurons.

Third, more specifically, it has been shown in hippocampal slice preparations that CA2 neurons, in sharp contrast to CA1 neurons, receive strong feedforward inhibition as a result of stimulation of CA3 afferents[87] (Schaffer collateral fibers). This finding is noteworthy in light of prior knowledge that CA3 transiently becomes the dominant source of excitatory synaptic input in the hippocampus during the sharp wave-ripple (SWR) network pattern[2-4,170]. Thus, based on these facts alone, we would expect that CA2 neurons would fail to excite or possibly become inhibited when SWRs occur (**Illustration 1**). As we show in Chapter 1, this is precisely the case in the CA2 N unit population, thereby supporting the view that CA2 N units are CA2 neurons.

Fourth, a recent study conducting intracellular recordings *in vivo* showed that three molecularly identified CA2 neurons were hyperpolarized and failed to fire during SWRs[97]. This finding indicates that the CA2 N unit population and CA2 neurons are at least partially overlapping neuron populations.

To resolve the matter, future work will need to sample the SWR responses of a sufficiently large number of molecularly identified CA2 neurons, in addition to hippocampal neurons interspersed with and neighboring CA2 neurons. This latter control is necessary given our observation of both non-SWR-firing (N units) and SWR-firing (P units) neurons at single CA2 recording sites. Currently, CA2 neurons are only conclusively identified using standard neurochemical or genetic markers[92]. In the future, approaches using genetic drivers may prove especially efficient for identifying CA2 neurons in physiological experiments.

It remains possible that there exist CA2 neuron subpopulations that, for example, fire more during SWRs, or show no consistent anti-correlation between firing rate and speed. Indeed recent reports indicate compelling functional heterogeneity in the CA1 principal neuron population[95,96,160,209,210], suggesting that a similar scenario may be the case for principal neurons in other hippocampal subregions.

Importantly, genetic targeting of CA2 neurons has been achieved in mice[94,146]. In one notable study, inactivation of labeled CA2 neurons led to no discernible deficits in an array of conventional behavioral tasks – including standard spatial memory tasks – known to require the hippocampus. Rather, a deficit was found in social memory assays in which subjects are tested on their ability to recognize a previously encountered conspecific. This study suggests that CA2 has a unique role in behavior, and has motivated subsequent assessment of whether CA2 neurons respond to social stimuli[211]. These studies provide important clues about the functional correlates of CA2. At the broadest level, findings along these lines (and others[174,175,212]) suggest that the function of spatial representation, by itself, may be too limited of a concept for more advanced understanding of the hippocampus. On the other hand, the lack of behavioral deficits on conventional spatial memory tasks does not rule out a necessary role of CA2 in spatial cognition under native conditions[146]. In the future, it may be informative to design and apply new behavioral paradigms – in the simplest case, more challenging versions of existing spatial paradigms, or, alternatively, paradigms explicitly involving periods of immobility, particularly during task phases in which subjects must encode their location. Analogously, for physiological studies, a potentially informative approach would be to study neuron responses in CA2 using either spatial paradigms involving immobility or non-spatial paradigms tested under conditions of immobility.

K. Study limitation

There has been no demonstration that any particular spatial representation in the brain – including those described in this thesis – has a role in behavior, much less in particular cognitive faculties. While interventional studies targeting physiological and anatomical markers of spatial representation have been shown to affect behavior[213-215], what is required are manipulations that target spatial representations of specific experiences. Concordantly specific behavioral outcomes as a result of such manipulations would then constitute adequate demonstration. Specificity is critical since without non-targeted spatial representations as a control, it is easy to argue that manipulation of spatially specific neural activity changes behavior due to collateral effects unrelated to spatial representation itself. Interestingly, a recent study has shown that median forebrain bundle stimulation at the time of re-activated spatial firing in sleep was sufficient to bias subsequent behavior to the location represented by the spatial firing[216]. In general, future studies will need to increase the anatomical, temporal, and representational specificity of interventional methods, demonstrate even more specific behavioral outcomes, and target additional types of spatial representations. At the same time, it is also true that the overarching limitation described here can only be overcome with sufficient knowledge of the neural activity in question.

Illustration 1
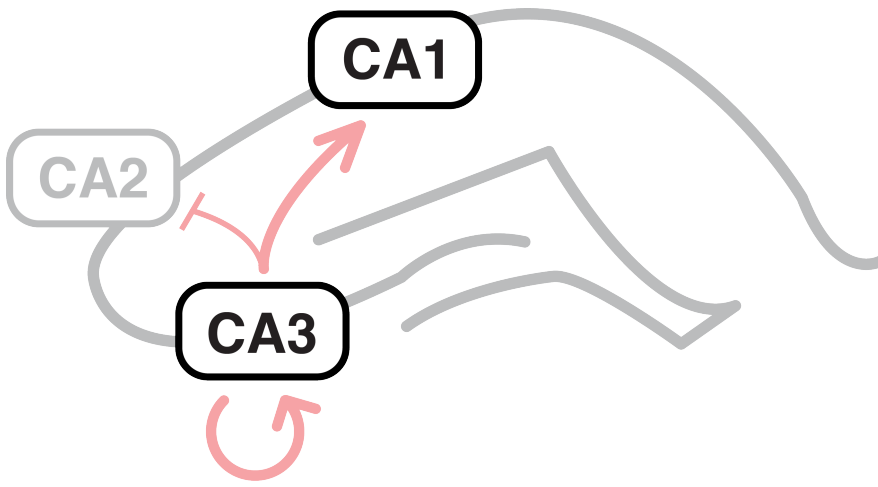
Model of excitatory synaptic input during hippocampal sharp wave-ripples (SWRs).

Illustration 2

Ripple
(~180 Hz)

CA1

CA2

DG

CA3

Wave gamma
(~100 Hz)

CA1

EC

CA2

DG

CA3
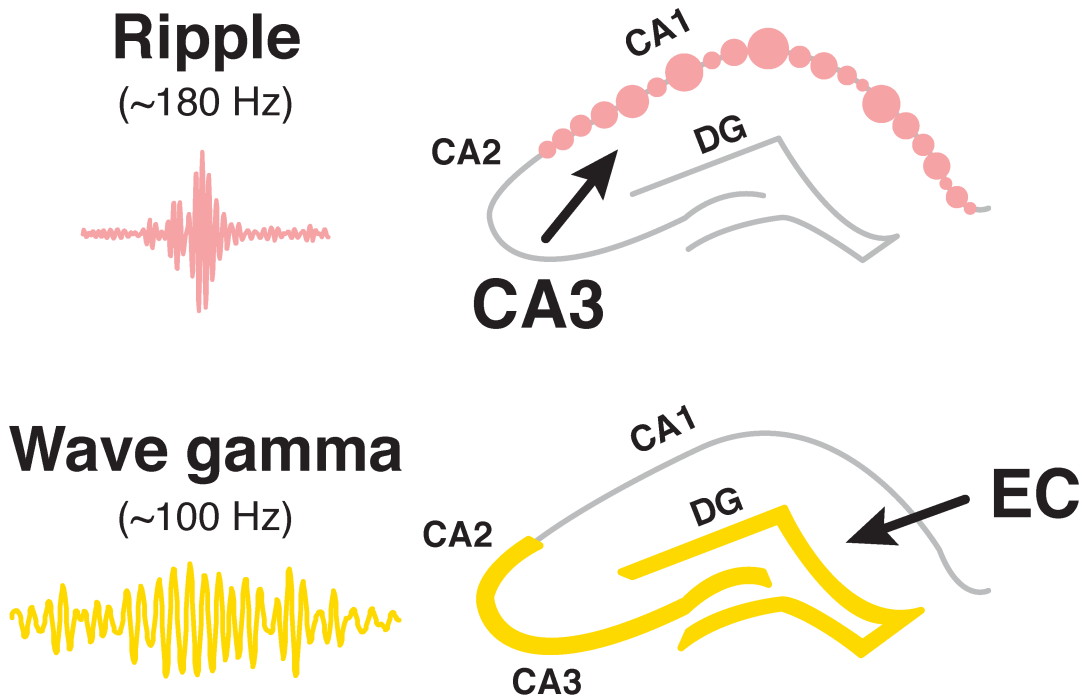
Two high frequency network rhythms in the hippocampus: ripple and wave gamma (WG). Arrows indicate predominant source of synaptic excitation. The ripple pattern becomes active in limited spatial domains in CA1, while WG becomes active synchronously throughout CA2, CA3, and DG, as reflected by widespread phase entrainment of neural units (see Chapter 2).

1   Bragin, A., Jando, G., Nadasdy, Z., van Landeghem, M. & Buzsaki, G. Dentate EEG spikes and associated interneuronal population bursts in the hippocampal hilar region of the rat. J Neurophysiol 73, 1691-1705 (1995).

2   Penttonen, M., Kamondi, A., Sik, A., Acsady, L. & Buzsaki, G. Feed-forward and feed-back activation of the dentate gyrus in vivo during dentate spikes and sharp wave bursts. Hippocampus 7, 437-450 (1997).

3   Buzsáki, G. Hippocampal sharp waves: their origin and significance. Brain research 398, 242-252 (1986).

4   Ylinen, A. *et al.* Sharp wave-associated high-frequency oscillation (200 Hz) in the intact hippocampus: network and intracellular mechanisms. J Neurosci 15, 30-46 (1995).

5   Foster, D. J. & Wilson, M. A. Reverse replay of behavioural sequences in hippocampal place cells during the awake state. Nature 440, 680-683 (2006).

6   Diba, K. & Buzsaki, G. Forward and reverse hippocampal place-cell sequences during ripples. Nat Neurosci 10, 1241-1242 (2007).

7   Csicsvari, J., O'Neill, J., Allen, K. & Senior, T. Place-selective firing contributes to the reverse-order reactivation of CA1 pyramidal cells during sharp waves in open-field exploration. Eur J Neurosci 26, 704-716 (2007).

8   Karlsson, M. P. & Frank, L. M. Awake replay of remote experiences in the hippocampus. Nat Neurosci 12, 913-918 (2009).

9   Davidson, T. J., Kloosterman, F. & Wilson, M. A. Hippocampal replay of extended experience. Neuron 63, 497-507 (2009).

10   O'Keefe, J. & Nadel, L. The hippocampus as a cognitive map. (Oxford University Press, 1978).

11   Olafsdottir, H. F., Carpenter, F. & Barry, C. Coordinated grid and place cell replay during rest. Nat Neurosci (2016).

12   Chrobak, J. J. & Buzsaki, G. Gamma oscillations in the entorhinal cortex of the freely behaving rat. Journal of Neuroscience 18, 388-398 (1998).

13   Hafting, T., Fyhn, M., Bonnevie, T., Moser, M. B. & Moser, E. I. Hippocampus-independent phase precession in entorhinal grid cells. Nature 453, 1248-1252 (2008).

14   Colgin, L. L. *et al.* Frequency of gamma oscillations routes flow of information in the hippocampus. Nature 462, 353-357 (2009).

15   Mizuseki, K., Sirota, A., Pastalkova, E. & Buzsaki, G. Theta oscillations provide temporal windows for local circuit computation in the entorhinal-hippocampal loop. Neuron 64, 267-280 (2009).

16   Deshmukh, S. S., Yoganarasimha, D., Voicu, H. & Knierim, J. J. Theta modulation in the medial and the lateral entorhinal cortices. J Neurophysiol 104, 994-1006 (2010).

17   Schomburg, E. W. *et al.* Theta phase segregation of input-specific gamma patterns in entorhinal-hippocampal networks. Neuron 84, 470-485 (2014).

18   Hafting, T., Fyhn, M., Molden, S., Moser, M. B. & Moser, E. I. Microstructure of a spatial map in the entorhinal cortex. Nature 436, 801-806 (2005).

19   Hargreaves, E. L., Rao, G., Lee, I. & Knierim, J. J. Major dissociation between medial and lateral entorhinal input to dorsal hippocampus. Science 308, 1792-1794 (2005).

20   Sargolini, F. *et al.* Conjunctive representation of position, direction, and velocity in entorhinal cortex. Science 312, 758-762 (2006).

21   Deshmukh, S. S. & Knierim, J. J. Representation of non-spatial and spatial information in the lateral entorhinal cortex. Frontiers in behavioral neuroscience 5, 69 (2011).

22   Krupic, J., Burgess, N. & O'Keefe, J. Neural representations of location composed of spatially periodic bands. Science 337, 853-857 (2012).

23   Tsao, A., Moser, M. B. & Moser, E. I. Traces of experience in the lateral entorhinal cortex. Curr Biol 23, 399-405 (2013).

24   Luczak, A., Bartho, P., Marguet, S. L., Buzsaki, G. & Harris, K. D. Sequential structure of neocortical spontaneous activity in vivo. Proc Natl Acad Sci U S A 104, 347-352 (2007).

25   Fontanini, A. & Katz, D. B. Behavioral states, network states, and sensory response variability. J Neurophysiol 100, 1160-1168 (2008).

26   Niell, C. M. & Stryker, M. P. Modulation of visual responses by behavioral state in mouse visual cortex. Neuron 65, 472-479 (2010).

27   Poulet, J. F., Fernandez, L. M., Crochet, S. & Petersen, C. C. Thalamic control of cortical states. Nat Neurosci 15, 370-372 (2012).

28   Fu, Y. *et al.* A cortical circuit for gain control by behavioral state. Cell 156, 1139-1152 (2014).

29   Reimer, J. *et al.* Pupil fluctuations track fast switching of cortical states during quiet wakefulness. Neuron 84, 355-362 (2014).

30   McGinley, M. J. *et al.* Waking State: Rapid Variations Modulate Neural and Behavioral Responses. Neuron 87, 1143-1161 (2015).

31   Suzuki, S. S. & Smith, G. K. Spontaneous EEG spikes in the normal hippocampus. I. Behavioral correlates, laminar profiles and bilateral synchrony. Electroencephalogr Clin Neurophysiol 67, 348-359 (1987).

32   Buzsaki, G. Two-stage model of memory trace formation: a role for "noisy" brain states. Neuroscience 31, 551-570 (1989).

33   Buzsaki, G. Hippocampal sharp wave-ripple: A cognitive biomarker for episodic memory and planning. Hippocampus 25, 1073-1188 (2015).

34   Kay, K. *et al.* A hippocampal network for spatial coding during immobility and sleep. Nature 531, 185-190 (2016).

35   Gray, A. M. & McNaughton, N. The Neuropsychology of Anxiety: An Enquiry into the Functions of the Septo-hippocampal System. 2nd edn, (Oxford University Press, 2000).

36   Bannerman, D. M. *et al.* Regional dissociations within the hippocampus--memory and anxiety. Neurosci Biobehav Rev 28, 273-283 (2004).

37   Whishaw, I. Q. & Kolb, B. The Behavior of the Laboratory Rat: A Handbook with Tests. (Oxford University Press, 2005).

38   Pentkowski, N. S., Blanchard, D. C., Lever, C., Litvin, Y. & Blanchard, R. J. Effects of lesions to the dorsal and ventral hippocampus on defensive behaviors in rats. Eur J Neurosci 23, 2185-2196 (2006).

39   Andersen, P. in The Hippocampus Book (eds P. Andersen *et al.*) 37-114 (Oxford Univ. Press, 2007).

40   Maren, S., Phan, K. L. & Liberzon, I. The contextual brain: implications for fear conditioning, extinction and psychopathology. Nat Rev Neurosci 14, 417-428 (2013).

41   Morris, R. G., Garrud, P., Rawlins, J. N. & O'Keefe, J. Place navigation impaired in rats with hippocampal lesions. Nature 297, 681-683 (1982).

42   Whishaw, I. Q., McKenna, J. E. & Maaswinkel, H. Hippocampal lesions and path integration. Curr Opin Neurobiol 7, 228-234 (1997).

43   Eilam, D. & Golani, I. Home base behavior of rats (Rattus norvegicus) exploring a novel environment. Behav Brain Res 34, 199-211 (1989).

44   Wallace, D. G., Hamilton, D. A. & Whishaw, I. Q. Movement characteristics support a role for dead reckoning in organizing exploratory behavior. Anim Cogn 9, 219-228 (2006).

45   Tchernichovski, O., Benjamini, Y. & Golani, I. The dynamics of long-term exploration in the rat. Part I. A phase-plane analysis of the relationship between location and velocity. Biol Cybern 78, 423-432 (1998).

46   Drai, D., Kafkafi, N., Benjamini, Y., Elmer, G. & Golani, I. Rats and mice share common ethologically relevant parameters of exploratory behavior. Behav Brain Res 125, 133--140 (2001).

47   Drai, D., Benjamini, Y. & Golani, I. Statistical discrimination of natural modes of motion in rat exploratory behavior. J Neurosci Methods 96, 119-131 (2000).

48   Olton, D. S. & Samuelson, R. J. Remembrance of places passed: spatial memory in rats. J Exp Psychol: Ani.Behav.Proc. 2, 97-116 (1976).

49   Ainge, J. A., van der Meer, M. A., Langston, R. F. & Wood, E. R. Exploring the role of context-dependent hippocampal activity in spatial alternation behavior. Hippocampus. 17, 988-1002 (2007).

50   Dupret, D., O'Neill, J., Pleydell-Bouverie, B. & Csicsvari, J. The reorganization and reactivation of hippocampal maps predict spatial memory performance. Nat Neurosci 13, 995-1002 (2010).

51   Singer, A. C., Carr, M. F., Karlsson, M. P. & Frank, L. M. Hippocampal SWR Activity Predicts Correct Decisions during the Initial Learning of an Alternation Task. Neuron 77, 1163-1173 (2013).

52   Wikenheiser, A. M. & Redish, A. D. in Nat Neurosci Vol. 18 289-294 (2015).

53   Tolman, E. C. Cognitive maps in rats and men. Psychological review 55, 189-208 (1948).

54   Pfeiffer, B. E. & Foster, D. J. Hippocampal place-cell sequences depict future paths to remembered goals. Nature 497, 74-79 (2013).

55   Burgess, N. & O'Keefe, J. Neuronal computations underlying the firing of place cells and their role in navigation. Hippocampus. 6, 749-762 (1996).

56   Redish, A. D. & Touretzky, D. S. The role of the hippocampus in solving the Morris water maze. Neural Comput. 10, 73-111 (1998).

57   Hok, V. *et al.* Goal-related activity in hippocampal place cells. J Neurosci 27, 472-482 (2007).

58   Scoville, W. B. & Milner, B. Loss of recent memory after bilateral hippocampal lesions. J Neurol Neurosurg Psychiatry 20, 11-21 (1957).

59   Tulving, E., Donaldson, W., Bower, G. H. & United States. Office of Naval Research. Organization of memory. (Academic Press, 1972).

60   Squire, L. R. Memory and the hippocampus: a synthesis from findings with rats, monkeys, and humans [published erratum appears in Psychol Rev 1992 Jul;99(3):582]. Psychol.Rev. 99, 195-231 (1992).

61   Tulving, E. & Markowitsch, H. J. Episodic and declarative memory: role of the hippocampus. Hippocampus. 8, 198-204 (1998).

62   Tulving, E. Episodic memory: from mind to brain. Annu Rev Psychol 53, 1-25 (2002).

63   Buzsaki, G. & Moser, E. I. Memory, navigation and theta rhythm in the hippocampal-entorhinal system. Nat Neurosci 16, 130-138 (2013).

64   Miller, J. F. *et al.* Neural activity in human hippocampal formation reveals the spatial context of retrieved memories. Science 342, 1111-1114 (2013).

65   Morris, R. G. & Frey, U. Hippocampal synaptic plasticity: role in spatial learning or the automatic recording of attended experience? Philos Trans R Soc Lond B Biol Sci 352, 1489-1503 (1997).

66   Buzsaki, G. Neural syntax: cell assemblies, synapsembles, and readers. Neuron 68, 362-385 (2010).

67   Takahashi, M., Lauwereyns, J., Sakurai, Y. & Tsukada, M. A code for spatial alternation during fixation in rat hippocampal CA1 neurons. J Neurophysiol 102, 556-567 (2009).

68   MacDonald, C. J., Carrow, S., Place, R. & Eichenbaum, H. Distinct hippocampal time cell sequences represent odor memories in immobilized rats. J Neurosci 33, 14607-14616 (2013).

69   Hattori, S., Chen, L., Weiss, C. & Disterhoft, J. F. Robust hippocampal responsivity during retrieval of consolidated associative memory. Hippocampus 25, 655-669 (2015).

70   Gelbard-Sagiv, H., Mukamel, R., Harel, M., Malach, R. & Fried, I. Internally Generated Reactivation of Single Neurons in Human Hippocampus During Free Recall. Science. (2008).

71   Quiroga, R. Q. Concept cells: the building blocks of declarative memory functions. Nat Rev Neurosci 13, 587-597 (2012).

72   McNaughton, B. L., Barnes, C. A. & O'Keefe, J. The contributions of position, direction, and velocity to single unit activity in the hippocampus of freely-moving rats. Exp Brain Res 52, 41-49 (1983).

73   Breese, C. R., Hampson, R. E. & Deadwyler, S. A. Hippocampal place cells: stereotypy and plasticity. Journal of Neuroscience 9, 1097-1111 (1989).

74   Wiener, S. I., Paul, C. A. & Eichenbaum, H. Spatial and behavioral correlates of hippocampal neuronal activity. Journal of Neuroscience 9, 2737-2763 (1989).

75   Markus, E. J. *et al.* Interactions between location and task affect the spatial and directional firing of hippocampal neurons. J Neurosci 15, 7079-7094 (1995).

76   Gothard, K. M., Skaggs, W. E., Moore, K. M. & McNaughton, B. L. Binding of hippocampal CA1 neural activity to multiple reference frames in a landmark-based navigation task. Journal of Neuroscience 16, 823-835 (1996).

77   Eichenbaum, H., Dudchenko, P., Wood, E., Shapiro, M. & Tanila, H. The hippocampus, memory, and place cells: is it spatial memory or a memory space? Neuron 23, 209-226 (1999).

78   Frank, L. M., Brown, E. N. & Wilson, M. Trajectory encoding in the hippocampus and entorhinal cortex. Neuron 27, 169-178 (2000).

79   Wood, E. R., Dudchenko, P. A., Robitsek, R. J. & Eichenbaum, H. Hippocampal neurons encode information about different types of memory episodes occurring in the same location. Neuron 27, 623-633 (2000).

80   Aghajan, Z. M. *et al.* Impaired spatial selectivity and intact phase precession in two-dimensional virtual reality. Nat Neurosci 18, 121-128 (2015).

81   Eichenbaum, H. in Hippocampal place fields: relevance to learning and memory (ed S. Mizumori) 409 p. (Oxford University Press, 2008).

82   Jarosiewicz, B., McNaughton, B. L. & Skaggs, W. E. Hippocampal population activity during the small-amplitude irregular activity state in the rat. J Neurosci 22, 1373-1384 (2002).

83   Jarosiewicz, B. & Skaggs, W. E. Hippocampal place cells are not controlled by visual input during the small irregular activity state in the rat. J Neurosci 24, 5070-5077 (2004).

84   Jarosiewicz, B. & Skaggs, W. E. Level of arousal during the small irregular activity state in the rat hippocampal EEG. J Neurophysiol 91, 2649-2657 (2004).

85   Bartesaghi, R. & Gessi, T. Parallel activation of field CA2 and dentate gyrus by synaptically elicited perforant path volleys. Hippocampus 14, 948-963 (2004).

86   Bartesaghi, R., Migliore, M. & Gessi, T. Input-output relations in the entorhinal cortex-dentate-hippocampal system: Evidence for a non-linear transfer of signals. Neuroscience 142, 247-265 (2006).

87   Chevaleyre, V. & Siegelbaum, S. A. Strong CA2 pyramidal neuron synapses define a powerful disynaptic cortico-hippocampal loop. Neuron 66, 560-572 (2010).

88   Lorente de Nó, R. Studies on the structure of the cerebral cortex. II. Continuation of the study of the ammonic system. J Psychol Neurol 46, 113-177 (1934).

89   Tamamaki, N., Abe, K. & Nojyo, Y. Three-dimensional analysis of the whole axonal arbors originating from single CA2 pyramidal neurons in the rat hippocampus with the aid of a computer graphic technique. Brain Res 452, 255-272 (1988).

90   Ishizuka, N., Weber, J. & Amaral, D. G. Organization of intrahippocampal projections originating from CA3 pyramidal cells in the rat. J Comp Neurol 295, 580-623 (1990).

91   Mercer, A., Trigg, H. L. & Thomson, A. M. Characterization of neurons in the CA2 subfield of the adult rat hippocampus. J Neurosci 27, 7329-7338 (2007).

92   Dudek, S. M., Alexander, G. M. & Farris, S. Rediscovering area CA2: unique properties and functions. Nat Rev Neurosci 17, 89-102 (2016).

93   Rowland, D. C. et al. Transgenically targeted rabies virus demonstrates a major monosynaptic projection from hippocampal area CA2 to medial entorhinal layer II neurons. J Neurosci 33, 14889-14898 (2013).

94   Kohara, K. et al. Cell type-specific genetic and optogenetic tools reveal hippocampal CA2 circuits. Nat Neurosci 17, 269-279 (2014).

95   Mizuseki, K., Diba, K., Pastalkova, E. & Buzsaki, G. Hippocampal CA1 pyramidal cells form functionally distinct sublayers. Nat Neurosci 14, 1174-1181 (2011).

96   Lee, S. H. et al. Parvalbumin-positive basket cells differentiate among hippocampal pyramidal cells. Neuron 82, 1129-1144 (2014).

97   Valero, M. et al. Determinants of different deep and superficial CA1 pyramidal cell dynamics during sharp-wave ripples. Nat Neurosci 18, 1281-1290 (2015).

98   Pavlides, C. & Winson, J. Influences of Hippocampal Place Cell Firing in the Awake State on the Activity of These Cells during Subsequent Sleep Episodes. Journal of Neuroscience 9, 2907-2918 (1989).

99   Wilson, M. A. & McNaughton, B. L. Reactivation of hippocampal ensemble memories during sleep. Science 265, 676-679 (1994).

100   Skaggs, W. E. & McNaughton, B. L. Replay of neuronal firing sequences in rat hippocampus during sleep following spatial experience. Science 271, 1870-1873 (1996).

101   Nadasdy, Z., Hirase, H., Czurko, A., Csicsvari, J. & Buzsaki, G. Replay and time compression of recurring spike sequences in the hippocampus. J Neurosci 19, 9497-9507 (1999).

102   Lee, A. K. & Wilson, M. A. Memory of sequential experience in the hippocampus during slow wave sleep. Neuron 36, 1183-1194 (2002).

103   Moser, E. I., Kropff, E. & Moser, M. B. Place Cells, Grid Cells, and the Brain's Spatial Representation System. Annu Rev Neurosci 19 (2008).

104   Hartley, T., Lever, C., Burgess, N. & O'Keefe, J. Space in the brain: how the hippocampal formation supports spatial cognition. Philos Trans R Soc Lond B Biol Sci 369, 20120510 (2014).

105   Brandon, M. P., Koenig, J., Leutgeb, J. K. & Leutgeb, S. New and distinct hippocampal place codes are generated in a new environment during septal inactivation. Neuron 82, 789-796 (2014).

106   Hales, J. B. *et al.* Medial entorhinal cortex lesions only partially disrupt hippocampal place cells and hippocampus-dependent place memory. Cell reports 9, 893-901 (2014).

107   Schlesiger, M. I. *et al.* The medial entorhinal cortex is necessary for temporal organization of hippocampal neuronal activity. Nat Neurosci 18, 1123-1132 (2015).

108   Sanders, H., Renno-Costa, C., Idiart, M. & Lisman, J. Grid Cells and Place Cells: An Integrated View of their Navigational and Memory Function. Trends Neurosci 38, 763-775 (2015).

109   O'Keefe, J. & Conway, D. H. Hippocampal place units in the freely moving rat: why they fire where they fire. Exp Brain Res 31, 573-590 (1978).

110   Knierim, J. J. & Hamilton, D. A. Framing spatial cognition: neural representations of proximal and distal frames of reference and their roles in navigation. Physiol Rev 91, 1245-1279 (2011).

111   McNaughton, B. L. *et al.* Deciphering the hippocampal polyglot: the hippocampus as a path integration system. J Exp Biol 199, 173-185 (1996).

112   Gothard, K. M., Skaggs, W. E. & McNaughton, B. L. Dynamics of mismatch correction in the hippocampal ensemble code for space: interaction between path integration and environmental cues. Journal of Neuroscience 16, 8027-8040 (1996).

113   Terrazas, A. *et al.* Self-motion and the hippocampal spatial metric. J Neurosci 25, 8085-8096 (2005).

114   Chen, G., King, J. A., Burgess, N. & O'Keefe, J. How vision and movement combine in the hippocampal place code. Proc Natl Acad Sci U S A 110, 378-383 (2013).

115   Kelemen, E. & Fenton, A. A. Coordinating different representations in the hippocampus. Neurobiol Learn Mem 129, 50-59 (2016).

116   O'Keefe, J. & Recce, M. L. Phase relationship between hippocampal place units and the EEG theta rhythm. Hippocampus 3, 317-330 (1993).

117   Jezek, K., Henriksen, E. J., Treves, A., Moser, E. I. & Moser, M. B. Theta-paced flickering between place-cell maps in the hippocampus. Nature 478, 246-249 (2011).

118   Carr, M. F., Karlsson, M. P. & Frank, L. M. Transient slow gamma synchrony underlies hippocampal memory replay. Neuron 75, 700-713 (2012).

119   Dupret, D., O'Neill, J. & Csicsvari, J. Dynamic reconfiguration of hippocampal interneuron circuits during spatial learning. Neuron 78, 166-180 (2013).

120   Pfeiffer, B. E. & Foster, D. J. Autoassociative dynamics in the generation of sequences of hippocampal place cells. Science 349, 180-183 (2015).

121   Feng, T., Silva, D. & Foster, D. J. Dissociation between the experience-dependent development of hippocampal theta sequences and single-trial phase precession. J Neurosci 35, 4890-4902 (2015).

122   Colgin, L. L. Rhythms of the hippocampal network. Nat Rev Neurosci 17, 239-249 (2016).

123   Andersen, P., Holmqvist, B. & Voorhoeve, P. E. Excitatory synapses on hippocampal apical dendrites activated by entorhinal stimulation. Acta physiologica Scandinavica 66, 461-472 (1966).

124   Amaral, D. G. & Witter, M. P. The three-dimensional organization of the hippocampal formation: a review of anatomical data. Neuroscience 31, 571-591 (1989).

125   McNaughton, B. L., Barnes, C. A., Meltzer, J. & Sutherland, R. J. Hippocampal granule cells are necessary for normal spatial learning but not for spatially-selective pyramidal cell discharge. Exp Brain Res 76, 485-496 (1989).

126   Brun, V. H. *et al.* Place cells and place recognition maintained by direct entorhinal-hippocampal circuitry. Science 296, 2243-2246 (2002).

127   Nakashiba, T., Buhl, D. L., McHugh, T. J. & Tonegawa, S. Hippocampal CA3 output is crucial for ripple-associated reactivation and consolidation of memory. Neuron 62, 781-787 (2009).

128   Brun, V. H. *et al.* Impaired spatial representation in CA1 after lesion of direct input from entorhinal cortex. Neuron 57, 290-302 (2008).

129   Suh, J., Rivest, A. J., Nakashiba, T., Tominaga, T. & Tonegawa, S. Entorhinal cortex layer III input to the hippocampus is crucial for temporal association memory. Science 334, 1415-1420 (2011).

130   Witter, M. P., Groenewegen, H. J., Lopes da Silva, F. H. & Lohman, A. H. Functional organization of the extrinsic and intrinsic circuitry of the parahippocampal region. Prog Neurobiol 33, 161-253 (1989).

131   Solstad, T., Boccara, C. N., Kropff, E., Moser, M. B. & Moser, E. I. Representation of geometric borders in the entorhinal cortex. Science 322, 1865-1868 (2008).

132   de, A. L., Idiart, M. & Lisman, J. E. The input-output transformation of the hippocampal granule cells: from grid cells to place fields. J Neurosci 29, 7504-7512 (2009).

133   Cheng, S. & Frank, L. M. The structure of networks that produce the transformation from grid cells to place cells. Neuroscience 197, 293-306 (2011).

134   Monaco, J. D. & Abbott, L. F. Modular realignment of entorhinal grid cell activity as a basis for hippocampal remapping. J Neurosci 31, 9414-9425 (2011).

135   Lu, L. *et al.* Impaired hippocampal rate coding after lesions of the lateral entorhinal cortex. Nat Neurosci 16, 1085-1093 (2013).

136   Mizumori, S. J., McNaughton, B. L., Barnes, C. A. & Fox, K. B. Preserved spatial coding in hippocampal CA1 pyramidal cells during reversible suppression of CA3c output: evidence for pattern completion in hippocampus. J Neurosci 9, 3915-3928 (1989).

137   Ulanovsky, N. & Moss, C. F. Hippocampal cellular and network activity in freely moving echolocating bats. Nat Neurosci 10, 224-233 (2007).

138   Wills, T. J., Cacucci, F., Burgess, N. & O'Keefe, J. Development of the hippocampal cognitive map in preweanling rats. Science 328, 1573-1576 (2010).

139   Langston, R. F. *et al.* Development of the spatial representation system in the rat. Science 328, 1576-1580 (2010).

140   Koenig, J., Linder, A. N., Leutgeb, J. K. & Leutgeb, S. The spatial periodicity of grid cells is not sustained during reduced theta oscillations. Science 332, 592-595 (2011).

141   Brandon, M. P. *et al.* Reduction of theta rhythm dissociates grid cell spatial periodicity from directional tuning. Science 332, 595-599 (2011).

142   Yartsev, M. M. & Ulanovsky, N. Representation of three-dimensional space in the hippocampus of flying bats. Science 340, 367-372 (2013).

143   Foster, T. C., Castro, C. A. & McNaughton, B. L. Spatial selectivity of rat hippocampal neurons: dependence on preparedness for movement. Science 244, 1580-1582 (1989).

144   McNaughton, B. L., Battaglia, F. P., Jensen, O., Moser, E. I. & Moser, M. B. Path integration and the neural basis of the 'cognitive map'. Nat Rev Neurosci 7, 663-678 (2006).

145   Cui, Z., Gerfen, C. R. & Young, W. S., 3rd. Hypothalamic and other connections with dorsal CA2 area of the mouse hippocampus. J Comp Neurol 521, 1844-1866 (2013).

146   Hitti, F. L. & Siegelbaum, S. A. The hippocampal CA2 region is essential for social memory. Nature 508, 88-92 (2014).

147   Zheng, C., Bieri, K. W., Trettel, S. G. & Colgin, L. L. The relationship between gamma frequency and running speed differs for slow and fast gamma rhythms in freely behaving rats. Hippocampus (2015).

148   San Antonio, A., Liban, K., Ikrar, T., Tsyganovskiy, E. & Xu, X. Distinct physiological and developmental properties of hippocampal CA2 subfield revealed by using anti-Purkinje cell protein 4 (PCP4) immunostaining. J Comp Neurol 522, 1333-1354 (2014).

149   Deshmukh, S. S. in Space, Time, and Memory in the Hippocampal Formation (eds Dori Derdikman & James J. Knierim) viii, 571 pages (Springer Verlag Wien, 2014).

150   Burak, Y. & Fiete, I. R. Accurate path integration in continuous attractor network models of grid cells. PLoS Comput Biol 5, e1000291 (2009).

151   Hardcastle, K., Ganguli, S. & Giocomo, L. M. Environmental boundaries as an error correction mechanism for grid cells. Neuron 86, 827-839 (2015).

152   Gallistel, C. R. The organization of learning. (MIT Press, 1990).

153   Fyhn, M., Hafting, T., Treves, A., Moser, M. B. & Moser, E. I. Hippocampal remapping and grid realignment in entorhinal cortex. Nature. 446, 190-194 (2007).

154   Stensola, T., Stensola, H., Moser, M. B. & Moser, E. I. Shearing-induced asymmetry in entorhinal grid cells. Nature 518, 207-212 (2015).

155   Krupic, J., Bauza, M., Burton, S., Barry, C. & O'Keefe, J. Grid cell symmetry is shaped by environmental geometry. Nature 518, 232-235 (2015).

156   Geva-Sagiv, M., Romani, S., Las, L. & Ulanovsky, N. Hippocampal global remapping for different sensory modalities in flying bats. Nat Neurosci (2016).

157   Jackson, J. C. & Redish, A. D. Detecting dynamical changes within a simulated neural ensemble using a measure of representational quality. Network.14, 629-645 (2003).

158   Jackson, J. & Redish, A. D. Network dynamics of hippocampal cell-assemblies resemble multiple spatial maps within single tasks. Hippocampus 17, 1209-1229 (2007).

159   Kelemen, E. & Fenton, A. A. Dynamic grouping of hippocampal neural activity during cognitive control of two spatial frames. PLoS.Biol. 8, e1000403 (2010).

160   Graves, A. R. *et al.* Hippocampal pyramidal neurons comprise two distinct cell types that are countermodulated by metabotropic receptors. Neuron 76, 776-789 (2012).

161   Grosmark, A. D. & Buzsaki, G. Diversity in neural firing dynamics supports both rigid and learned hippocampal sequences. Science 351, 1440-1443 (2016).

162   Wilson, M. A. & McNaughton, B. L. Dynamics of the hippocampal ensemble code for space. Science 261, 1055-1058 (1993).

163   Cheng, S. & Frank, L. M. New experiences enhance coordinated neural activity in the hippocampus. Neuron 57, 303-313 (2008).

164   Singer, A. C., Karlsson, M. P., Nathe, A. R., Carr, M. F. & Frank, L. M. Experience-dependent development of coordinated hippocampal spatial activity representing the similarity of related locations. J Neurosci 30, 11586-11604 (2010).

165   Carr, M. F., Jadhav, S. P. & Frank, L. M. Hippocampal replay in the awake state: a potential substrate for memory consolidation and retrieval. Nat Neurosci 14, 147-153 (2011).

166   Foster, D. J. & Knierim, J. J. Sequence learning and the role of the hippocampus in rodent navigation. Curr Opin Neurobiol 22, 294-300 (2012).

167   Wu, X. & Foster, D. J. Hippocampal replay captures the unique topological structure of a novel environment. J Neurosci 34, 6459-6469 (2014).

168   Bendor, D. & Wilson, M. A. Biasing the content of hippocampal replay during sleep. Nat Neurosci 15, 1439-1444 (2012).

169   O'Neill, J., Senior, T. & Csicsvari, J. Place-selective firing of CA1 pyramidal cells during sharp wave/ripple network patterns in exploratory behavior. Neuron 49, 143-155 (2006).

170   Csicsvari, J., Hirase, H., Mamiya, A. & Buzsaki, G. Ensemble patterns of hippocampal CA3-CA1 neurons during sharp wave-associated population events. Neuron 28, 585-594 (2000).

171   Li, X. G., Somogyi, P., Ylinen, A. & Buzsaki, G. The hippocampal CA3 network: an in vivo intracellular labeling study. J Comp Neurol 339, 181--208 (1994).

172   Csicsvari, J., Jamieson, B., Wise, K. D. & Buzsaki, G. Mechanisms of gamma oscillations in the hippocampus of the behaving rat. Neuron 37, 311-322 (2003).

173   Wong, R. K. & Traub, R. D. Synchronized burst discharge in disinhibited hippocampal slice. I. Initiation in CA2-CA3 region. J Neurophysiol 49, 442-458 (1983).

174   Lee, H., Wang, C., Deshmukh, S. S. & Knierim, J. J. Neural Population Evidence of Functional Heterogeneity along the CA3 Transverse Axis: Pattern Completion versus Pattern Separation. Neuron 87, 1093-1105 (2015).

175   Lu, L., Igarashi, K. M., Witter, M. P., Moser, E. I. & Moser, M. B. Topography of place maps along the CA3-to-CA2 axis of the hippocampus. Neuron 87, 1078-1092 (2015).

176   Singer, W. Neuronal synchrony: a versatile code for the definition of relations? Neuron 24, 49-65, 111-125 (1999).

177   Shadlen, M. N. & Movshon, J. A. Synchrony unbound: a critical evaluation of the temporal binding hypothesis. Neuron 24, 67-77, 111-125 (1999).

178   Buzsaki, G. & Draguhn, A. Neuronal oscillations in cortical networks. Science. 304, 1926-1929 (2004).

179   Buzsaki, G. Rhythms of the brain. (Oxford University Press, 2006).

180   Colgin, L. L. & Moser, E. I. Gamma oscillations in the hippocampus. Physiology (Bethesda) 25, 319-329 (2010).

181   Fell, J. & Axmacher, N. The role of phase synchronization in memory processes. Nat Rev Neurosci 12, 105-118 (2011).

182   Siegle, J. H. & Massachusetts Institute of Technology. Department of Brain and Cognitive Sciences. Causal evidence for the behavioral impact of oscillations in neocortex and hippocampus. (2014).

183   Ray, S. & Maunsell, J. H. Do gamma oscillations play a role in cerebral cortex? Trends Cogn Sci 19, 78-85 (2015).

184   Ahmed, O. J. & Mehta, M. R. Running speed alters the frequency of hippocampal gamma oscillations. J Neurosci 32, 7373-7383 (2012).

185   Kemere, C., Carr, M. F., Karlsson, M. P. & Frank, L. M. Rapid and continuous modulation of hippocampal network state during exploration of new places. PLoS ONE 8, e73114 (2013).

186   Takahashi, M., Nishida, H., Redish, A. D. & Lauwereyns, J. Theta phase shift in spike timing and modulation of gamma oscillation: a dynamic code for spatial alternation during fixation in rat hippocampal area CA1. J Neurophysiol 111, 1601-1614 (2014).

187   Cabral, H. O. *et al.* Oscillatory dynamics and place field maps reflect hippocampal ensemble processing of sequence and place memory under NMDA receptor control. Neuron 81, 402-415 (2014).

188   Igarashi, K. M., Lu, L., Colgin, L. L., Moser, M. B. & Moser, E. I. Coordination of entorhinal-hippocampal ensemble activity during associative learning. Nature 510, 143-147 (2014).

189   Zheng, C., Bieri, K. W., Hsiao, Y. T. & Colgin, L. L. Spatial Sequence Coding Differs during Slow and Fast Gamma Rhythms in the Hippocampus. Neuron 89, 398-408 (2016).

190   Bragin, A. *et al.* Gamma (40-100 Hz) oscillation in the hippocampus of the behaving rat. J Neurosci 15, 47-60 (1995).

191   Csicsvari, J., Jamieson, B., Wise, K. D. & Buzsaki, G. Mechanisms of gamma oscillations in the hippocampus of the behaving rat. Neuron 37, 311-322 (2003).

192   Belluscio, M. A., Mizuseki, K., Schmidt, R., Kempter, R. & Buzsaki, G. Cross-frequency phase-phase coupling between theta and gamma oscillations in the hippocampus. J Neurosci 32, 423-435 (2012).

193   Scheffer-Teixeira, R., Belchior, H., Leao, R. N., Ribeiro, S. & Tort, A. B. On high-frequency field oscillations (>100 Hz) and the spectral leakage of spiking activity. J Neurosci 33, 1535-1539 (2013).

194   Lasztoczi, B. & Klausberger, T. Layer-specific GABAergic control of distinct gamma oscillations in the CA1 hippocampus. Neuron 81, 1126-1139 (2014).

195   Buzsaki, G., Horvath, Z., Urioste, R., Hetke, J. & Wise, K. High-frequency network oscillation in the hippocampus. Science 256, 1025-1027 (1992).

196   Csicsvari, J., Hirase, H., Czurko, A., Mamiya, A. & Buzsaki, G. Fast Network Oscillations in the Hippocampal CA1 Region of the Behaving Rat. J Neurosci 19, RC20 (1999).

197   Patel, J., Schomburg, E. W., Berenyi, A., Fujisawa, S. & Buzsaki, G. Local generation and propagation of ripples along the septotemporal axis of the hippocampus. J Neurosci 33, 17029-17041 (2013).

198   Mercer, A., Eastlake, K., Trigg, H. L. & Thomson, A. M. Local circuitry involving parvalbumin-positive basket cells in the CA2 region of the hippocampus. Hippocampus 22, 43-56 (2012).

199   Botcher, N. A., Falck, J. E., Thomson, A. M. & Mercer, A. Distribution of interneurons in the CA2 region of the rat hippocampus. Front Neuroanat 8, 104 (2014).

200   Ranck, J. B., Jr. Studies on single neurons in dorsal hippocampal formation and septum in unrestrained rats. I. Behavioral correlates and firing repertoires. Exp Neurol 41, 461-531 (1973).

201   Fox, S. E. & Ranck, J. B., Jr. Electrophysiological characteristics of hippocampal complex-spike cells and theta cells. Exp Brain Res 41, 399-410 (1981).

202   Buzsaki, G., Leung, L. W. & Vanderwolf, C. H. Cellular bases of hippocampal EEG in the behaving rat. Brain Res 287, 139-171 (1983).

203   Skaggs, W. E., McNaughton, B. L., Wilson, M. A. & Barnes, C. A. Theta phase precession in hippocampal neuronal populations and the compression of temporal sequences. Hippocampus 6, 149-172 (1996).
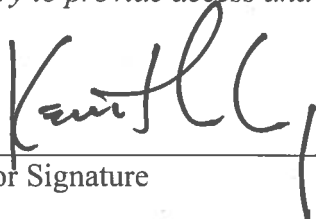
204   Csicsvari, J., Hirase, H., Czurko, A., Mamiya, A. & Buzsaki, G. Oscillatory coupling of hippocampal pyramidal cells and interneurons in the behaving rat. J Neurosci 19, 274-287 (1999).

205   Harvey, C. D., Collman, F., Dombeck, D. A. & Tank, D. W. Intracellular dynamics of hippocampal place cells during virtual navigation. Nature 461, 941-946 (2009).

206   Epsztein, J., Brecht, M. & Lee, A. K. Intracellular determinants of hippocampal CA1 place and silent cell activity in a novel environment. Neuron 70, 109-120 (2011).

207   Grienberger, C., Chen, X. & Konnerth, A. NMDA receptor-dependent multidendrite Ca(2+) spikes required for hippocampal burst firing in vivo. Neuron 81, 1274-1281 (2014).

208   Bittner, K. C. *et al.* Conjunctive input processing drives feature selectivity in hippocampal CA1 neurons. Nat Neurosci 18, 1133-1142 (2015).

209   Jarsky, T., Mady, R., Kennedy, B. & Spruston, N. Distribution of bursting neurons in the CA1 region and the subiculum of the rat hippocampus. J Comp Neurol 506, 535-547 (2008).

210   Slomianka, L., Amrein, I., Knuesel, I., Sorensen, J. C. & Wolfer, D. P. Hippocampal pyramidal cells: the reemergence of cortical lamination. Brain Struct Funct 216, 301-317 (2011).

211   Alexander, G. M. *et al.* Social and novel contexts modify hippocampal CA2 representations of space. Nat Commun 7, 10300 (2016).

212   Mankin, E. A., Diehl, G. W., Sparks, F. T., Leutgeb, S. & Leutgeb, J. K. Hippocampal CA2 activity patterns change over time to a larger extent than between spatial contexts. Neuron 85, 190-201 (2015).

213   Girardeau, G., Benchenane, K., Wiener, S. I., Buzsaki, G. & Zugaro, M. B. Selective suppression of hippocampal ripples impairs spatial memory. Nat Neurosci 12, 1222-1223 (2009).

214   Ego-Stengel, V. & Wilson, M. A. Disruption of ripple-associated hippocampal activity during rest impairs spatial learning in the rat. Hippocampus 20, 1-10 (2010).

215   Jadhav, S. P., Kemere, C., German, P. W. & Frank, L. M. Awake hippocampal sharp-wave ripples support spatial memory. Science 336, 1454-1458 (2012).

216   de Lavilleon, G., Lacroix, M. M., Rondi-Reig, L. & Benchenane, K. Explicit memory creation during sleep demonstrates a causal role of place cells in navigation. Nat Neurosci 18, 493-495 (2015).

Publishing Agreement

It is the policy of the University to encourage the distribution of all theses, dissertations, and manuscripts. Copies of all UCSF theses, dissertations, and manuscripts will be routed to the library via the Graduate Division. The library will make all theses, dissertations, and manuscripts accessible to the public and will preserve these to the best of their abilities, in perpetuity.

Please sign the following statement:

I hereby grant permission to the Graduate Division of the University of California, San Francisco to release copies of my thesis, dissertation, or manuscript to the Campus Library to provide access and preservation, in whole or in part, in perpetuity.

Author Signature

6 · 7 · 16

Date